CRITICAL SPEED PHENOMENON FOR FLOATING ICE SHEETS

JOHN JOSEPH WHITTEN

CRITICAL SPEED PHENOMENON

FOR FLOATING ICE SHEETS

BY

(c) JOHN JOSEPH WHITTEN, B.Eng.

A thesis submitted to the School of Graduate Studies in partial fulfillment of the requirements for the degree of Master of Engineering

FACULTY OF ENGINEERING AND APPLIED SCIENCE

MEMORIAL UNIVERSITY OF NEWFOUNDLAND

November, 1987

St. John's Newfoundland Canada

ISBN 0-315-43358-2

Abstract

In Canada's Northern Regions floating ice sheets are often used as roads for vehicular traffic, including large trucks, and as runways for aircraft. Operators have found that a critical speed exists for movement over these roads and runways. Movement over the ice sheet at this critical speed causes large amplitude waves to be generated in the sheet near the load. Thus, it is very important that operators avoid this speed.

Experimental work has been done on this phenomenon, and researchers have developed theoretical means to determine this critical speed. Until quite recently (mid 1980s), there had been no measurements or predictions of the wave patterns generated in ice sheets, and the limited predictions were conflicting.

In this thesis, an experimental approach was taken to determine the wave patterns generated in a floating ice sheet by a moving load. Several different moving loads were used, and the ice was modelled in various ways: EG/AD/S model ice, styrofoam sheeting, and polyethylene sheeting. Theoretical predictions of the patterns were also produced. The generated patterns agreed with the predictions.

It was also determined that the deflection depression caused by the load at speeds less than the critical changed shape with speed. The tests also indicated that the critical speed is much more a function of sheet characteristics than load characteristics.

Acknowledgements

The author wishes to extend his sincere appreciation for the help and guidance given to him by his supervisor, Dr. M.J. Hinchey, during work on this thesis.

This work would have been very difficult to complete if not for the help and co-operation of several individuals. The experimental work at the Institute for Marine Dynamics went well in part due to the help afforded the author by Brian Hill and the rest of the technical staff of the ice group. A word of appreciation must also go to Dr. S. Jones, head of the ice group at IMD, for the use of such a world class facility.

The author would also like to thank the technical staff of the MUN Wave/Towing Tank for their help during several series of tests.

In closing, the author would like to express his gratitude to the School of Graduate Studies for financial assistance in the form of a bursary.

TABLE OF CONTENTS

TABLE OF CONTENTS (cont'd.)

TABLE OF CONTENTS (cont'd.)

TABLE OF CONTENTS (cont'd.)

LIST OF TABLES

C_g	Group Speed
C_p	Phase Speed
D	Flexural Rigidity
D_c	Cushion Diameter
D_d	Depression Diameter
E_a	Energy Absorbed
E_t	Energy Transmitted
E	Young's Modulus
H	Water Depth
K	Spring Constant
L	Characteristic Length
N_f	Froude Number
P	Pressure
P_s	Interface Pressure
R	Towing Resistance
T	Surface Tension
V	Velocity
V_c	Critical Velocity
V_r	Resonant Velocity
W	Vehicle Weight
X	Distance (Wave Pattern Geometry)

g	Gravitational Acceleration
h	Ice Thickness
h_w	Wave Height
k	Wave Number
q	Load
t	Time
$\bar{v}$	Velocity Vector
w	Vertical Deflection of Ice
x, y, z	Stationary Cartesian Coordinate System
θ	Angle
ϕ	Velocity Potential
σ	Ice Sheet Density (mass/area)
ρ_i	Density of Ice
ρ_f	Density of Fluid
ρ_w	Water Density
υ	Poisson's Ratio
π	3.14159
Δ	Vehicle Weight
ω	Circular Frequency
λ	Wavelength

CHAPTER 1 INTRODUCTION

1.1 General

The ability to transport people and goods over floating ice sheets in the Canadian North is of great importance. Floating ice roadways have been used in several locations in Canada for many years. These ice roads are used by operators to move a variety of goods to and from isolated communities not serviced by all-weather roads. They are used by mining, logging and oil companies to get to sites which would be otherwise inaccessible. Winter landing strips are also set up on floating ice sheets to allow conventional aircraft access to sites otherwise inaccessible.

To predict the safe use of these floating ice roads and runways, two conditions must be considered. First, the static condition must be considered. This is a bearing capacity problem and involves the determination of the maximum static or quasi-static load an ice sheet can support. This problem has been the subject of much study. Kerr (1975) has developed both theoretical and empirical formulae giving the allowable load based on mechanical properties of the ice, ice thickness, and (in the case of long duration loads where creep can come into play) time.

Secondly, the dynamic condition must be considered. Loads moving over a floating ice sheet at high speeds generate flexural gravity waves in the ice sheet in the vicinity of the load. At a certain "critical speed", the amplitude of these waves is a maximum, and the deflection under the load is greatest and can be two to three times the static deflection for the same load. Thus, it can be seen that a load which is determined to be safe in a static condition could be quite unsafe if it were to travel at the critical speed. Although transport operators generally try to avoid the critical speed, the Canadian Coast Guard has recently used hovercraft to take advantage of the phenomenon for icebreaking purposes.

Several aspects of this critical speed phenomenon will be examined in this thesis.

1.2 Scope of Work

Although many researchers have studied this phenomenon experimentally and theoretically, it is still not well understood. This thesis reports on recent work done on the critical speed phenomenon at Memorial University and at the National Research Council's Institute for Marine Dynamics.

To understand how a floating ice sheet fails under the action of waves induced by a moving load, we must understand how the ice sheet deforms under the moving load. That is to say we require an understanding of the wave patterns generated in a floating ice sheet by a moving load. This thesis will study wave pattern generation in ice sheets. In previous studies, data on wave generation in floating ice sheets was obtained using single sensors. This data was not sufficient to determine the wave patterns generated. The thesis will try to obtain improved data by using multiple sensors. It will also attempt to predict these generated wave patterns. The only predictions in the literature are quite recent (Shinbrot (1983) and Davys et al (1985)) and are conflicting. In predicting these wave patterns, ideally, we would like to predict the wave amplitudes as well as the crest patterns. Amplitude predictions, however, can be expected to be poor due to dissipation and non-linear factors, both of which, are ignored. For this reason, it was decided to concentrate on the wave crest patterns.

The thesis is organized into six main chapters.

Chapter 1 is an introduction. Chapter 2 is a literature review on the critical speed phenomenon. Transport over ice is covered as is high speed Air Cushion Vehicle (ACV) ice breaking.

Chapter 3 contains wave pattern predictions reported in literature and also some developed at Memorial University of Newfoundland. For this, ice was modelled as membranes, thick plates and thin plates. The various models are compared. Chapter 4 outlines the objectives of the experimental work. Chapter 5 describes the experimental work which was done. The experimental facilities are described. Each set of experiments is treated separately. Included is a description of the experimental apparatus and instrumentation followed by experimental procedures, presentation and discussion of results. Chapter 6 contains conclusions and suggestions for future work.

CHAPTER 2 LITERATURE REVIEW

2.1 General

A stationary load resting on a floating ice sheet creates a bowl-shaped depression centered at the load. If the load moves at low velocities, a "quasi-static" condition exists where the bowl-shaped depression moves with the load. If, however, the load moves at high velocities, flexural gravity waves are generated in the ice sheet in the vicinity of the load. In this condition, two distinct wave forms are generated. Short wave length, high frequency waves precede the load and longer wavelength, low frequency waves follow it. It has been observed in the field (Eyre, 1977) and in laboratory experiments (Whitten et al 1986) that the wave patterns generated by a load moving at constant speed are fixed relative to it.

There is a certain cut-off velocity below which no waves are generated by the moving load. This velocity is also a critical velocity, and at this velocity the amplitude of the generated waves (as well as deflection of the ice sheet under the load) is a maximum (Eyre, 1977).

2.2 Theoretical Work on Critical Speed

The generation of waves in a floating ice sheet induced by a moving load was first observed by the Russians on an ice sheet over Lake Ladoga during World War II. Shortly after the war, Ivanov & Assoc. (1946) published the first paper which discussed the deformation of ice covers by moving loads.

Holl (1950) considered a load moving vertically up and down on a thin plate resting on a Winkler foundation. The Winkler foundation assumes foundation pressure proportional to deflection.

Livesley (1953) extended this solution to a uniformly distributed rectangular load travelling at a constant velocity on a thin plate resting on a Winkler foundation. He incorrectly analyzed the singularities in his results and came to the erroneous conclusion that at velocities above critical, deflections under the load became infinite. This incorrect analysis was pointed out by Nevel (1970). Livesley treated the water base as a series of ideal springs and the action of the water on the sheet was represented by simple Kw terms; K being a spring constant and w, being the vertical deflection. The inertia of the water and the load was not considered and, thus, results obtained using this type of analysis can be considered

qualitative at best. This type of analysis was extended by Piszczek (1958). He considered a plate resting on a Winkler foundation and analyzed the effects of a moving load, including its inertia.

Even though inertia effects of the load were now considered, the response of the liquid base was still being described by simple Kw terms. To do a proper analysis of the response of a floating ice sheet to a moving load, it is necessary to describe the response (including inertia effects) of the liquid base with equations of hydrodynamics.

The theory of flexural waves in ice covers was presented by Greenhill (1887). This theory outlined the response of floating ice sheets to water waves. Wilson (1955) attempted to analyze the problem of waves in ice caused by moving loads by applying Greenhill's theory and a theory by Hertz (1884) (deflection of floating plates by static loads) to the critical speed problem. He obtained the following expression for the critical velocity.

$$V_c = \left[\frac{922\, h^{3/4}}{\cot\left(0.0150 \frac{H}{h^{3/4}} + 0.0135\, h^{1/4}\right)} \right]^{1/2} \qquad (2\text{-}1)$$

where H = water depth

h = thickness of sheet

Ice properties were as follows:

$$\frac{E}{12(1-\upsilon^2)} = 8.0 \times 10^9 \text{ dyne cm}$$

where E = Young's modulus

υ = Poisson's Ratio

Wilson also carried out two series of experiments on lakes in Chelsea, Michigan in February, 1954 and Mille Lacs near Brainerd, Minnesota in February, 1955. The results showed the critical speed phenomenon very well. The author concluded that the match between results and theory was good considering the theory was only first order and the test conditions were less than ideal.

Assur (1956) who had worked with Wilson on the 1955 field tests attempted to improve on Wilson's approach. According to Nevel (1970), both Wilson's and Ivanov's approaches are incorrect, but both do give approximately correct critical velocities.

The first systematic formulation of the critical speed phenomenon for moving loads on floating ice sheets is attributed to Kheisin (1963). His analysis is linear. He uses plate theory and equations of hydrodynamics to model the system. The differential equation for the motion of the plate is:

$$D\nabla^4 w + P_s + \rho_i \frac{\partial^2 w}{\partial t^2} = q(x, y, t) \qquad (2\text{-}2)$$

where $D = Eh^3/12(1 - \nu^2)$

h = ice thickness

$$\nabla^4 = \frac{\partial^4}{\partial x^4} + \frac{2\,\partial^4}{\partial x^2\,\partial y^2} + \frac{\partial^4}{\partial y^4}$$

x,y,z: stationary cartesian coordinate system

w: vertical deflection of ice

P_s: interface pressure (pressure of water on ice)

ρ_i: mass density of ice

t: time

q: load

The liquid which supports the plate is assumed to be inviscid and incompressible. Its motion is assumed to be irrotational. Thus, the continuity equation becomes

$$\frac{\partial^2\phi}{\partial x^2} + \frac{\partial^2\phi}{\partial y^2} + \frac{\partial^2\phi}{\partial z^2} = 0 \qquad (2\text{-}3)$$

or

$$\nabla^2\phi = 0 \qquad (2\text{-}4)$$

where ϕ = velocity potential. This is basically a statement of conservation of mass for the liquid.

For an irrotational flow:

$$\nabla \times \bar{V} = 0 \qquad (2\text{-}5)$$

$\bar{V}$ must take the form:

$$\bar{V} = -\nabla\phi \qquad (2\text{-}6)$$

where $\bar{V}$ is the velocity vector.

Next, Bernoulli's equation for unsteady flow is used to solve for the pressure at the plate liquid interface.

$$P_s = \rho_f gz - \rho_f \frac{v^2}{2} + \rho_f \frac{\partial\phi}{\partial t} + \rho_f F(t) \qquad (2\text{-}7)$$

Since as $(x^2 + y^2) \to \infty$, $P_s = \rho_f gz$ and $v = \phi = 0$, it follows that $F(t) = 0$.

Also, since the $\rho_f v^2/2$ term is non-linear, it is neglected. The value of this term tends to be negligible anyway.

The resulting pressure is as follows:

$$P_s = \rho_f gz + \rho_f \frac{\partial\phi}{\partial t} \qquad (2\text{-}8)$$

Equation 2-8 was then substituted into Equation 2-2 to give the plate equation as follows:

$$D \nabla^4 w + \frac{\partial^2 w}{\partial t^2} + \rho_f g z + \rho_f \frac{\partial \phi}{\partial t} = q \qquad (2\text{-}9)$$

This equation along with Equation 2-3 constituted two simultaneous equations in two unknowns, w and ϕ.

The following boundary conditions were also used. At the surface, it is assumed that there is no separation between the ice and the water:

$$\frac{\partial \phi}{\partial z} = - V \frac{\partial w}{\partial x} \qquad \text{at } z = 0 \qquad (2\text{-}10)$$

This equation simply states that the vertical velocity of the water at the interface is equal to the velocity of the ice. The bottom boundary condition is

$$\frac{\partial \phi}{\partial z} = 0 \qquad \text{at } z = H \qquad (2\text{-}11)$$

which merely states that the vertical velocity of the water at $z = H$ (the bottom) is zero.

Kheisin considered two loading situations. The first was a concentrated load moving at constant velocity along the x axis over an infinite plate of thickness h resting on an ideal fluid. He also considered the case of a constant moving line load. In both cases, it was assumed that the load had been travelling at constant speed for a sufficient time to allow transient effects to die out, and thus the problem could be treated as steady state.

Kheisin now solved the two equations, 2-3 and 2-9, and obtained expressions for w and ϕ in integral form. At this point, he restricts his discussion to the shallow water case. From his results, Kheisin concluded that the deflection under the load was finite at the critical velocity. He also concluded that for the three dimensional case no critical velocity existed.

Nevel (1970) attributes Kheisin's prediction of a finite deflection at the critical velocity to an incorrect analysis of the singularities in his final equations. Nevel also found that Kheisin was incorrect in his conclusion that no critical velocity existed for the three dimensional case.

Nevel (1970) extended on Kheisin's approach. Where Kheisin considered only a concentrated force, Nevel also considered a force distributed uniformly over a circular area and computed stresses in the plates as well as deflections. Nevel made the problem as general as possible and didn't limit ice thickness or water depth though both were considered to be constant. Much as Kheisin had done, Nevel considered an infinite elastic plate floating on a liquid. The liquid was assumed inviscid and incompressible, and the motion of the liquid was assumed to be irrotational. The vertical load P moved along the x axis at constant velocity. The ice sheet was assumed to be homogeneous, isotropic and elastic. The first assumption (homogeneous) isn't too bad an assumption for freshwater ice; however, sea ice with its brine cells can't as easily be considered homogeneous. The assumption that ice is isotropic is only a rough approximation. The elastic assumption is good as long as static or quasi-static conditions are avoided where creep can come into play and make the ice behave in a visco-elastic manner.

Using thin plate theory and hydrodynamics, Nevel starts with the same equations as Kheisin, Equations 2-2 and 2-3. He uses Bernoulli's equation and makes similar assumptions to obtain Equation 2-8.

Then, using the method of Fourier transforms, he obtained explicit equations for the sheet deflection and also for plate curvature in the x and y directions.

These equations contain complicated integrals and calculation of deflections and curvatures using them is not a simple task. Nevel does, however, solve these equations for varying depths of water and thicknesses of ice and presents his results graphically.

Figure 1 shows critical velocity as a function of ice thickness and water depth. It is based on the following ice properties:

$\rho_i = \rho_w = 1$ gm / cm^3	densities
E = 50,000 kg/cm^2	Young's Modulis of ice
$\upsilon = 0.33$	Poisson's Ratio of ice

If ice properties (E, ρ and υ) are known and different from those assumed in Figure 1 then Figure 2 can be used. In this figure, the critical velocity is a function of water depth and characteristic length. Characteristic length is given as follows:

$$L = \left[\frac{E h^3}{12 (1 \neq v^2) \rho_i} \right]^{1/4} \qquad (2\text{-}12)$$

Figure 3 shows a ratio of deflection over static deflection as a function of velocity over critical velocity. The critical speed phenomenon is illustrated very well in this figure. It should be noted that at the critical velocity the deflection becomes infinite. This is not the case in practice, and Nevel attributes the discrepancy to assumptions made in the formulation of the problem. Namely, (1) The v^2 term was dropped from Bernoulli's equation to make it linear. (2) Dissipation in the ice and water was neglected (especially ice). (3) H and h were assumed to be constant as were the mechanical properties of the ice sheet. Since in practice any or all of these may vary, it could change the problem from a steady state one to a forced vibration problem under a general force.

Kerr (1982) extended the study of critical speed phenomenon by considering the effects of in-plane forces. All earlier work had considered the in-plane forces to be zero; however, due to constrained thermal strain, these in-plane forces can be non-zero. Kerr determined that compression fields reduce the critical speed, whereas tension fields have the opposite effect.

Davys, Hosking and Sneyd (1985), and Squire (1985) approach the critical speed phenomenon in a different way. Since the critical speed occurs at the minimum phase speed for waves in an ice sheet water environment, they start with a dispersion relationship. The dispersion relationship for deep water is as follows:

$$D k^5 + (\rho_w g - \rho_i h \omega^2) k - \rho_w \omega^2 = 0 \qquad (2\text{-}13)$$

k = wave number = $2\pi/\lambda$

ρ_i = ice density

ρ_w = water density

D = flexural rigidity

ω = circular frequency

h = ice thickness

λ = wave length

Since phase velocity, $C_p = \omega/k$, the above dispersion relationship may be expressed in terms of C_p:

$$C_p^2 = \frac{Dk^3 + \rho_w g/k}{\rho_i h k + \rho_w} \qquad (2\text{-}14)$$

By differentiating this equation and setting the result to zero, the minimum phase velocity can be found:

$$C_p{}^2_{min} = \frac{4Dk^3}{(2\rho_i hk + \rho_w)} \qquad (2\text{-}15)$$

Waves can only exist at speeds above C_{pmin}. The group velocity is $C_g = d\omega/dk$, and can be written:

$$C_g = \frac{4Dk^3 + \rho_w C_p{}^2}{2C_p(\rho_i hk + \rho_w)} \qquad (2\text{-}16)$$

This is the speed at which energy travels.

This group speed is numerically the same as the phase speed when $C_p = C_{pmin}$, indicating that the phase speed and group speed are the same at C_{pmin}. In ice, the waves created by moving loads appear stationary with respect to the moving load. That is to say the waves travel at the same speed or have a phase speed equal to the vehicle speed. This implies that at the critical speed, C_{pmin}, the energy travels at the same speed as the moving load which is the source of energy. Thus, at the critical speed, the energy is trapped and can not get away from the vehicle. This excess energy increases the wave amplitude at the critical speed. Hinchey (1986) has gone through a similar analysis and reached the same conclusion.

2.3 Experimental Work on Critical Speed

To date, the number of field studies on the dynamic response of ice covers is limited. Field tests were carried out by Wilson (1955) as mentioned earlier, Anderson (1958), Eyre (1977) and Beltaos (1977). The results of these four authors' work are summarized in Table 1 (From Beltaos).

All the authors measured sheet deflections (although in various ways) induced by moving loads. As can be seen in Table 1, the observed critical speeds, although they had a marked tendency to be higher than predicted by Nevel's theory, all tend to be within about 10% of it. Also, the deflections at the critical speed are finite, and the critical deflection amplification factor (dynamic deflection/static deflection) varies from 1.4 (Wilson) to 4.6 (Anderson). Deflection amplitute factors all tend to be about 2.0 with the exception being Anderson (4.6). Beltaos explains this by suggesting that such a high deflection amplitude factor could exist, but in a narrow band of speed not hit in any of the other field tests.

This statement proved correct when Takizawa (1978) concluded a series of field trials and obtained a deflection amplitude factor of almost 4.0. High deflection amplification factors (about 5.0 - 6.0) were also obtained by the author in tests on

a model ice sheet at Memorial University of Newfoundland. These results will be discussed later in this thesis.

Eyre's experiments were the most extensive of the field tests. His tests included various stages of ice growth, vehicles ranging in weight from 2,200 to 23,500 kg with velocities varying from 0 to 31 m/s. The elastic modulus derived from static load tests varied from 2 to 13 x 10^9 Pa. Eyre conducted more than 150 test runs, most producing useful results. He concluded that his data tended to support Nevel's theory.

Eyre also made use of a vibration transducer in his tests to measure the noise intensity in the ice. He argued that the maximum noise intensity would occur at the point when maximum fracturing was taking place in the ice sheet. He observed that maximum noise intensity did not occur at the critical speed but at about 85% of it. If, as Eyre assumes, maximum fracturing is occurring at this point, then the critical speed is not the speed to be concerned with, but rather a speed which is .85 of the critical speed. This, however, cannot be explained by Nevel's theory.

Eyre also studied the effect of vehicle speed on wave frequency. He found that the frequency of the stern wave increased with vehicle speed in a linear fashion. It was found

that on a given day (ice conditions unchanged) a variety of vehicles varying drastically in mass all fell on the same line on a plot of frequency versus vehicle speed. However, on different days, these lines varied (Figure 4). Eyre attributed this to varying ice conditions and, as Eyre stated, this is "always a confounding factor in experiments on floating ice sheets."

Takizawa (1978) came up with a similar result. He concluded that the vehicle weight only affected the depression depth and wave amplitude and had no significant effect on wave length or frequency. He also observed that, at the critical speed, while the maximum depression depth occurred, the depression width was a minimum. This means the ice sheet would undergo maximum bending at the critical speed and, if ice failure was to occur, it would be under these conditions. Squire (1985) conducted a series of field tests on the dynamic strain response of ice to moving loads. He measured strains directly with the use of strain gauges. He presents wavelength data that agrees well with the results reported by Takizawa which were obtained from deflection measurements.

Beltaos observed that the maximum stress amplification factor was about 1.4, and it occurred near the critical speed. He concluded this from strain measurements on the ice cover

(using elastic assumption, stress is proportional to strain). This stress amplification factor was lower than the deflection amplification factor which varied from 1.9 to 2.3. Nevel had predicted that the stress amplification factor would be less than the deflection amplification factor. It should be noted that, even though most papers report deflection amplification factors, the more important result is the stress amplification factor, since it and not deflection will dictate when the ice cover will fail.

2.4 High Speed Air Cushion Vehicle Ice Breaking

In the mid 1970's, the critical speed phenomenon became the subject of renewed attention when it was discovered that under certain conditions air cushion vehicles (ACVs), which operated at or near the critical speed, could be used to break ice.

Hovercraft icebreaking was first observed in Yellowknife in the winter of 1971-72. The ACT-100 was towed by cable and broke 27 inches (68.6 cm) of freshwater ice continuously at speeds up to 4 mph (6.2 km/hr).

The Canadian Government became involved in this work in the winter of 1972-73 (Dutfield, D.O and Dickens, D.F., 1974). The ice-breaking capabilities of the ACT-100 were further tested at

Tuktoyaktuk that year. In simulated cable ferry trials, the available 22 inches (56 cm) of ice was broken, and successive passes broke up the ice floes considerably.

Those tests demonstrated what has become known as slow speed air cushion ice breaking. Several tests were carried out subsequently with several air cushion vehicles (ACVs) ranging in size, weight and cushion pressure. Most early testing was done using non-self-propelled ACVs. These ACVs were either towed or pushed.

In the winter of 1973-74, the Canadian Government decided to test a self-propelled ACV to see if its lower cushion pressures would have an effect on the ability of the vehicle to break ice.

The self-propelled ACV Voyageur was tested at Parry Sound, Ontario, and it was clearly demonstrated that ice could be broken. Ice 10 inches (25 cm) thick was broken continuously at speeds up to about 7 mph (11.2 km/hr). This again was slow speed ACV ice-breaking.

A startling discovery came one day as the Voyageur was on its way to the low speed test area. As it accelerated between 12 to 18 mph (19 - 30 km/hr), a much more powerful ice-breaking

action was observed. Ice about 20 inches (51 cm) thick was broken by waves set up in the ice sheet. This new method broke ice twice as thick, over a path three times as wide, while operating at twice the speed of the low speed mode.

This powerful new method of ice breaking became known as high speed ACV ice breaking.

As mentioned earlier, the Parry Sound experiments were meant to investigate the slow speed ice breaking capabilities of a self-propelled ACV. This new phenomenon, however, appeared so important that some time was devoted to further investigation of it. Tests were conducted and the results are given in Table 2. In all cases, the ice was broken by flexural waves in the ice sheet. On February 18, 1974, eight separate runs were made with special care taken to measure speed accurately. Critical speeds were estimated using Nevel's (1970) theory.

Although the flexural gravity waves caused the ice sheet to fail (extensive cracking), multiple successive passes were required to obtain the same degree of track clearance as that obtained in the slow speed mode. While much greater ice thicknesses can be broken in the high speed mode the speed of advancement may be close to that of the slow speed mode. One big plus of high speed ACV ice breaking is the speed and

mobility of the craft. An ACV could make a two hundred mile trip in five hours whereas a conventional ice breaker could take as long as thirty hours.

An ACV travelling over open water generates a wave train. This wave train grows with speed up to a maximum at a certain speed and above that speed the wave train disappears and the water surface is relatively undisturbed. This generation of waves causes a large drag on the ACV and, in fact, it is the drag encountered at this certain speed (open water hump speed) which dictates the propulsion power requirements of the vehicle. In order to exploit the high speed capabilities of ACVs, they must be able to overcome this drag.

It has been suggested (Landel, 1977) that, when an ACV travels over ice at the open water hump speed, the ice sheet behaves much like the water surface would if no ice were present. The ice fails in flexural bending as the wave train moves across it.

This implies that theories for loads moving over flat ice sheets, such as Nevel's, are not valid. It also suggests that the water under the ice is responding to a pressure disturbance (depression in the ice). The length of this depression will determine the speed at which waves are formed in the sub-ice

water. It is noted that the length of this depression is dependent on vehicle length and ice characteristics. It appears, with these assumptions, that the depression length is constant over all speeds (under speed where waves form); however, field tests (Takizawa) have shown that this depression length is not constant. Tests done at MUN have also shown that the depression length varies with speed.

Carter (1977) assumes that the ice breaks under the hovercraft and, thus, the cushion pressure is applied to the water surface. He also assumes the presence of broken ice pieces has a negligible damping effect under and in the vicinity of the ACV. Carter has basically assumed that the ACV is travelling on open water and, thus, the response of the ice sheet is that of open water as if no ice sheet existed. Carter does not explain how the ice breaks.

Under these conditions, the ice will see maximum deflection when the ACV travels at the open water hump speed. This is probably the case once the ice sheet fails (cracks) and no longer has flexural rigidity. The open water hump speed is probably the important speed on successive passes once the ice is cracked by an initial pass at the critical speed for waves in the floating ice sheet.

Lecourt and Kotras (1975) presented the results of model tests of an ACV over model ice. The object was to determine the resistance to forward motion experienced by an ACV operating over a floating ice sheet. The model tested was a 1/7.5 scale of the SK-5 and had characteristics as shown in Table 3. Tests were done at the ARCTEC ice model basin. The tank was sixty (60) feet long, eight (8) feet wide and four (4) feet deep. Water depth was 2.9 feet during testing. The test instrumentation included measurements of velocity, resistance, roll, pitch, heave, cushion pressure and ice sheet deflection. The model ice used was a multi-component wax-like material which exhibited the desired properties. Properties of the model ice sheets were routinely measured as part of each test.

The results of the experiments can be seen in Table 4. Figure 5 shows a plot of R/Δ (the dimensionless resistance) against V/V_c (the dimensionless velocity ratio). It shows that a peak occurs at the critical velocity for waves in the sheet.

Figure 6 is a plot of R/Δ against Froude Number $V/(gL)^{1/2}$. Also included is a plot of open water resistance. The following conclusions were made based on these results. The presence of the floating ice sheet effects the velocity of peak resistance (V_c). This critical velocity V_c is a function of ice properties and not vehicle properties as in the case of

open water hump speed. It was also noted that the peak resistance was less than the open water hump resistance. Also of importance to be noted from Figure 5 and 6 is that not only is the resistance a maximum at the critical wave making velocity but that there is an abrupt change. Resistance is at a low level below the critical speed and it rises to a peak at the critical speed and drops off again at speeds above V_c. It acts much like sheet deflections which would be expected since the relationship between resistance and wave height is well known.

During several tests, the model pitched down at the bow and the hull made contact with the ice. Also, negative resistance (or thrust) was recorded for some test runs. The negative resistance is attributed to the skirt leaking most of its air out the back and creating thrust. This could also be a partial explanation of the model nosing in if the rear air leakage became excessive. The authors attributed the nose-in to interaction between the skirt and ice caused by the shape of the flexural waves induced by the vehicle. All nose-ins occurred on thin sheets at or near the critical speed. The nose-in problem was overcome by shifting the centre of gravity of the model rearward. The authors also made note of the fact that the model was towed at constant velocity and was not free to surge. Normally, an ACV which is self-propelled is free to

surge and would tend to slow down when added resistance was encountered. Towing at constant speed without the ability to surge gave some interesting results during testing at IMD. These results will be presented later in this thesis.

Decker (1978) postulates that there is a resonant speed at which high speed ACV ice breaking takes place and that this speed is dependent upon vehicle characteristics and ice characteristics. He suggests that, when an ACV operates at a speed for which the free gravity wave of the water body and the depression in the ice are the same length, a resonance will be set up. At this resonance point, the resulting wave height and resistance are maximum and the potential to break ice is greatest.

Decker determined the resonant Froude Number to be in the range of $0.46 < N_{fres} < 0.56$ for the model tests done by Lecourt and Koutras. This was calculated using the following equation:

$$V_r = \left[\frac{g\ D_d}{2}\right]^{.5} \qquad (2\text{-}17)$$

where D_d is the depression diameter and is calculated for the test conditions using Equation 2-18:

$$D_d = \frac{5.98\ L}{(1 - 3/2\ D_c/D_d)^{.25}} \qquad (2\text{-}18)$$

D_d = Depression Diameter

L = Characteristic Length of Ice Sheet

D_c = Diameter of Cushion

In Decker's analysis, the depression diameter is a function of ice characteristics and air cushion size, and is independent of speed.

Decker plots resistance against Froude number as did Lecourt and Kotras except Decker lumps all data together and doesn't differentiate between different L/D_c ratios. He draws a single curve through all the data and concludes that the data supports his resonance hypothesis. He also plots resistance against speed ratio (V/V_c) and again doesn't differentiate the data as to L/D_c ratio and concludes that Nevel's theory is not as well supported as his concept. It is difficult to understand Decker's reasoning in presenting the data in this way. As originally presented (Figure 5 and Figure 6) by Lecourt and Kotras with separate curves through data with similar L/D_c ratios (basically similar sheet thickness), Nevel's theory seems to be much better supported than does Decker's. In

Figure 6, the data for L/D_c = .162 seems to support Decker's concept, whereas the L/D_c = .248 data has a Froude number above the resonant range determined by Decker. This data, however, supports Nevel's theory since the sheet with higher characteristic length (L) has a higher critical speed.

Decker makes note of the rapid rise in resistance near the critical speed and states that any theory which attempts to explain high speed ACV ice breaking must explain this experimental result.

Since the jump in resistance level coincides with the onset of wave generation, it is reasonable to assume that the added resistance is wave resistance. Under these conditions, it is also reasonable to assume that the ACV is adding energy to the ice sheet water environment. Based on those assumptions, Decker balances the energy input into the ice sheet water system with the energy output of the vehicle moving over the ice sheet. He determines energy absorbed by the ice-water environment to be

$$E_a = (13/70)\rho_w g D_d^2 h_w^2 \qquad (2\text{-}19)$$

where:

h_w = wave height.

He next determines the energy transmitted by the ACV to be

$$E_t = 3 W h_w \qquad (2\text{-}20)$$

where:

W = vehicle weight.

Equating energy transmitted with energy absorbed, (2-19) and (2-20), Decker obtains h_w to be

$$h_w = \frac{210 W}{13 \rho_w g D_d^2} \qquad (2\text{-}21)$$

Recent work on critical speed has been related to wave patterns generated in ice sheets. A series of predictions of generated wave patterns will be presented in the following chapter.

CHAPTER 3 PREDICTIONS OF GENERATED WAVE PATTERNS

3.1 General

Most experimental work done on wave generation in floating ice sheets induced by moving loads has results presented in the form of deflection and wavelength data versus speed usually measured (in various ways) at a single point on the ice sheet.

To gain an understanding of how a floating ice sheet fails under the action of waves generated by a moving load, we require information on how the ice sheet is deformed under this wave action. It is not sufficient to just know at what speeds waves are generated in the ice sheet. For a proper understanding of the mechanisms which are taking place, we require information on the wave patterns which are generated in the floating ice sheet by the moving load. Wave patterns here refer to wave crest patterns as viewed from above.

3.2 Wave Pattern Predictions in Open Literature

Mathematical predictions of wave patterns have been reported by Shinbrot (1983) and Davys et al (1985). Hinchey (1987) has also made wave pattern predictions.

Shinbrot treats the ice as an intact thin plate of uniform thickness floating on deep water. An analysis found in Whitman (1974) is used to derive the wave patterns. Shinbrot's predicted wave patterns can be seen in Figure 7. As can be seen, his bow waves bend ahead of the moving disturbance. He suggests that this could explain radial the cracks observed in the field.

Experimental work at MUN and IMD has yielded quite a different result, and these results will be discussed later in this thesis.

Davys et al (1985) have also reported wave pattern predictions. The ice sheet is assumed to be an infinite, homogeneous, elastic plate floating on water. The method of asymptotic Fourier analysis was used to give a description of the wave patterns. Their analysis starts with the dispersion relationship:

$$\omega^2 = \left[\frac{Dk^4}{\rho_w g} + 1 \right] gk \ \text{Tanh} \ kH \qquad (3\text{-}1)$$

This equation was arrived at by taking the more general relationship and assuming sheet thickness goes to zero and thus inertia effects of the sheet are ignored. Davys et al state that they were only concerned with waves longer than 50 m and that Equation 3-1 is accurate under these conditions. All calculations of wave patterns were done using a sheet thickness of 2.5 m and a water depth of 350 m. For this depth and waves of 50 m, Tanh kH = 1 and remains 1 for waves over 500 m long. This means a depth of 350 m gives the same result as infinitely deep water. The resulting wave pattern predictions can be seen in Figure 8.

3.3 Wave Pattern Prediction Developed at MUN

3.3.1 General Formulation of Problem

All wave pattern predictions developed at Memorial University are based on Lighthill's (1978) general formulation. A definition sketch for this is shown in Figure 9. Since the wave patterns are fixed relative to the load, the following equation must be satisfied:

$$C_p = V \cos \quad (3\text{-}2)$$

C_p = Phase speed

V = Load speed

Groups of waves generated by the load at any location propagate from that location at the group speed C_g. Below the critical speed no waves are formed but above it two distinct waveforms are produced; bow waves and stern waves. Thus, any value of θ whose corresponding value of $C_p = V \cos \theta$ is above the critical speed will produce two waves which will each propagate from the generation site at their own group speeds.

As shown in Figure 9, a group of waves generated by a load when it was at $x = X$ can now be found at:

$$x = X - C_g t \cos \theta \qquad (3\text{-}3)$$

$$y = C_g t \sin \theta \qquad t = X/V \qquad (3\text{-}4)$$

Multiple X locations contribute to each constant phase line, crests and troughs being examples of such a line. For any particular line:

$$\frac{dy}{dx} = \frac{\cos\theta}{\sin\theta} \qquad (3\text{-}5)$$

but

$$\frac{dy}{dx} = \frac{dy/d\theta}{dx/d\theta} \qquad (3\text{-}6)$$

Differentiation of 3-3 and 3-4 gives

$$\frac{dy}{d\theta} = \frac{C_g X}{V} \cos\theta + \frac{\sin\theta}{V} \left[C_g \frac{dX}{d\theta} + X \frac{dC_g}{d\theta} \right] \qquad (3\text{-}7)$$

$$\frac{dx}{d\theta} = \frac{dX}{d\theta} + \frac{C_g X}{V} \sin\theta - \frac{\cos\theta}{V} \left[C_g \frac{dX}{d\theta} + X \frac{dC_g}{d\theta} \right] \qquad (3\text{-}8)$$

Substitution back into 3-5 gives:

$$\frac{\cos\theta}{\sin\theta} = \frac{\frac{C_g X}{V} \cos\theta + \frac{\sin\theta}{V} \left[C_g \frac{dX}{d\theta} + X \frac{dC_g}{d\theta} \right]}{\frac{dX}{d\theta} + \frac{C_g X}{V} \sin\theta - \frac{\cos\theta}{V} \left[C_g \frac{dX}{d\theta} + X \frac{dC_g}{d\theta} \right]} \qquad (3\text{-}9)$$

This reduces to

$$\frac{dX}{d\theta} = \frac{\frac{dC_g}{d\theta} X}{V \cos\theta - C_g} \qquad (3\text{-}10)$$

By inserting values for C_g and $dC_g/d\theta$ into Equation 3-10 and integrating, values of X in terms of θ can be found. Once X is known, x and y coordinates along a crest or trough can be found using Equations 3-3 and 3-4.

A check on this method can be made by inserting the group speed for open water waves to see if the well known Kelvin wedge results.

For open water (deep)

$$C_g = C_p/2 = V\cos\theta/2 \qquad (3\text{-}11)$$

$$\frac{dC_g}{d\theta} = \frac{-V\sin\theta}{2} \qquad (3\text{-}12)$$

Substitution into Equation 3-10 gives:

$$\frac{dX}{d\theta} = \frac{-V/2\ \sin\theta\ X}{V\cos - V\cos\theta/2}$$

$$= \frac{-V/2\ \sin\theta\ X}{V/2\ \cos\theta}$$

$$\frac{dX}{d\theta} = -\tan\theta\ X \qquad (3\text{-}13)$$

Integration yields:

$$X = X_o \cos\theta \qquad (3\text{-}14)$$

Substitution into 3-3 and 3-4 gives:

$$x = X_o \cos\theta \left(1 - \frac{\cos^2\theta}{2}\right) \qquad (3\text{-}15)$$

$$y = X_o \frac{\sin\theta \cos^2\theta}{2} \qquad (3\text{-}16)$$

Picking a value of $X_o = 10$ results in Figure 10 which is the Kelvin wedge as expected. Different values of X change the size of the pattern but the same shape results.

3.3.2 Sheet Inertia Effect

Hinchey (1987) used Lighthill's general formulation to predict wave patterns in a floating ice sheet. To do this, he required C_g and $dC_g/d\theta$ for waves in a floating ice sheet where:

$$C_g = C_p + k \frac{\partial C_p}{\partial k} \qquad (3\text{-}17)$$

C_g can be determined using Equation 3-17 once C_p and $\partial C_p/\partial k$ are known.

The general equation for phase speed of waves in a floating elastic plate is given by:

$$C_p^2 = \frac{1}{k^2} \frac{(Dk^4/\rho_w + g) \; k \; \text{Tanh} \; kH}{(1 + \sigma/\rho_w \; k \; \text{Tanh} \; kH)} \qquad (3\text{-}18)$$

In the deep water limit as $H \to \infty$, Tanh $kH \to 1$, and Equation 3-18 reduces to:

$$C_p^2 = \frac{Dk^4/\rho_w + g}{k \; (1 + \frac{\sigma}{\rho_w} k)} \qquad (3\text{-}19)$$

σ is the ice sheet density and is defined as mass per unit surface area. At this point, Hinchey assumes the sheet to be thin and sets σ to 0 which basically ignores the inertia of the ice sheet. Since $\sigma = \rho_i h$, it follows that as h becomes small, σ also becomes small, as $h \to 0$, $\sigma \to 0$.

This reduces Equation 3-19 further to:

$$C_p^2 = \frac{Dk^3}{\rho_w} + \frac{g}{k} \qquad (3\text{-}20)$$

Equation 3-20 is the dispersion relationship for a thin plate floating on deep water. There is a minimum value of C_p which occurs at a certain value of k. This minimum phase speed corresponds to the critical speed for generation of waves in the ice sheet. Below this speed, no waves are formed and, above it, a certain C_p will have two corresponding k values. One of the k values is the wave number for the bow wave and the other is the wave number for the stern wave.

The critical speed can be determined by differentiating C_p with respect to k and setting the result to zero. The result will be the k value which corresponds to C_{pmin}. Inserting this k value back into Equation 3-20 will yield the critical speed (C_{pmin}).

Hinchey used Equation 3-17 to determine C_g and differentiated the result with respect to θ to obtain $dC_g/d\theta$. C_g and $dC_g/d\theta$ for the thin plate were then inserted into Equation 3-10 which was subsequently integrated numerically to give values of X in terms of θ. From this, the x and y coordinates which correspond to a constant phase line were determined. Figure 11 shows wave patterns produced using this method.

A similar analysis to that of Hinchey's was carried out to

determine the effect of assuming $\sigma = 0$. In this formulation, the water is again assumed to be deep, and this yields Equation 3-19 as before. At this point, however, the assumption that $\sigma = 0$ is not made. Since $\sigma = \rho_i h$ and $\rho_i/\rho_w = .9$:

$$\frac{\sigma}{\rho_w} = \frac{\rho_i}{\rho_w} h = .9h$$

This reduces Equation 3-19 to:

$$C_p^2 = \frac{\frac{Dk^4}{\rho_w} + g}{k + .9h\,k^2} \qquad (3\text{-}21)$$

C_{pmin} can be determined from Equation 3-21 as can V_{cr}.

Equation 3-21 can be used to determine wave numbers for bow and stern waves for values of C_p greater than V_{cr}. Values of C_g and $dC_g/d\theta$ were determined using Equations 3-17 and 3-21. These values were substituted into Equation 3-10 which was then numerically integrated to give X in terms of θ. From these values, wave patterns were plotted. Figure 12 shows wave patterns for various speeds produced using this formulation.

As can be seen from comparing the two sets of plots, the assumption that $\sigma = 0$ appears to have very little effect on the wave patterns produced. This result was not surprising, since Hinchey (1987) determined that assuming $\sigma = 0$ had only a small effect on the wavelength of the waves produced.

To further check on this finding, critical speeds were calculated using both models for a series of sheet thicknesses. It was found that the assumption that $\sigma = 0$ had only a small effect on the critical speed obtained. The thin sheet model yielded critical speeds a maximum of 2% higher than the inertia model for sheet thicknesses up to 2.5 m. As can be seen in Figure 13, the inertia model and the thin sheet model yield an almost identical critical speed versus ice thickness plot. For comparison purposes, Nevel's deep water results are also plotted on the same chart. As can be seen, the models presented here give the same critical speed as determined by Nevel, although the approach is very different.

3.3.3 Depth Effect

The analysis with inertia included was done in an effort to make the problem as general as possible. In Hinchey's analysis, the dispersion relationship was differentiated manually to obtain C_g and $dC_g/d\theta$. The assumption of deep water

and a thin sheet simplified the dispersion relationship and aided in this analysis. In the analysis which included inertia effects, the dispersion relationship had several extra terms and manual differentiation was much more involved, and so it was decided to switch to numerical differentiation. Once this was done and the wave patterns for a thin sheet and a sheet with inertia (both floating on deep water) were compared, it became obvious that the deep water limitation was no longer required. With numerical techniques being employed, the more complex general dispersion relationship (Equation 3-18) could now be used and the effect of water depth could also be studied.

This final analysis using the general dispersion relationship for an elastic plate floating on water turned out to be the most useful. Using this analysis, the two previous analyses could also be studied by setting appropriate values to parameters in the dispersion relationship.

Finite depth has the effect of creating a shadow zone behind the load where no waves are present. Figure 14 is a plot showing this shadow zone.

3.3.4 Membrane Model

The study of critical speed phenomenon is not recent and is not restricted to floating ice sheets. Critical speeds related to rails, beam and membranes have been studied for many years. Lamb, in his text originally published in 1897, studied waves generated in open water by a uniform disturbance travelling over the water. This critical speed is related to surface tension which acts like a membrane stretched over the surface of the water. The dispersion relationship for waves in a membrane on water is:

$$C_p^2 = \frac{Tk}{\rho_w} + \frac{g}{k} \qquad (3\text{-}22)$$

T = surface tension

Using Equation 3-22 and the same general formulation as in the previous analyses, wave patterns for a membrane were determined. These can be seen in Figure 15. They compare favourably with patterns produced by Lamb (1945).

3.4 Discussion

From comparing the wave patterns for the sheet with inertia and the thin plate, it seems reasonable to assume the thin plate

model is valid since it yielded the same result as the sheet with inertia. The simpler mathematics of the thin plate model make it easier to use although, as mentioned in 3.3.4, the use of numerical techniques eliminates this problem.

As can be seen by comparing the various models, they all result in a stern wave which resembles the Kelvin wedge when speeds are much greater than the critical speed. This is due to the fact that the long wavelength stern waves are gravity dominated in all of the models.

The wave patterns presented in this thesis, although generated in a different way, agree fairly well with those predicted by Davys et al. The wave patterns presented by Davys et al, however, seem to show the bow waves and stern waves of similar wavelength even at speeds over twice the critical speed. In actuality, however, at these speeds, the bow wave tends to be compressed and have a significantly shorter wavelength than the stern wave.

The wave patterns presented by Shinbrot (1983) at first appeared to be very different than those presented in this thesis. However, a closer look revealed similar stern waves. The bow waves were also similar except Shinbrot's bend in the opposite direction, and actually bend ahead of the load in contrast to the bent back bow waves revealed in our research.

CHAPTER 4 OBJECTIVES OF THE EXPERIMENTS

The main objective of the experimental work carried out was to obtain a better understanding of the generation of waves in floating ice sheets induced by moving loads. Of concern was not just the speed at which maximum wave generation occurred but also the geometric shape of wave patterns produced in the ice sheet. The wave patterns here refer to the wave crest patterns as observed from above.

Most researchers (Wilson, Anderson, Eyre and Beltaos) have simply measured deflection of the ice sheet (by various means) at a single point as the load passed. This was repeated for various speeds and the main result was a wave amplitude versus speed plot, as well as wave length information. Beltaos also made strain measurements as did Davys, Hosking and Sneyd. Eyre made use of a vibration transducer in some of his tests. All of these tests resulted in valuable information about the critical speed phenomenon; however, none gave any indication of the actual shape of the generated wave patterns.

Until very recently, there has been no work done on the actual wave patterns produced by moving loads. Shinbrot and Davys et al both make theoretical predictions of the wave patterns generated, but their results are conflicting. One major

objective of the experiments described was to determine the wave patterns generated in a floating ice sheet induced by a moving load. The objective was to determine the wave patterns by instrumenting a model ice sheet and actually measuring the wave patterns by comparing deflections at various points on the sheet, measured simultaneously. In some cases, photographs of the wave patterns were also taken.

For comparison purposes, open water wave patterns were also observed and photographed. Waves in open water exhibit a critical speed the same way they do in ice sheets. Below a certain speed, no waves are produced in water by a moving pressure disturbance. This critical speed effect is a result of surface tension in open water. This speed is very low in comparison to the critical speed in floating ice sheets; however, wave patterns for similar V/V_{cr} can be compared for open water and floating ice sheets. Surface tension acts like a membrane stretched over the water surface. It has been suggested (Hinchey) that it may be possible to model ice as a membrane and, if this was a correct assumption, the wave patterns for open water should be similar to those found in ice sheets. In this analysis, thicker ice sheets would correspond to membranes with higher tension.

Another objective was to study the relationship between towing

resistance and speed for loads moving over floating ice sheets. The purpose of this was to study the energy being put into the ice sheet water system by the moving load in an attempt to balance it with the energy carried away from the load by waves. It has been postulated that, at the critical speed, the speed of the energy being taken away by waves is equivalent to the vehicle speed and, thus, no energy can escape. This energy trap would result in a very high towing resistance for loads travelling at the critical speed.

In addition to these objectives, a general study of the critical speed phenomenon was carried out. Multiple deflection sensors were used to give amplitude and wavelength data for comparison with earlier researchers' results.

A final objective of the experimental work was to obtain a better understanding of the mechanism of high speed air cushion vehicle ice breaking. Various air cushion vehicle models was towed over ice sheets at a variety of speeds in an attempt to determine the most favourable conditions for this phenomenon to occur. Careful observations were made of the ice sheet in an attempt to see where the ice failed initially and also how cracks propagated once formed.

CHAPTER 5 EXPERIMENTAL WORK

5.1 General

Several different sets of experiments were carried out during the course of work on this project. The moving load was modelled in a variety of ways ranging from a simple downward acting air jet, to single and double tires, a roller and, finally, some simple air cushion vehicles. The testing was carried out at two locations, the National Research Council's Institute for Marine Dynamics' recently opened ice tank, and Memorial University's Wave/Towing Tank facility. At the MUN wave tank, testing was done over open water, or with the ice sheet modelled by styrofoam and plastic sheets. At IMD, the ice sheets were frozen to thicknesses as required.

5.2 Tank Facilities

5.2.1 Memorial University's Wave/Towing Tank Facility

The MUN wave/towing tank facility is located in the basement of the S.J. Carew Building and is operated by the Department of Ocean Engineering. The tank is a reinforced concrete structure with a length of 58 m, a width of 4.5 m and a depth of 3 m.

For the tests carried out on this project, the water depth was 1.83 m (6 ft.). The wave board and hydraulic actuator which drive it are installed at one end of the tank, and a parabolic beach is installed at the opposite end. These features restrict the actual operating length of the tank to approximately 50 m. The wave/towing tank also has a fully equipped control room which contains a complete range of data acquisition and analysis equipment. Another important feature of the facility is the towing carriage. It has a net weight of 3.9 tonnes and is capable of speeds up to 5.0 m/s.

5.2.2 IMD Ice Tank

The Institute for Marine Dynamics is located next to the S.J. Carew Building on the campus of Memorial University in St. John's. The new IMD ice model basin is a world class facility. It has a usable ice sheet size of 76 m by 12 m and a tank depth of 3 m. These dimensions make it the largest ice model basin in the world today.

A 15 m setup area which houses the towing carriage is located at one end of the tank. It is separated from the tank by a thermal barrier door. The opposite end has a ramp leading into an insulated melt pit. The remains of an ice sheet are pushed into this pit by a service carriage and allowed to melt while

the next sheet is growing. The tank was designed with sufficient corrosion resistance to handle saline ice but, presently, EG/AD/S ice (Timco; 1986) is being used.

The facility has a very sophisticated refrigeration system comprised of computer-controlled two-stage mechanical compression utilizing ammonia as the working fluid. Along with compressor capacity, evaporator pressures and fan speeds are also computer controlled to ensure uniform temperature distribution near the water surface. The air temperature can be controlled from +15°C down to -30°C and ice thicknesses up to 15 cm have been achieved. A separate chiller system is used to initially cool the water. Rejected heat from the system is reclaimed for ice melting in the melt pit, perimeter tank wall heating for ice sheet release and domestic water pre-heating.

The towing carriage is 14 m long and weighs 80 tonnes. It has two speed ranges with a maximum speed of 4.0 m/s in its high range. The model test bay has a test frame which is adjustable vertically and horizontally to accommodate a variety of testing situations.

5.3 Air Cushion Vehicle Model Tests at IMD

5.3.1 General

Several series of tests were carried out at IMD's ice basin with the ACV being modelled in three different ways: an air cell, a simple downward acting air jet and, finally, a pneumatic tube model. All models were towed over the ice sheets at various speeds. The air cell model was instrumented in an attempt to measure its towing resistance. Attempts were also made to observe and photograph waves generated by the air cell model. The downward acting air jet was used to give an unobstructed view of the sheet in an attempt to better observe and photograph the waves it generated.

The more advanced pneumatic tube model was used in towing resistance tests. This ACV model was also used to break ice while operating in the high speed mode (velocities in the range of the critical velocity).

5.3.2 Ice Sheet Properties

In order to scale down the strength properties of the ice sheets, several dopants have been added to the tank water. As mentioned in section 5.2.2, EG/AD/S model ice is used in the

IMD ice basin. Information on the mechanical properties of this ice can be found in Timco (1986).

The normal procedure for making an ice sheet consists of cooling the air in the tank to about -20°C (which supercools the tank water) and seeding. Seeding consists of spraying a very fine mist into the atmosphere above the supercooled tank water. These very fine droplets freeze and fall into the tank water and act as nuclei which results in an initial layer which is very fine grained. Below this very fine and very thin top layer, the ice grows down in columnar grains to the desired sheet thickness.

The top layer produced by seeding has a high porosity, and when thin sheets are used (as in our tests), deflections tend to cause flooding of the sheet. In an effort to overcome this problem, sheets were grown without seeding. With the absence of seeding, the rate of nucleation was much slower and the result was a much larger grained top layer. Also, at slow growth rates of these grains, the dopants could more effectively be rejected by the ice. The resulting top layer obtained was very coarse grained with no porosity and almost no dopants present. This top layer, approximately 2 mm thick, was much like natural ice. The ice below this top layer was typical EG/AD/S ice.

A typical day of testing at IMD consisted of several hours of testing. During this time, the properties of the ice would change for a variety of reasons. For example, the ice would continue to grow from its original thickness, and also tempering would occur since testing was done at a temperature higher than the temperature at which the sheet was formed.

Even though much testing has been done on the mechanical properties of EG/AD/S model ice, it was all done on seeded sheets, and thus the results were not applicable to these unseeded sheets. These unseeded ice sheets were unfamiliar to the IMD staff.

Because these unseeded sheets were basically composites of natural ice and model ice and because the properties tended to change throughout the course of testing (as did thickness), it was difficult to determine values for elastic modulus needed to calculate critical speed for comparison purposes.

Critical speeds found in testing did turn out to be in the range of those calculated but the amount of uncertainty involved in determining mechanical properties makes it difficult to make any definitive statements.

5.3.3 Air Cushion Vehicle Models and Experimental Procedures

5.3.3.1 Truncated Cone Air Cell

The first ACV model used was a simple truncated cone air cell. The cell was 30.5 cm in diameter at the top with a taper of 15°. The cell was 10 cm high. The top of the cell was made of plywood, and the skirt was made of nylon. Air was supplied to the cell by a Spencer vortex blower. It had an input power of 2.2 kw, a maximum volume of 160 cfm and an maximum operating pressure of 65" H_2O. Since the fan had an output in excess of the requirements of the cell, an arrangement of valves was used which enabled excess air to be blown off. Figure 16 shows the arrangement of the cell with the fan and valves. Valve #1 allowed air to be blown off while valve #2 controlled the amount of air which entered the cell. The cell was instrumented with a pressure transducer to monitor cushion pressure, but when it failed an inclined manometer was used in its place. An attempt was made to measure the towing resistance between the cell and the ice sheet; however, resulting resistances were too low to measure with the load cell used. The cell was attached to the 38 mm pipe with standard ABS threaded fittings so it could be attached by simply screwing it on. Initial testing of the cell showed premature failure of the sheet caused by the concentrated

central air jet; however, the addition of a diffuser solved this problem. This model was towed at various speeds, and attempts were made to observe and photograph wave patterns generated in the ice sheet.

5.3.3.2 Air Jet

A similar set of tests were carried out except with the air cell removed from the 38 mm pipe. For these tests, the ACV was modelled by the pressure disturbance caused by the downward acting air jet. This downward acting air jet is the simplest model for an ACV. The results are presented and discussed in Sections 5.3.4 and 5.3.5.

5.3.3.3 Pneumatic Tube Model

While the air cell model and the downward acting air jet worked well, these models were not suited to towing resistance tests. For the towing resistance tests, a new and more advanced ACV model was constructed. The model was as seen in Figure 17. For the skirt of this model, a pneumatic tube was used. The central hole in the tube was blocked with a disk of styrofoam, and weight was added to the model as shown. Pressure in the tube skirt was independent of cushion pressure. Air was put into the tube, and the amount remained constant. The tube had

very low pressure, slightly above atmosphere. Air was introduced through a central hole in the styrofoam, and pressure built up until the model rose allowing air to leak under the skirt. The model had very good stability and, with the high pressure fan used, it was capable of hovering with loads up to 300 N on smooth floors. Much lower loads were used during resistance tests.

The fan and valve arrangement used for the air cell was also used for this model (see Figure 16). The only difference was that the 38 mm rigid plastic pipe from valve #2 to the air cell was replaced by a flexible plastic hose to the pneumatic tube ACV model. This was required since the pneumatic tube model had to be free to heave in towing resistance tests. The output of the load cell was recorded on the H/P FM recorder.

The total mass of the model as it was towed over the ice was 5.0 kg.

During the resistance tests, two video cameras recorded the events, one from the front and one from the side. This model was also used to break ice in the high speed mode.

In an attempt to determine the open water hump speed of the model, a set of resistance tests were carried out at the MUN

wave/towing tank on January 26, 1987. These tests did not yield any useful results due to instability of the model in open water. While the model hovered very well on smooth floors and ice sheets, it did not hover well in water. Excessive air leakage was experienced under the skirt since the skirt did not deflate (and reseal itself) when leaks were encountered. Because of the model's instability, towing it resulted in water flooding over the model and, thus, since it was not behaving like a hovercraft, the results were useless.

Due to the test failure, the hump speed had to be estimated. According to Lamb (1945), the hump speed occurs when the generated waves have a wavelength equal to two vehicle lengths. Since the vehicle length (cushion length) is 37 cm, the wavelength of waves at the hump speed will be 74 cm. This coincides with a wave number (k) of 8.491 m^{-1}. The speed corresponding to this wave number is determined using the following dispersion relationship:

$$c_p^2 = \frac{g \ \text{Tanh} \ kH}{k} \qquad (5\text{-}1)$$

For deep water as $H \to \infty$, Tanh $kH \to 1$. Thus

$$c_p^2 = g/k \qquad (5\text{-}2)$$

For $k = 8.491\ m^{-1}$ $C_p = 1.075$ m/s

The estimated open water hump speed is 1.075 m/s.

A check on this method was made using test results from LeCourt et al (1975). The cushion length of this model was 1.237 m, corresponding to a wavelength of 2.475 m and a wave number k of $2.539\ m^{-1}$. The corresponding open water hump speed was calculated to be 1.966 m/s. This compares very favourably with the open water hump speed of the model determined experimentally to be 2.09 m/s, a difference of only 6%. Based on this, the calculated open water hump speed of the pneumatic tube model (1.075 m/s) seems to be a reasonable estimate.

5.3.4 Results of Experiments

5.3.4.1 General

Air Cushion Vehicles were modelled in various ways during testing at IMD. While much useful data was acquired, both numerical and photographic, actual observations of the testing also provided a better understanding of the phenomenon. Wave patterns were photographed using the air jet model. Resistance data was obtained by towing the pneumatic tube model.

5.3.4.2 Truncated Cone Air Cell

As discussed in Section 5.3.3.1, problems were encountered with the air cell model. The problem of premature sheet failure caused by the concentrated central air jet was overcome by the addition of a diffuser. When instrumentation problems persisted, the instrumentation was abandoned, and test runs were made in an attempt to observe and photograph waves generated in the ice sheet. After several runs, it became obvious that photographing these wave patterns would be more difficult than had been anticipated. Although no waves were visible in the sheet during constant speed runs, a large amplitude (7 - 10 cm) stern wave was generated on deceleration from 4 m/s. This wave caused the ice sheet to fail. This test was repeated yielding the same result.

5.3.4.3 Air Jet Model

At this point in testing, it was decided to remove the air cell, leaving only the 38 mm pipe. The result was a small downward-acting air jet, the simplest possible model of an ACV. The removal of the air cell gave an unobstructed view of the sheet, and it was hoped that this would aid in observing and photographing waves in the sheet. Also, with the large air supply used, the ability was now there to induce larger forces

due to the small area of the jet. It was hoped that the resulting larger deflections would make the wave patterns more visible. On June 24, 1986, several runs were made at various speeds up to 4 m/s, with both video and still pictures taken from various angles. When viewed from behind at low angles, a bowl-shaped depression could be seen in the ice under the air jet when the fan was turned on. As the carriage accelerated to 4 m/s, a transition was observed as the bowl-shaped depression grew out into what appeared to be a wave. Since the wave was moving away from the point of observation, it was difficult to define its shape. The wave could not be seen from the carriage since the available points of observation were above the air jet. Although these tests showed signs of waves in the ice sheet, the wave patterns could not be well defined.

A series of similar tests was run a month later. Knowledge gained in the earlier tests and in the open water tests aided in the setting up of these tests. Since the waves appeared to be best seen from low angles, an attachment was fabricated which enabled a camera to be mounted on the carriage close to the ice. This setup also eliminated the problem of the waves moving away from the point of observation. The additional fact that the waves are fixed relative the load (which moved at the same speed as the camera) also aided in photography. This setup provided the first good photographs of the waves

generated in the ice sheet. Figure 18 shows a typical result. The photograph was taken from a point directly in front of the air jet. The bowed back bow wave can be seen travelling in front of the air jet. The absence of a stern wave in the photograph is attributed to its long wavelength in comparison to its amplitude which makes it hard to see and thus hard to photograph.

5.3.4.4 Pneumatic Tube Model

Two series of towing resistance tests were carried out on December 30, 1986 and January 2, 1987 at IMD. A series of tests was attempted on December 29, 1986, but a premature sheet failure forced an early halt to testing. The December 29, 1986 sheet was a seeded sheet and, as a result, had properties of the EG/AD/S model ice. This type of ice has high porosity, and this caused the ice to flood when deflections were encountered. Because of the low strength, the ice could not support the 5 kg model (even under static conditions). The remaining two days of testing were done on unseeded ice sheets. These sheets were much stronger and did not have the porosity problems encountered with the seeded sheet. As mentioned in Section 5.3.2, these sheets were much like natural ice.

The December 30, 1986 resistance tests were conducted without any problems being encountered. Resistances were recorded for a series of towing speeds, and this data is seen in Table 5 and is plotted in Figure 19. The ice thickness was 12 - 13 mm, and no waves could be seen in the ice sheet. The ice sheet was not damaged during these tests.

A similar series of resistance tests was carried out on January 2, 1987 except the ice sheet thickness this time was only 8 - 9 mm. The thinner ice sheet was deflected much more by the model and waves could be seen in the sheet during some tests. At speeds near the critical speed, the amplitudes of the waves were maximum and cracking occurred in the sheet. The presence of waves could be seen on the video tapes of the tests. Because cracking was encountered, to continue testing, the entire sheet had to be utilized. In some cases, the ice failed at one end of the tank only, and successive runs were shorter, and they were run only over the remaining intact portions of the sheet. The model was also moved to the two quarter points of the tank to maximize the number of test runs. The results of these resistance tests can be seen in Table 6. The results are also plotted in Figure 20.

There was an interesting occurrence at the end of this series of testing. A final run was done at what was estimated (based

on the day's testing) to be the critical speed for the ice sheet (1.75 m/s). At previous tests at speeds just above this, waves could be seen in the sheet (and were filmed on video) and cracking occurred. In this final run as the model reached test speed, bowed back bow waves were observed in the sheet immediately. These bow waves grew in amplitude as the test continued. The waves continued to grow in amplitude and, after about 15 m had been covered, cracks started to appear in the ice sheet. The cracks propagated along the bowed back bow waves. The amplitude of the waves grew further still until, at about 20 m into the test, there was a sudden and massive failure of the ice sheet. The model broke through the ice and, since it wasn't free to surge (since it was towed by the carriage at constant speed), the model continued but the pneumatic tube skirt hooked in the ice and was dislodged from the remainder of the model. The plot of resistance against time for that test is given in Figure 21, and it shows a continual increase in resistance up to the point of failure.

5.3.5 Comments

The IMD tests were quite extensive and much useful data was obtained. For the first time, the actual shape of a wave pattern generated in an ice sheet by a moving load was determined. This bowed back bow wave photographed agreed with

the predictions made earlier in this thesis, and with those made by Davys et al (1985). It shows that Shinbrot (1983) appears to have the bow wave pointing in the wrong direction in his predictions.

The towing resistance tests carried out with the pneumatic tube model gave results as expected. The resistance increased with speed to a maximum and dropped off at higher speeds. As expected, it gave a curve of similar shape to a deflection versus speed curve. Also, the tests carried out on the thinner sheet produced a point of maximum resistance at a lower speed. This too would be expected since the thinner sheet would have a lower critical speed. The thin sheet also resulted in larger deflections and towing resistance.

The ice failure caused by the pneumatic tube model being towed at the critical speed also gave interesting results. It appeared from observations of the test (and review of video tapes) that the wave amplitude grew as the test progressed. This, coupled with the resistance data which showed a continual rise to the point of failure, appears to backup the energy trap hypothesis. Since the energy was travelling at the same speed as the model, it could not propagate away from the load and the increased amplitude resulted, which also led to increased towing resistance. A comparison of energy input (towing

resistance) to energy output (wave generation) was not possible since the ice sheet was not instrumented and no wave amplitude or frequency data was obtained.

Another important observation made during this test was the manner in which the ice sheet failed. The initial cracking in the sheet appeared to be a circumferential crack in front of the load which followed along the crest of the bow wave.

Although the IMD tests provided many good results, they also showed the need for more testing. The thinnest ice sheet which could be grown had a critical speed near 2 m/s, and with a maximum carriage speed of 4 m/s, testing was limited to speeds only twice the critical speed. This was a drawback but the fragility of the very thin ice sheets proved a bigger drawback. Several days of testing had to be cut short when the ice sheets were broken.

Also, as is a problem whenever testing with ice, the properties of the ice sheet changed as testing progressed. Since testing sometimes continued for several hours, the ice sheet would continue to grow, sometimes to a thickness 40% greater than when testing started. This made comparisons of expected critical speed with observed critical speed difficult.

5.4 Styrofoam Sheet Experiment

5.4.1 General

The styrofoam sheet experiment was carried out in the MUN wave/towing tank. During these tests, three different loads were towed over a floating sheet of styrofoam. The loads were a single tire (pneumatic tube) with a downward force of 58 N (13 lb), two tires, towed one behind the other, with a total combined force of 116 N (26 lb) downward and a 28 cm diameter roller which spanned the width of the sheet. The single and two-tire models can be seen in Figure 22, while the roller can be seen in Figure 23. Sheet deflections were measured at several locations simultaneously for the single and two tire tests. The roller, because it spanned the total width of the sheet, basically reduced the problem to one of two dimensions and thus deflection was only measured at one point. A load cell was used to measure towing resistance.

5.4.2 Styrofoam Sheet

The overall size of the styrofoam sheet used was 30 m by 4.27 m by 3.175 cm thick. Ideally, to ensure continuity throughout the sheet, it should consist of one continuous piece of styrofoam. Unfortunately, reality did not allow this, and

commercially available sizes of styrofoam limited the sheet to 4.27 m by 1.22 m (14 ft by 4 ft) pieces. A construction technique was devised in an effort to reduce discontinuities in the sheet to a minimum. Butt joints were ruled out because of the discontinuities they would produce. Each section of the sheet was constructed using two pieces of styrofoam 4.27 m by 1.22 m by 1.59 cm (14 ft by 4 ft by 0.625 in) glued together to produce the total thickness of 3.175 cm (1.25 in). The two pieces were offset before they were glued together as shown in Figure 24.

This produced a lap joint which increased glue area of one panel to the next and eliminated butt joints. There was still concern that discontinuities would result from this joint. Since at every 1.22 m (4 ft) there was a discontinuity where layers of the sheet butted together, it was decided to add several more cuts to the sheet in an orderly pattern in both directions. This, in fact, would mean the sheet had uniformly distributed discontinuities which approximates a continuous sheet, although with less flexural rigidity. The cuts were 3/4 the thickness of each layer and staggered in both directions. The distance between the cuts had to be small compared to the wavelength of a wave in the sheet so as not to have an adverse effect on it. It was decided to make the cuts 15.24 cm (6 in) apart since this was small compared to expected wavelengths

around the critical speed (in the order of 1m). The cuts in the sheet were as shown in Figure 25.

The presence of the cuts reduces the flexural rigidity of the sheet. The sheet will have a flexural rigidity equal to that of an uncut sheet of less thickness. This sheet therefore has an effective thickness which is less than the actual sheet thickness.

To calculate the expected critical velocity the sheet's flexural rigidity is required. To calculate the flexural rigidity, Elastic Modulus, and the sheet thickness, (in this case effective sheet thickness) are required. Samples of the styrofoam sheet were prepared and tested in an Instron (tension/compression) testing machine. The modulus of elasticity was determined to be 13.4 MPa. To obtain the sheet's effective thickness, a static deflection test was done. Knowing the modulus and measuring deflection for a given load, the effective sheet thickness was determined to be 2.60 cm. This seems reasonable since the total sheet thickness is 3.175 cm and the minimum sheet thickness at a cut is 1.98 cm.

Using this information, the flexural rigidity was determined, and the anticipated critical velocity was calculated to be 1.94 m/sec.

The two layers of each section were glued, and the cuts were made. All gluing was done using a glue recommended by the insulation manufacturer. All sections were prepared ahead of time to reduce setup time in the tank to a minimum.

To install and assemble the sheet, the tank was emptied. The sections of the sheet were laid out and arranged properly on the tank floor, and then the lap joints were glued. Once the glue was cured, the tank was refilled floating the sheet. The sheet was attached with mooring lines at both ends of the tank. Small blocks of styrofoam were placed loosely along both sides of the sheet. These blocks stopped lateral movement of the sheet but did not affect its vertical deflection.

5.4.3 Instrumentation

For the tire tests, the sheet was instrumented with six deflection sensors. They were located as seen in Figure 26. Since the wave patterns generated are symmetric with respect to the sheet centerline, it was decided to instrument only half the sheet. In this way, twice the data would be available for plotting wave crest patterns. The deflection sensors were rotating variable potentiometers with an input voltage of ± 5 V. Lines attached to the sheet rode over pulleys as the sheet deflected. A photograph of the deflection sensors in place

with the lines attached to the sheet can be seen in Figure 27. This photograph also shows the arrangement of the cuts which were made in the sheet. As can be seen, the carriage can pass by the sensors and, thus, deflections are measured as the load (towed by the carriage) passes. An output of 1.0 V D.C. corresponds to a sheet deflection of 3.14 cm. The analog outputs of the deflection sensors were recorded on tape on an 8 channel FM recorder (Hewlett-Packard 3968A Instrumentation Recorder). Data was analyzed on a H/P 5420 B digital signal analyzer in conjunction with a H/P 54410A analog/digital converter. In the roller experiments, a single sensor located near the edge of the sheet was used to measure deflection.

A mechanism was fabricated to attach to the carriage to tow the various loads (single tire, two tire, and roller). It was arranged as shown in Figure 28. As can be seen, a load cell was incorporated into the mechanism for measuring the towing resistance of the loads.

5.4.4 Experimental Procedure

Several series of tests were run on the styrofoam sheet. The roller tests were the simplest since they involved only a single deflection sensor. Since the roller extended the width of the sheet, it essentially reduced the problem to one of two dimensions. The roller was towed the length of the sheet at

speeds varying from 1.0 m/s to 4.0 m/s. Towing resistance was recorded as was sheet deflection for all speeds. Tests were repeated to verify results.

The single pneumatic tube was towed the length of the sheet at speeds varying from 1.0 m/s to 5.0 m/s in .5 m/s increments. During these tests, deflections were measured, and a rough estimate of the critical speed for these conditions was determined. These tests were repeated with smaller increments of speed change in the range of the critical speed. During all testing, the loads were accelerated up to test speed quickly to ensure constant speed as the load passed the deflection sensors. This was done to reduce transient effects to a minimum.

A similar series of tests was carried out towing a load consisting of two pneumatic tubes, one behind the other, with a set spacing of 1 m. These tests were carried out to determine the effect of two vehicles travelling in close proximity on the waves produced (amplitude and wavelength). An attempt was made to measure the towing resistance generated by the single tire and two tire models; however, the loads encountered in these tests were below the range that could be measured with the load cell used.

5.4.5 Results of Experiments

5.4.5.1 General

The experiments carried out on the styrofoam sheet were extensive, and a large amount of useful data was obtained. The multiple deflection sensors produced deflection information for various points on the sheet. This was used to produce deflection versus speed graphs which defined the critical speed as well as giving the critical deflection amplification factor (deflection at critical speed divided by static deflection). Wavelength information was also obtained from the deflection data. From wavelength data at various points on the sheet, the overhead wave patterns were determined. Towing resistance data was also obtained.

5.4.5.2 Deflection Data

The output of the deflection sensors was a deflection versus time plot of the type shown in Figure 29. To obtain wavelength information, the time scale must be multiplied by the speed of the test. Deflection data was obtained for three different loads: single pneumatic tube model, two pneumatic tube model, and the roller model. The loads were towed at various speeds with several repeat tests to verify data

obtained. The deflection data for various speeds for the three loads is presented in Table 7. During the roller experiment, only one deflection sensor was used, and the data in Table 7 is from that sensor. During the single tire and two tire tests, six deflection sensors were used. The data in Table 7 for both single and two tire tests is from channel 7 which was located 305 mm (12") from the centreline of the sheet. The load was towed along the centreline. It should also be noted that deflections in Table 7 represent peak to peak deflections or double amplitudes as indicated by ΔY on the deflection plot (Figure 29). Deflection is plotted against load speed for the single tire model in Figure 30, two tire model in Figure 31, and for the roller model in Figure 32.

5.4.5.3 Overhead Wave Patterns

The wave patterns consist of plots of wave crests as viewed from above. The wave patterns presented here are for the single pneumatic tube model rolling up the centreline of the sheet. Since the wave pattern are symmetric about the centreline, the six deflection sensors actually supply us with twelve sets of data to generate the plots. The plots were generated using wavelength information from the deflection sensors. Figure 33 is a plot of deflection against time showing deflections from two adjacent sensors. Important to

note is that the deflections are different, the deflection closer to the load is greater. Of more importance to the determination of wave patterns is the phase difference between the two deflection plots. The absence of a phase difference here would indicate that the wave reached both sensors simultaneously or it was a plane wave perpendicular to the direction of travel of the load. The phase difference indicates that the waye is bent, since it reaches one sensor before it reaches the other. To determine how much the wave is bent, the phase difference in time can be measured and converted to distance by multiplying by the speed of the test. If, for example, this phase difference was 1 sec at a speed of 1 m/s (1 m phase difference) and the sensors were 1 m apart, the wave will be bent at an angle of 45° to the direction of travel.

This type of an analysis was done to obtain the wave patterns for various speeds. Since the digital signal analyzer had only two channels of input and six channels of data were recorded, the channels had to be compared to each other one at a time. Data was recorded on channels 3 through 8. The phase differences were determined from channel 8 to 7, then from 7 to 6, etc. The analysis was done as follows: a series of successive crests were chosen for examination (if possible at least one bow wave and one stern wave). For example, in Figure

33 (2 deflection), four successive crests were chosen. The times corresponding to the crests of both waves were obtained from the digital signal analyzer. This information was recorded in tables, and the phase differences were calculated (in time) and then converted to distance by multiplying by velocity. Once this analysis was carried out on all successive channels, the phase differences (in distances) were known for all sensors. The distance between successive crests can also be determined from this information. This is in fact the wavelength although it varies from one section of the wave pattern to another. The information required to plot the wave patterns is listed in Table 8. The sheet centreline is taken as 0 and, thus, distances to sensors are ± values since wave patterns are symmetric. The leading bow wave on channel 8 is chosen as a 0 point on the centreline axis. Wave patterns for various speeds are presented in Figure 34.

5.4.5.4 Towing Resistance Data

As mentioned previously, resistance data was not obtained for the single tire and two tire models. The roller, however, did produce usable resistance data. The analog output of the load cell was recorded and analyzed using the digital signal analyzer. Plots of towing resistance against time were produced for a series of speeds. Figure 35 is an example of

one of the plots obtained. The towing resistance for the test is taken to be the mean of the data over the time of constant speed. This is the data after the initial high resistance caused by accelerating up to test speed. Table 9 lists the towing resistance of the roller over a series of speeds. Figure 36 is a plot of this data.

5.4.6 Comments

The styrofoam sheet tests produced a large amount and a variety of data. The constant mechanical properties and thickness of the styrofoam sheet made comparisons of various results and comparison of results with predictions much easier. The sheet also lacked the fragility of the ice sheets used at IMD. With instrumentation, including a load cell and multiple deflection sensors, information about sheet deflections, towing resistance and generated wave patterns was obtained.

Comparison of the deflection versus speed plots show a peak on all three (single tire, two tire and roller) which occurs at almost the same speed. This speed was also very close to the calculated critical speed of the styrofoam sheet which was determined to be 1.94 m/s. The maximum deflection for the single tire model occurred at 2.0 m/s and at 2.25 m/s for the two tire model. It should be noted, however, that no

deflection measurements were taken between 2.0 and 2.25 m/s. The maximum deflection for the roller occurred at 1.875 m/s. These three results obtained using vastly different moving loads would seem to indicate that the critical speed is more a function of sheet properties than load properties.

Even though the critical speed of the styrofoam sheet was 2.0 m/s, the higher speed of the MUN Wave/Towing Tank carriage (5 m/s) made it possible to determine wave patterns for speeds up to 2.5 times the critical speed. The strategically located deflection sensors made it possible to determine the shape of generated wave patterns for a variety of speeds. The wave patterns produced (Figure 34) agree quite well with the wave pattern predictions of Chapter 3.

Another interesting result of these tests was the deflection patterns in the sheet at speeds below the critical speed. Many researchers have assumed the depression in the ice sheet to be circular and of constant diameter at speeds below the critical speed. Figure 37 shows that the depression appears circular at very low speeds but, as speeds increase, it changes to an elliptical shape with its long axis perpendicular to the direction of motion. The long axis grew with increasing speed, and the short axis got shorter. At a speed of 1.0 m/s, the depression was about 1.8 m along the direction of motion by

1.5 m across; but, when the load travelled at 1.75 m/s (much closer to V_{cr}), the depression had changed to 1.6 m along the direction of motion and had grown to 3.0 m across. There appeared to be a gradual change from a bowl shape depression to a wave front at the critical speed.

The resistance tests done with the roller show a peak at a speed of 2.0 m/s (the same critical speed determined from deflection data) which seems to give further evidence in support of the notion that the critical speed is a function of sheet properties only.

When the resistance data was first obtained, the fairly high resistance values above the critical speed were unexpected, especially since the deflection data showed small deflections at these speeds. When the resistance of the large roller moving through air was factored out, the result was as seen in Figure 36, which was more as expected.

5.5 Open Water Wave Patterns

5.5.1 General

Researchers have been aware of the existence of a critical speed for waves in open water for many years. In his text,

originally published in 1879, Lamb goes through an analysis of an isolated pressure disturbance advancing over still water. He determined that a minimum wave velocity exists and calculated it to be 23.2 cm/sec with an associated wavelength of λ_m = 1.73 cm. At speeds below this, no waves are generated, and a depression associated with the disturbance follows the load. He determined that, at speeds above the minimum wave speed (critical speed), two distinct waves are produced. One was of short wavelength and had a group speed greater than the speed of the disturbance and preceded it. The other (long wavelength) had a group speed less than the disturbance and trailed it. This critical speed effect is associated with surface tension, which acts like a membrane stretched over the water surface.

Hinchey has postulated that a membrane sheet model may be valid for ice sheets. Here, increased tension in the membrane would represent increased ice thickness. In an attempt to verify Lamb's predictions of open water wave patterns and Hinchey's membrane model, open water wave patterns were determined experimentally in the wave/towing tank of MUN. The membrane model can be checked by comparing the wave patterns generated in open water with those generated in ice at similar V/V_{cr} values.

5.5.2 Experimental Setup and Procedure

These tests were designed to observe and photograph the wave patterns generated in open water by a moving pressure disturbance. Besides obtaining information on wave patterns, these tests were also very useful in aiding in the determination of the most favourable conditions for photographing wave patterns. From these tests, camera angles and lighting conditions which best show wave patterns were determined. This information aided in setting up cameras to photograph waves generated in floating ice sheets at IMD.

The pressure disturbance in these tests was a downward acting air jet, discharged from a brass tube of 5.0 mm inside diameter. The tube was fixed approximately 3 cm above the water surface. The air was supplied from a compressed air bottle, and a pressure regulator was used to avoid pressure fluctuations. The tube and air supply were mounted on the towing carriage at the MUN wave/towing tank and towed at various speeds to determine the critical speed. Since the wave patterns travel with the disturbance, the camera and lighting were attached to the carriage. A series of photographs of the generated wave patterns were taken.

5.5.3 Results of Expermiments

A series of experiments were conducted at the MUN wave/towing tank as described in Section 5.5.2. The results showed that a critical speed does exist for open water. At low speeds, the depression in the water caused by the air jet moved with it. At about 23 - 24 cm/sec, waves started to appear. This was in agreement with Lamb's prediction. In this speed range, the waves were bowed back slightly. There were bow waves which were ahead of the disturbance and stern waves behind it. As the speed increased, the bow waves bowed back more and the wavelength of the bow waves shortened while the wavelength of the stern waves lengthened. As the speed increased, the bow waves became compressed and above 1 m/s they could no longer be observed. Above this speed, the Kelvin wedge was produced behind the load. Some representative results of these tests can be seen as photographs of wave patterns in Figure 38.

5.5.4 Comments

The wave patterns generated in open water tended to agree with the membrane model (surface tension) predictions. The waves were only bowed back slightly at speeds just above the critical speed and bent back more as the speed of the disturbance increased. At speeds much greater than V_{cr}, the Kelvin wedge

wave pattern was produced behind the load. However, there was a discrepancy observed between the predictions and the actual waves produced. In the membrane model predictions, for speeds about four times the critical speed and above, the bow wave bent back and intersected the stern wave. In the tests, the wave patterns produced did not show this intersection. The bow waves always stayed ahead of the stern waves. The predictions for the thin plate and inertia models showed a similar intersection at these high speeds but limitations on carriage speed at IMD and MUN did not allow wave patterns at these speeds (four times V_{cr}) to be studied.

5.6 Polyethylene Sheet Tests

5.6.1 Experimental Setup and Procedure

In an effort to overcome the speed limitations of the MUN facility, a series of preliminary tests were carried out on a 12 mill polyethylene sheet. These tests were done in an effort to observe the more complicated wave patterns generated at higher speeds. The polyethylene sheet was .012 inches (3.05×10^{-4} m) thick and had an elastic modulus of 1.72×10^{8} Pa. Based on these values, the expected critical speed was .503 m/s, which meant much higher speed ratios were possible.

The plastic sheet was 54 inches (1.37 m) by 31 feet (9.5 m) and was draped over a frame fabricated from 2 inch x 4 inch (50 mm x 100 mm) wood. The frame had inside dimensions of 48 inches (1.22 m) by 30 feet (9.1 m). The plastic was allowed to lay on the water, and was stapled to the wooden frame to keep the edges out of the water to prevent sheet flooding. The air jet used in these tests was the same as used in the open water tests. The air jet was towed over the plastic sheet at a series of speeds, and the wave patterns produced were photographed.

5.6.2 Results of Experiment

Some representative photographs of the wave patterns generated in the plastic sheet can be seen in Figure 39. The plastic sheet exhibited a critical speed as expected. At low speeds, no waves were formed and the depression moved with the air jet. At a speed between 0.5 m/s and 0.6 m/s, waves started to appear in the sheet. As the speed increased, the waves tended (as predicted) to bend back more. At speed much greater than V_{cr}, the wave pattern at the reare started to resemble the Kelvin wedge.

5.6.3 Comments

The critical speed observed in the polyethylene sheet was very close to the value predicted. This is further proof that the minimum phase speed for waves determined from the dispersion relationship is a very satisfactory way of determining critical speed. As observed in the open water tests, there was a discrepancy between the predicted and observed wave patterns. The intersection of bow and stern waves at high speed ratios, which is present in the predictions, was not observed during testing. As in the open water tests, the bow waves always stayed ahead of the stern waves and seemed to be guided by them.

It should be noted that the plastic sheet tests were preliminary and only involved a day in total for setup and testing. This is a definite area for future study of generated wave patterns. The patterns produced in the plastic sheet agreed with earlier tests on the styrofoam sheet and with predictions.

CHAPTER 6 SUMMARY AND CONCLUSIONS

This thesis was undertaken primarily as a study of several aspects of the critical speed phenomenon for moving loads over floating ice sheets. Besides large amounts of quantitative data, much was also learned from qualitative observation, made during the tests. Several different moving loads were used ranging from a simple downward-acting air jet, single, two-tire and roller models, to models of Air Cushion Vehicles. Testing was carried out at two locations: the National Research Council's Institute for Marine Dynamics, and Memorial University's Wave/Towing Tank. Ice sheets were frozen at IMD, and a styrofoam sheet was used to model the ice sheet at MUN. Open water tests as well as tests on a polyethylene sheet were also carried out at MUN.

Instrumentation in the form of multiple deflection sensors and and a load cell allowed acquisition of deflection and towing resistance information. The actual wave patterns produced in the styrofoam sheet were also determined from deflection data generated at strategic locations on the sheet.

A series of theoretical models for predicting wave patterns generated in floating ice sheets were presented and the various models were compared. Experimental results were also compared

with these predictions. The observations made and the conclusions reached from the research are as follows:

(1) The thin sheet model and the inertia model yield almost identical results. Critical speeds calculated and wave patterns produced have values within 2%. Critical speeds calculated also agree with Nevel's predictions which were obtained in a completely different manner. This would indicate that the thin sheet model (with its much simpler mathematics) is valid although, as discussed earlier, the use of numerical techniques in the formulation allows the use of the general dispersion relationship which also allows for study of finite depth.

(2) Predictions of wave patterns agree with those presented by Davys et al and are similar to those presented by Shinbrot with the exception that Shinbrot's bow waves are bent in the opposite direction.

(3) IMD tests show a bent back bow wave which agrees with predictions presented in this thesis.

(4) At IMD, a large amplitude stern wave which caused the sheet to fail was generated by the air cell model on deceleration from 4 m/s. Constant speed testing done

with the same model at a series of speeds up to 4 m/s showed no visible waves.

(5) At IMD, resistance curves generated by the pneumatic tube ACV model were as expected. They rose to a maximum resistance and dropped off at higher speeds, similar to deflection versus speed curves.

(6) During a constant speed test at the critical speed at IMD, the sheet was observed to fail initially by cracking in front of the load along the crest of the bow wave. The output of the load cell for this test showed a steady and rapid increase in resistance to the point of failure. The amplitude of waves generated during this test was also observed to grow until the sheet failed.

(7) At MUN, resistance versus speed curves for the three moving loads used in the styrofoam sheet tests yielded a similar critical speed which was also very close to that calculated based on the dispersion relationship. This would seem to indicate that the critical speed is much more a function of sheet properties than load properties.

(8) Wave patterns obtained from the styrofoam sheet tests agree quite well with the wave pattern predictions of this thesis.

(9) Deflection patterns for the styrofoam sheet obtained at speeds below the critical speed show a bowl-shaped depression which is almost circular at very low speed, but, as the speed approaches the critical speed, the pattern becomes elliptical with its long axis perpendicular to the direction of motion. The long axis grew to twice its original length while the other axis actually shortened as speed increased. This is contradictory to some researchers' assumption that the depression stays circular and the same size.

(10) Resistance tests indicated a critical speed for the styrofoam sheet at the same speed as that determined from deflection data.

(11) The open water tests and the polyethylene sheet tests both give further proof that determining the minimum phase speed for waves from the dispersion relationships for surface tension and floating plates, respectively, is a valid way to obtain the critical speed.

(12) The open water tests and the polyethylene sheet tests produced wave patterns which agreed quite well with wave pattern predictions near the critical speed.

Based on the experimental work completed, it is felt that several aspects of the critical speed phenomenon for floating ice sheets require further study:

(1) Methods should be developed which can predict wave amplitudes as well as wave patterns. With amplitude information and wave patterns (including wavelength information), the actual curvature of an ice sheet could be determined. This would allow calculation of stresses and prediction of sheet failures.

(2) Further study of the energy trap hypothesis is required. An attempt should be made to determine wave-induced sheet failure based on vehicle mass.

(3) Since most work has been done on steady state problems, research should be done on loads which accelerate and decelerate.

(4) Vehicles which approach shore should also be studied. The effect of reflection needs study as does the effect of changing water depth.

(5) More work is also required into possible vehicle size effects and the effects of multiple vehicles. Multiple vehicles moving together, approaching each other from opposite directions or overtaking each other should be studied.

(6) A study of the wave patterns at higher speed ratios is another area of possible research. This would most easily be done with tests similar to the plastic sheet tests done as part of this thesis.

References

Assur, A. (1956), "Airfields on Floating Ice Sheets", U.S. Army, SIPRE Report No. 36

Bates, H. and Shapiro, L. (February, 1980), "Long Period Gravity Waves in Ice-Covered Sea", Journal of Geophysical Research, Volume 85, No. C2

Bates, H. and Shapiro, L (September, 1980), "Breaking Ice with Gravity Waves", Journal of Energy Resources Technology, Volume 102

Bates, H. and Shapiro, L. (1981), "Plane Waves in a Viscoelastic Floating Ice Sheet", Journal of Geophysical Research, Volume 86, No. C5

Beltaos, S (1977), "Field Studies on the Response of Floating Ice Sheets to Moving Loads", Alberta Research Council

Carter, D. (1977), "Mathematical Analysis of Ice-Breaking by Air Cushion Platforms", Transport Canada Research and Development Centre, Report No. TP 1238

Cohen, H., and Clayton, A. (1982), "Research into Transport Aspects of Ice Sheets", Civil Engineering Department, University of Manitoba

Davys, J., Hosking, R., and Sneyd, A. (1985), "Waves Due to a Steadily Moving Source on a Floating Ice Plate" , Journal of Fluid Mechanics

Decker, J. (1978), "The Applications of Air Cushion Configurations to Ice-Breaking", U.S. Department of Commerce Report No. MA-RD-940-78058

Dutfield, D.O., and Dickins, D.F. (1974), "Icebreaking Trials with Bell Aerospace Voyageur ACV", Canadian Aeronautics and Space Journal

Eyre, D. (1977), "The Flexural Motions of a Floating Ice Sheet Induced by Moving Vehicles", Journal of Glaciology, Volume 19, No. 81

Greenhill, A. (1887), "Wave Motion in Hydrodynamics", American Journal of Mathematics, Volume IX, pp 62 - 112

Hertz, H. (1884), "About the Equilibrium of a Floating Elastic Plate", Annalen der Physik and Chemie

Hinchey, M. (1986), "High Speed Air Cushion Icebreaking, Membrane Ice Sheet Model"

Hinchey, M.J. (1986), "Floating Ice Roads and Runways: Critical Speed Phenonemon", Canadian Aeronautics and Space Journal, Volume 32, No. 2

Hinchey, M.J. (1987), "Transport Over Floating Ice Sheets", Submitted to OMAE 87, Houston, Texas

Holl, D. (1950), "Dynamic Loads on Thin Plates on Elastic Foundations", Applied Mathematics Symposium of the American Mathematical Society, Volume 3,

Ivanov, K., Kobeko, P. and Shulman, A. (1946), "Deformation of an Ice Cover Under Moving Loads" (In Russian)

Jeffrey, N. and Jones, S. (1986), "Canada's New Institute for Marine Dynamics", International Polar Transportation Conference, Vancouver

Johnson, P. (1981), "Moving Loads on a Floating Ice Sheet", Phil Johnson, P.E., Consulting Engineer, Fairbanks, Alaska

Kerr, A.D. (1975), "The Bearing Capacity of Floating ice Plates Subjected to Static or Quasi-Static Loads", Cold Region Resources and Engineering Laboratory, Hanover, New Hampshire

Kerr, A.D. (1981), "Continuously Supported Beams and Plates Subjected to Moving Loads - A Survey", Solid Mechanics Archive, Volume 6, Issue 4

Kerr, A.D. (1983), "The Critical Velocities of a Load Moving on a Floating Ice Plate that is Subjected to In-Plane Forces", Cold Regions Science and Technology

Kheisin, D. (1967), "Dynamics of Floating Ice Covers" (In Russian)

Lamb, H. (1945), Hydrodynamics, Cambridge University Press, Dover Edition

Landel, D. (1977), "The Application of Air Cushion Technology to Icebreaking - Canadian Experience", Prepared by Air Cushion Vehicle Division, Canadian Coast Guard Report No. 1/77

Lecourt, E. and Kotras, T. (1975), "Model Tests of an Arctic SEV Over Model Ice", Society of Naval Architects and Marine Engineers, Ice Symposium, Montreal

LaFramboise, J. (1979), "Comparative Analysis of Ice-Breaking: Conventional vs Air-Cushion", Transport Canada Research and Development Centre, Canadian Symposium on Air Cushion Technology, Montreal

Lighthill, J. (1978), Waves in Fluids, Cambridge University Press

Livesley, R. (1953), "Some Notes on the Mathematical Theory of a Loaded Elastic Plate Resting on an Elastic Foundation", The Quarterly Journal of Mechanics and Applied Mathematics

Long, R. (1982), "Moving Loads on Floating Ice Sheets", Civil Engineering Department, University of Manitoba

Nevel, D. (1970), "Moving Loads on a Floating Ice Sheet", Cold Regions Research and Engineering Laboratory's, Hanover, New Hampshire

Piszczek, K. (1958), "The Possibility of Dynamic Stability Loss Under Moving Concentrated Loads"

Shinbrot, M. (1980), "A Preliminary Analysis of Dynamic Ice Rupture by Hovercraft", Transport Canada Report No. TP2461

Shinbrot, M. (1983), "A Mathematical Analysis of Dynamic Ice Rupture by Hovercraft", Transport Canada Report No. TP4235E

Squire, V. (1985), "On Deflections and Strains Induced by Loads Moving Over Ice", Scott Polar Research Institute, University of Cambridge, P.O.A.C.

Takizawa, T. (1978), "Deflection of a Floating Ice Sheet Subjected to a Moving Load", Low Temperature Science, Series A, Physical Sciences, ISSN 0439-3538

Timco, G. (At Press), "EG/AD/S: A New Type of ModelIce for Refrigerated Towing Tanks", Cold Regions Science and Technology

Wade, R., Edwards, R. and Kim, J. (1975), "Improvements in Icebreaking by Use of Air Cushion Technology", SNAME Ice Technology Symposium, Montreal

Whitham, G.B. (1974), Linear and Nonlinear Waves, John Wiley & Sons, New York

Whitten, J., Hinchey, M., Hill, B., and Jones, S. (1986), "Some Tests at the Institute for Marine Dynamics on High Speed Hovercraft Icebreaking", International Conference on Air Cushion Technology, Toronto

Wilson, J. (1953), "Coupling Between Moving Loads and Flexural Waves in Floating Ice Sheets", Engineering Research Institute, University of Michigan, Ann Arbor

Table 1. Summary of moving load data Beltaos (1977)

Source	ice thickness (m)	water depth (m)	observed critical speed (m/s)	predicted critical speed[1] (m/s)	amplification at crit. speed for: deflection	total height[2]	strain	Comments
Wilson (1955)	0.61	3.0	6.3	5.5	1.8	2.5	-	-
	0.28	3.5	5.7	5.9	1.4	2.1	-	motion parallel to, & 60 m off, shore
Anderson (1958)	1.37	15.2	14.4	12.2	4.6	-	-	approximate
Eyre (1977)	0.72	36.4 (avg)	≈14.9	13.7	2.1	-	-	-
Writer, Joseph Lake	0.66	1.8	4.9	4.3	2.1	2.3	-	average of two runs 12 & 18 Feb. 1976
	0.37	2.0	4.9	4.5	2.1	3.1	≈1.4	21 Dec. 1976
Writer, Cold Lake 1&2 Feb., 1977	0.59	4.3	7.3	6.4	1.9	2.4	-	
	0.65	11.6	11.0	10.5	1.9	2.5	≈1.4	
	0.64	27.1	13.7	12.9	2.3	3.3	-	obs'd critical speed not as reliable as above
	0.65	54.3	15.2	13.3	2.1	2.3	≈1.4	

[1] using Nevel's theory (1970)

[2] sum of absolute values of max. downward and max. upward deflections

Table 2 Voyageur High Speed Field Trials Dutfield et al (1974)

Date	Location	Ice Thickness (in)	(cm)	Average of Reported Water Depths (ft)	Estimated Critical Speed (mph)	Estimated Observed ACV Speed when Ice was Broken
5 Feb.	Killbear Point	11	(28.5)	114	20	12 mph
6 Feb.	Albert Channel McClelland Rock	12.5	(31.75)	21	17	12 mph
18 Feb.	Snake Island	15	(38)	10	12	12.2*

*Speed was measured accurately

Table 3 SK-5 Model Characteristics

Length Overall:	5.18 ft.
Beam:	3.17 ft.
Weight:	50.5 lbs.
Skirt Height:	0.47 ft.
Cushion Length:	4.06 ft.
Cushion Area:	9.78 ft.^{2}
Cushion Pressure:	5.16 psf
Fan Speed:	2800 rpm

Lecourt et al (1975)

Table 4 SK-5 Model Test Results Lecourt et al (1975)

Test No.	V (fps)	R** (lbs)	h (cm)	σ_f (kg/cm²)	ℓ (cm)	E (kg/cm²)	ω (in)	u_a (cm/sec)	$\frac{u}{u_a}$	$\frac{\ell}{L}$***	$\frac{R}{\Delta}$	$\frac{u}{\sqrt{gL}}$
1	3.87	3.51	0.72	0.653	7.55	91.1	----	110.1	1.071	0.061	0.0695	0.338
2	4.91	3.56	0.80	0.473	6.95	38.8	0.44	105.6	1.417	0.056	0.0685	0.429
3	6.10	2.30	0.88	-----	8.76	93.3	-----	118.6	1.568	0.071	0.0455	0.533
4	5.92	2.65	0.78	0.477	10.62	287.	----	130.6	1.382	0.086	0.0525	0.518
5	5.60	2.40	0.85	0.552	13.39	564.	----	146.6	1.159	0.108	0.0475	0.490
6	5.35	1.83	0.83	0.341	12.43	450.	1.37	141.3	1.154	0.100	0.0363	0.468
7A	5.93	-0.28	2.62	0.163	30.68	522.	0.52	222.0	0.814	0.248	-0.0055	0.519
7B	6.84	1.63	|	|	|	|	1.47	|	0.939	|	0.0323	0.598
7C	7.82	2.09	|	|	|	|	1.54	|	1.074	|	0.0414	0.684
7D	8.75	1.95	|	|	|	|	1.39	|	1.201	|	0.0386	0.765
7E*	6.31	1.86	|	-----	-----	-----	1.18	-----	-----	-----		0.0368	0.552
7F*	7.41	3.22	|	-----	-----	-----	1.83	-----	-----	-----		0.0638	0.648
8A	5.90	3.16	1.72	0.183	20.62	378.	1.40	182.0	0.988	0.167	0.0627	0.516
8B*	5.93	3.82	|	-----	-----	-----	1.84	-----	-----	-----		0.0757	0.519
9	4.86	0.14	1.62	0.230	18.94	321.	0.24	174.4	0.849	0.153	0.0028	0.425
10A	6.81	1.74	1.62	0.369	24.97	969.	1.39	200.3	1.037	0.202	0.0345	0.595
10B	6735	2.10	|	|	|	|	1.60	|	0.967	|	0.0416	0.555
10C*	2.96	-0.91	|	-----	-----	-----	----	-----	-----	-----	-0.0180	0.259
11	5.37	0.64	1.76	0.221	21.49	414.	0.28	185.8	0.881	0.174	0.0127	0.470
12A	6.18	2.20	1.37	0.281	16.26	288.	1.77	161.6	1.166	0.131	0.0436	0.540
13A	5.26	1.39	0.98	0.322	14.26	466.	0.56	151.3	1.059	0.115	0.0275	0.460
19	~5	----	1.20	0.132	14.90	304.	----	154.8	1.016	0.120	-----	0.437
20	~5	----	1.13	0.195	16.71	631.	----	163.9	0.929	0.135	-----	0.437
21	~5	----	1.38	0.175	15.60	192.	----	158.4	1.039	0.126	-----	0.437

* Flying over broken ice sheet.
** Sign convention: Positive is resistance; negative is thrust.
*** L = 123.8 cm.

TABLE 5 HOVERCRAFT RESISTANCE DATA - DECEMBER 30, 1986

Speed (m/s)	Towing Resistance (grams)
1.0	139
1.5	111
1.75	137
2.0	134
2.25	163
2.5	289
2.75	225
3.0	242
3.25	232
3.5	227
3.75	238
4.0	227

TABLE 6 HOVERCRAFT RESISTANCE DATA - JANUARY 2, 1987

Speed (m/s)	Towing Resistance (grams)
1.0	82
1.5	70
1.75	2310 *
2.0	985
2.25	425
2.5	381
4.0	261

* Sheet failure during test.

TABLE 7 STYROFOAM SHEET DEFLECTION DATA (Deflections Cm)

Speed m/s	Single Tire Tests		Two Tire Tests		Roller Tests
	Trial 1	Trial 2	Trial 1	Trial 2	
0.5		1.330		1.204	0.744
1.0	1.598	1.700		1.489	1.142
1.5	2.525	2.454		1.743	1.791
1.75		3.786	2.55	2.675	1.800
1.875					8.362
2.0	5.923	5.879	4.70/ 4.60	4.512/ 4.625	8.067
2.125					6.250
2.25		4.983		5.769	5.142
2.5	4.664	4.343	4.75	4.714/ 4.628	4.296
3.0	3.121	3.082	3.25	3.188	3.871
4.0	1.829	2.001	2.10	2.075	2.326
5.0		1.642			

(Fig. 30) (Fig. 31) (Fig. 32)

TABLE 8 WAVE PATTERN DATA - STYROFOAM SHEET TESTS

		Ch 8 ±7" (178mm)	Ch 7 ±12" (305)	Ch 6 ±24" (610)	Ch 5 ±36"(915)	Ch 4 ±54"(1372)	Ch 3 ±78"(1982)
	B1)	0	1.08	3.86	9.43	24.86	40.92
5 m/s	B2)	27.6	31.57	43.88	65.72	99.77	133.94
	S3)	201.7	202.51	202.92	253.33	304.25	359.64
	B1)	0	0.756	0.82	6.51	12.52	19.72
4 m/s	B2)	27.76	27.965	28.5	33.07	45.67	67.72
	B3)	54.11	56.9	67.09	79.06	110.11	158.71
	B1)	0	0.69	0.47	3.55	7.39	6.26
3 m/s	B2)	33.17	33.17	34.71	34.71	44.52	56.96
	B3)	65.07	66.68	73.34	85.89	98.96	124.44
	S1)	185.54	186.0	184.62	178.12	178.12	232.11
	B1)	0	0*	0*	4.28	13.96	15.27
2.5 m/s	B2)	39.73	38.74	37.46	44.24	60.38	72.19
	B3)	79.98	80.91	84.9	91.29	93.88	140.94
	S1)	192.43	192.43	192.15	189.76	201.67	210.05
	B1)	0	0.27	-1.88	0.61	1.24	12.54
2.25 m/s	B2)	42.26	42.8	47.82	54.28	61.28	77.44
	S1)	136.13	136.13	135.72	136.48	152.02	157.33
	B1)	0	0	0	0	0	6.75
2.0 m/s	B2)	58.35	58.35	60.9	64.05	71.07	82.2
	S1)	130.08	130.08	134.54	139.37	151.04	161.98

TABLE 9 ROLLER TOWING RESISTANCE

Speed (m/s)	Towing Resistance (Kg)
0.5	0.1
1.0	0.3
1.5	0.35
1.75	0.45/0.50
2.0	1.4/1.4
2.25	1.05
2.5	1.0
3.0	1.0
4.0	1.25

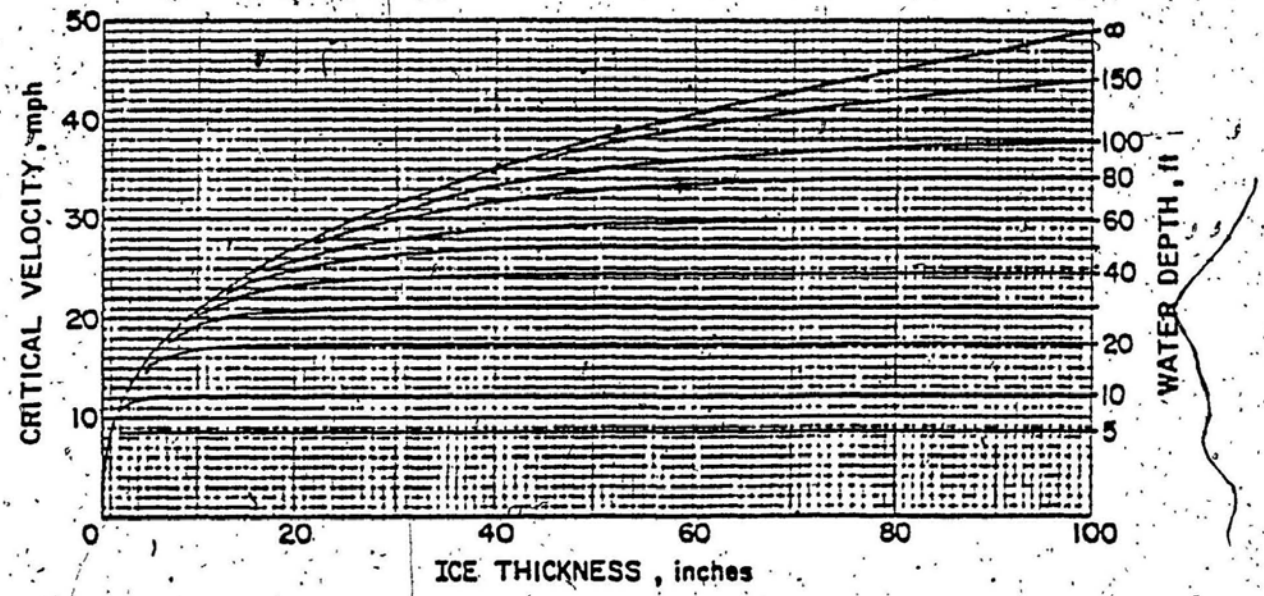

FIGURE 1 CRITICAL SPEED FOR VARIOUS H AND h (NEVEL 1970)

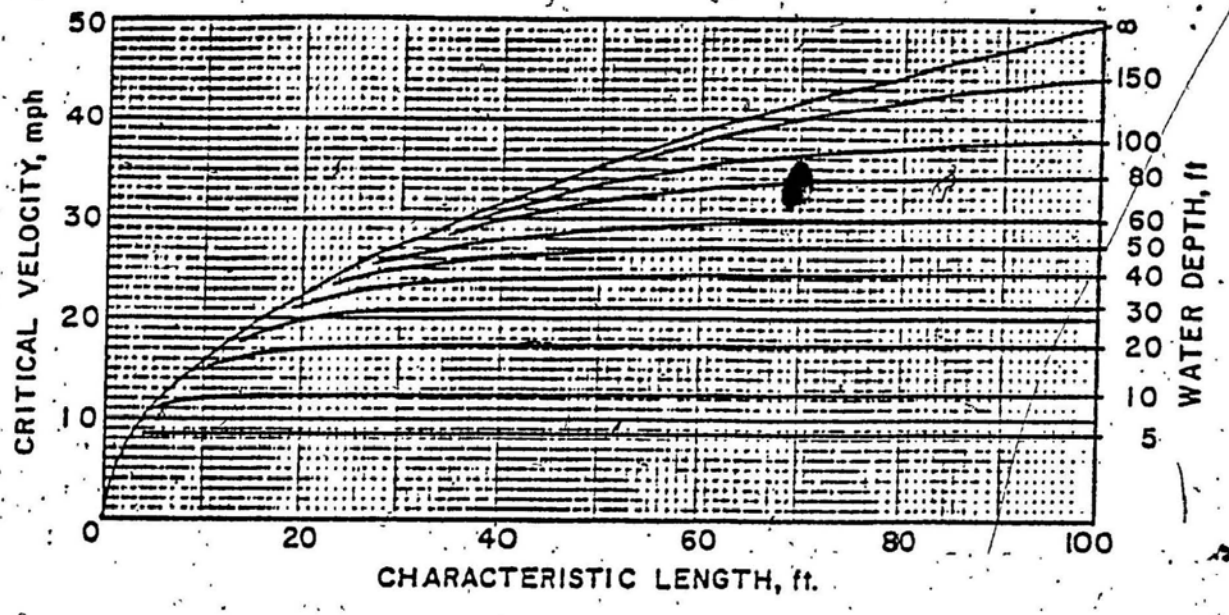

FIGURE 2 CRITICAL SPEED FOR VARIOUS H AND L (NEVEL 1970)

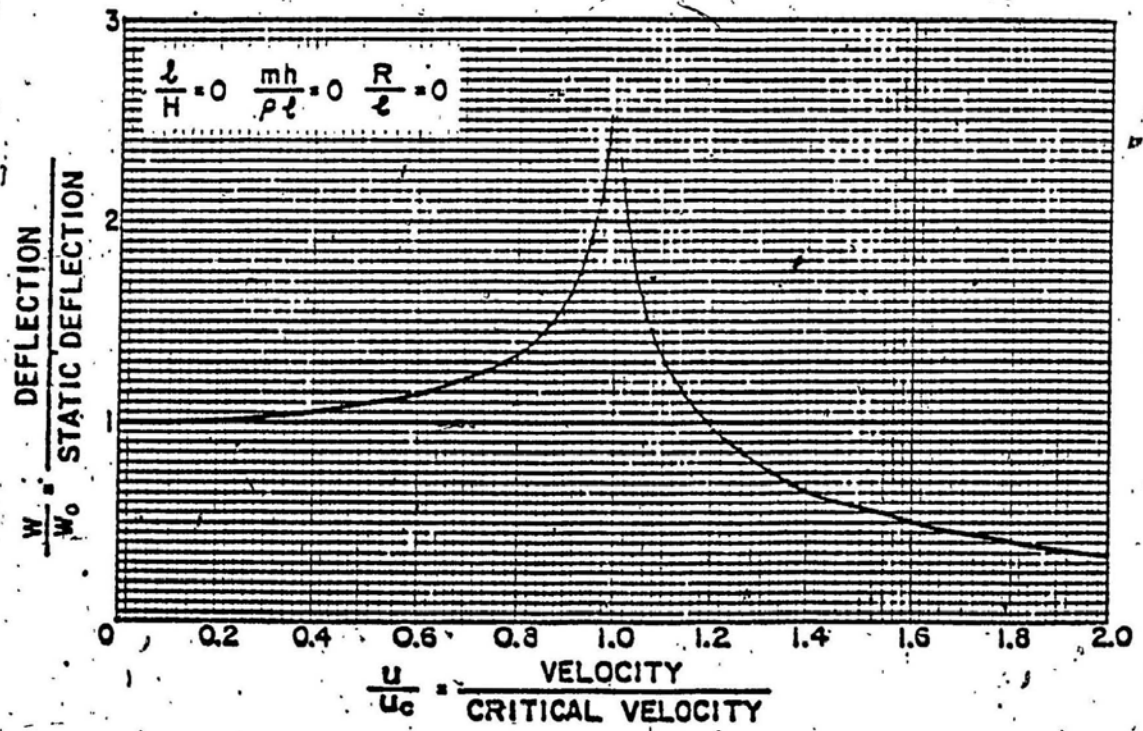

FIGURE 3 DEFLECTION AMPLIFICATION FACTOR (NEVEL 1970)

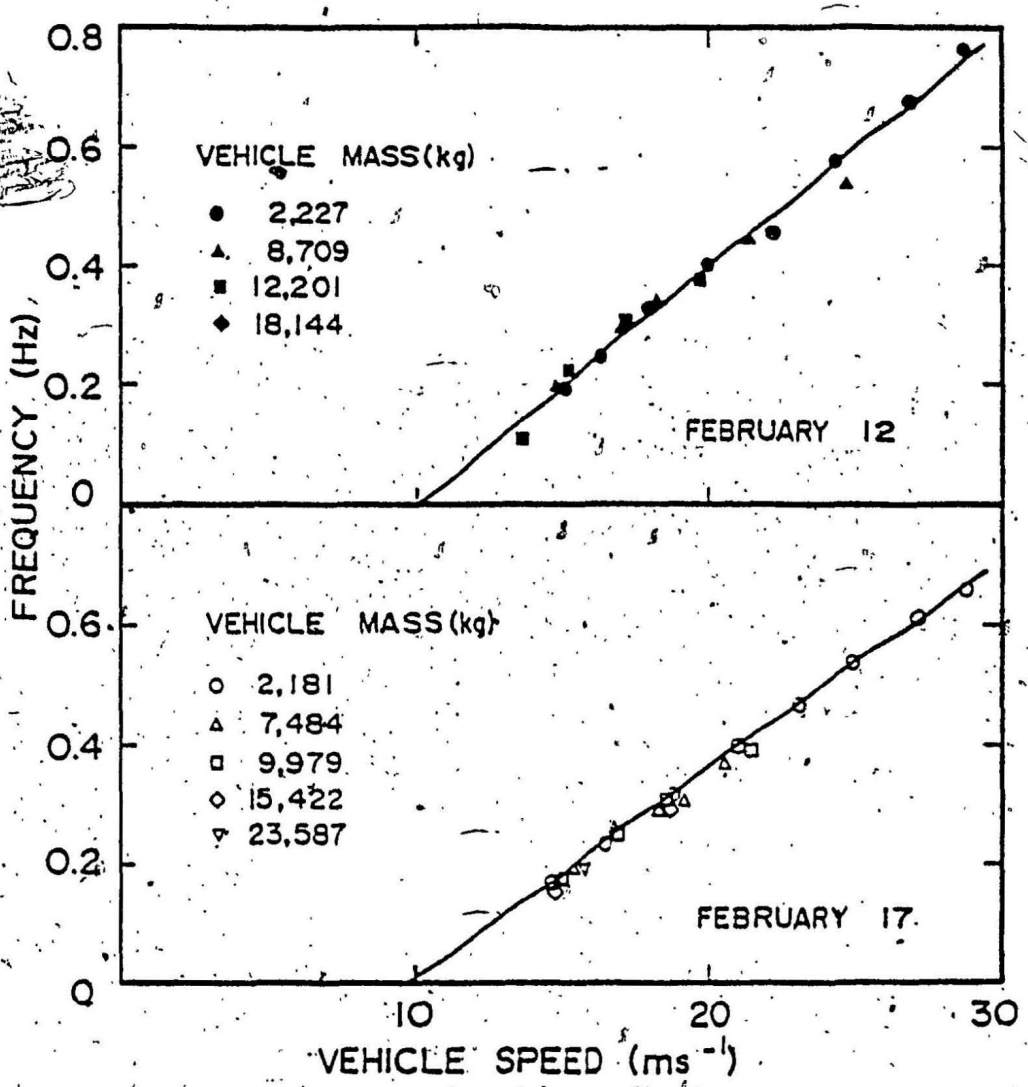

FIGURE 4 FREQUENCY VERSUS VEHICLE SPEED (EYRE.1977)

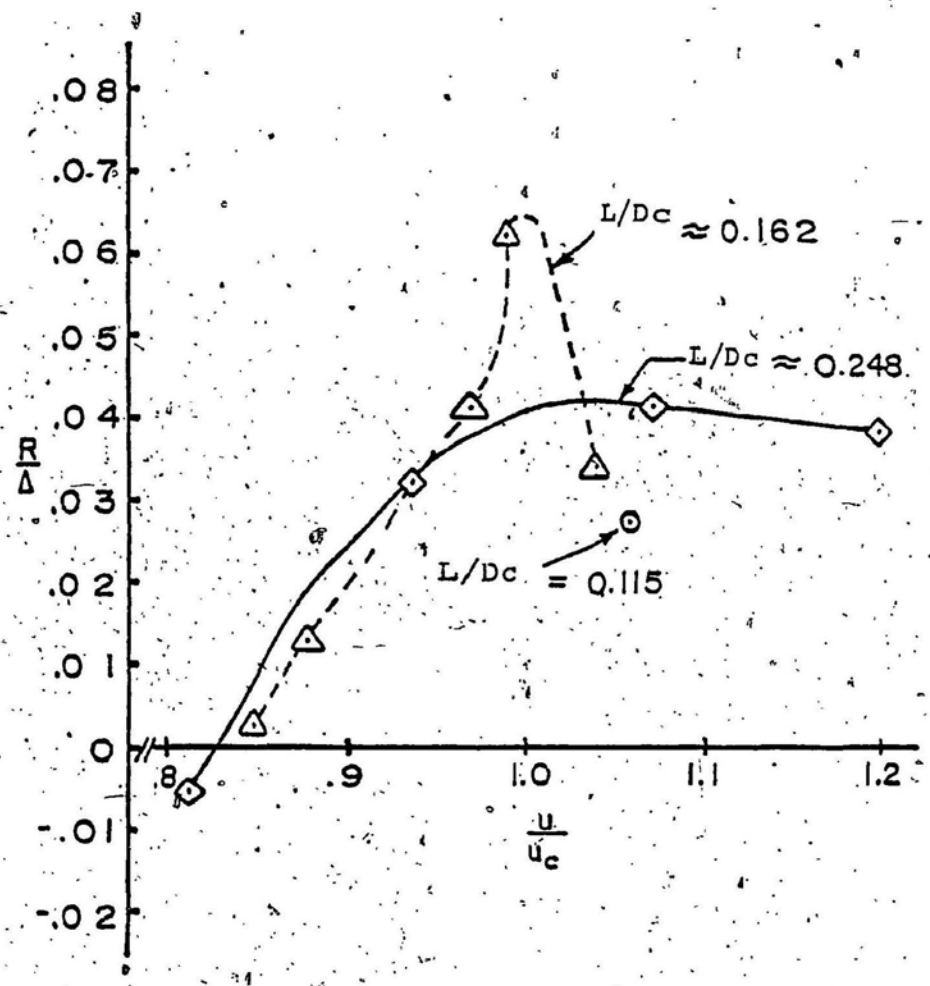

Fig. 5 Nondimensional resistance over ice versus critical velocity ratio

(LECOURT et al 1975)

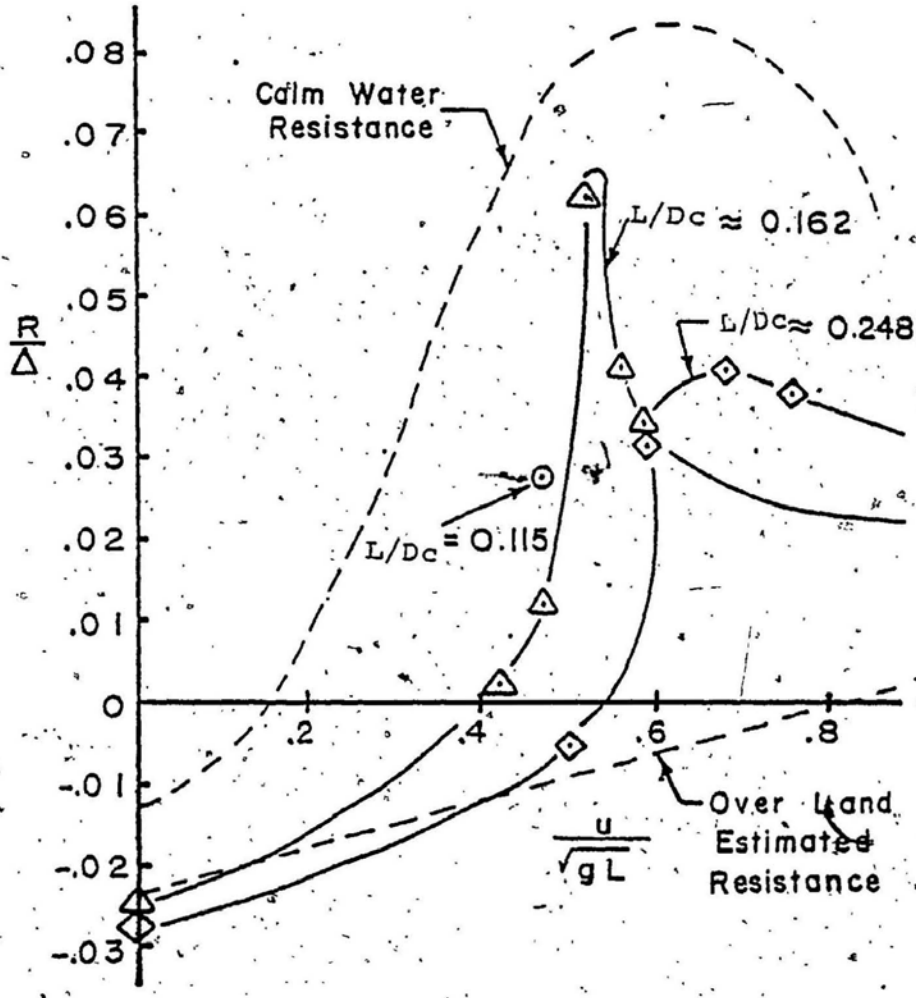

Fig. 6 Nondimensional resistance over ice versus Froude number

(LECOURT et al 1975)

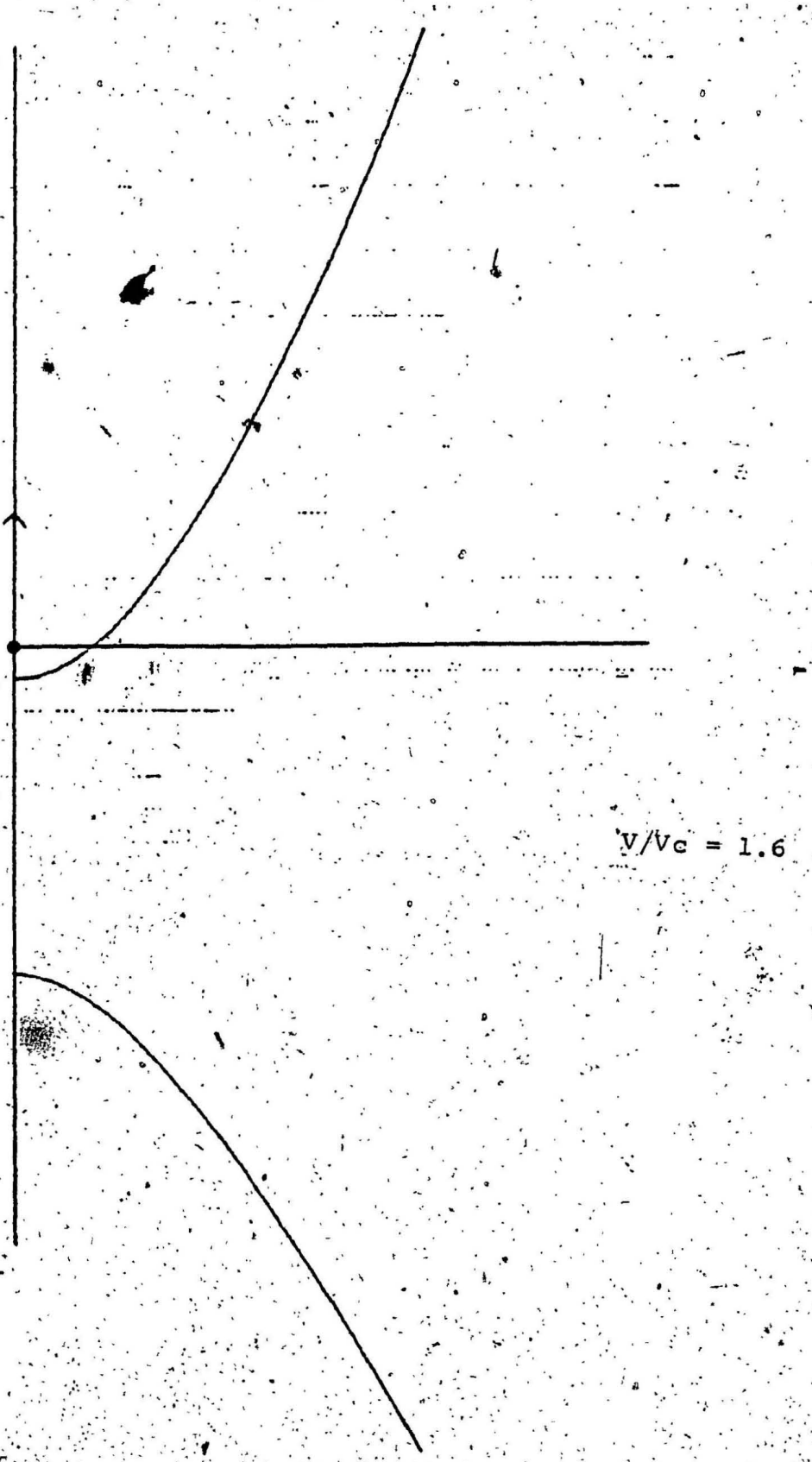

Fig. 7 Wave Pattern Predictions (Shinbrot):

Sheet Thickness h = 0.05 m.

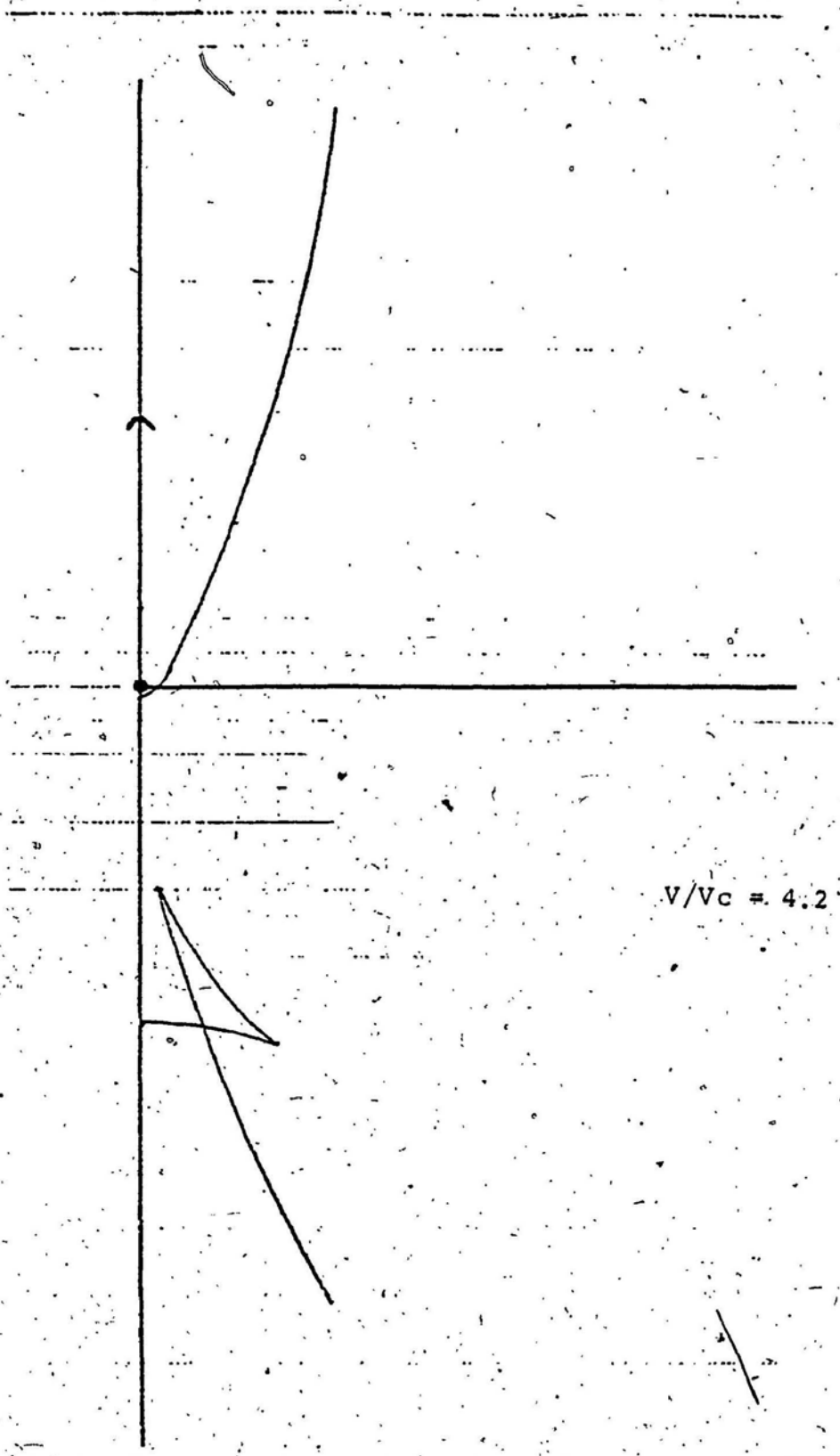

Fig. 7 (cont'd.)

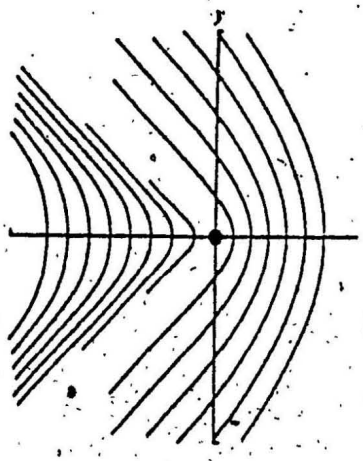

V/Vc = 1.33

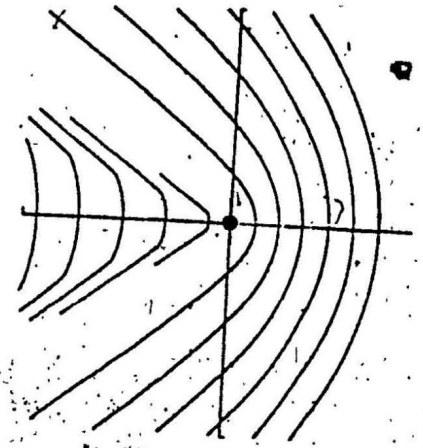

V/Vc = 1.67

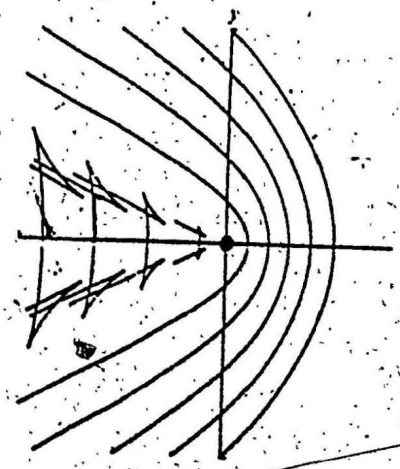

V/Vc = 2.22

FIGURE 8 WAVE PATTERN PREDICTIONS (Davys et al 1985)

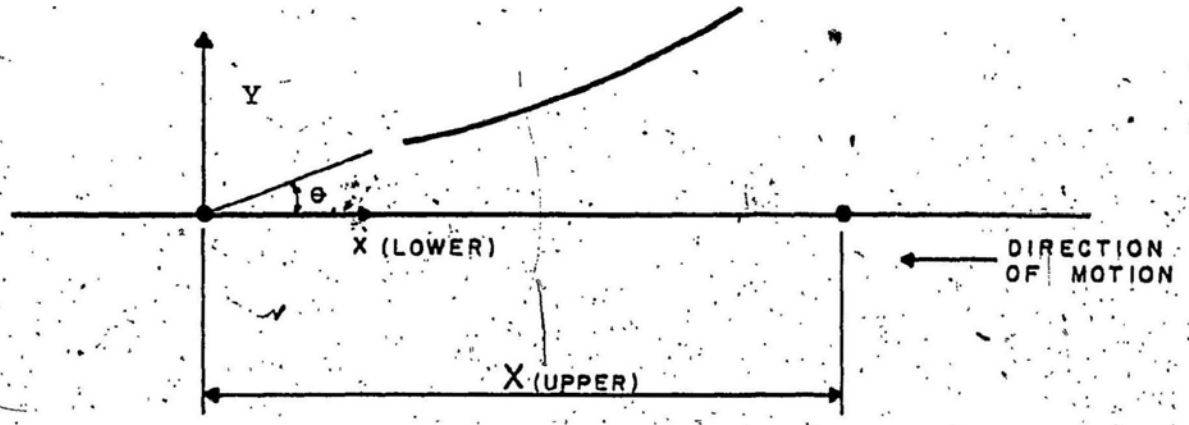

FIGURE 9 WAVE PATTERN GEOMETRY

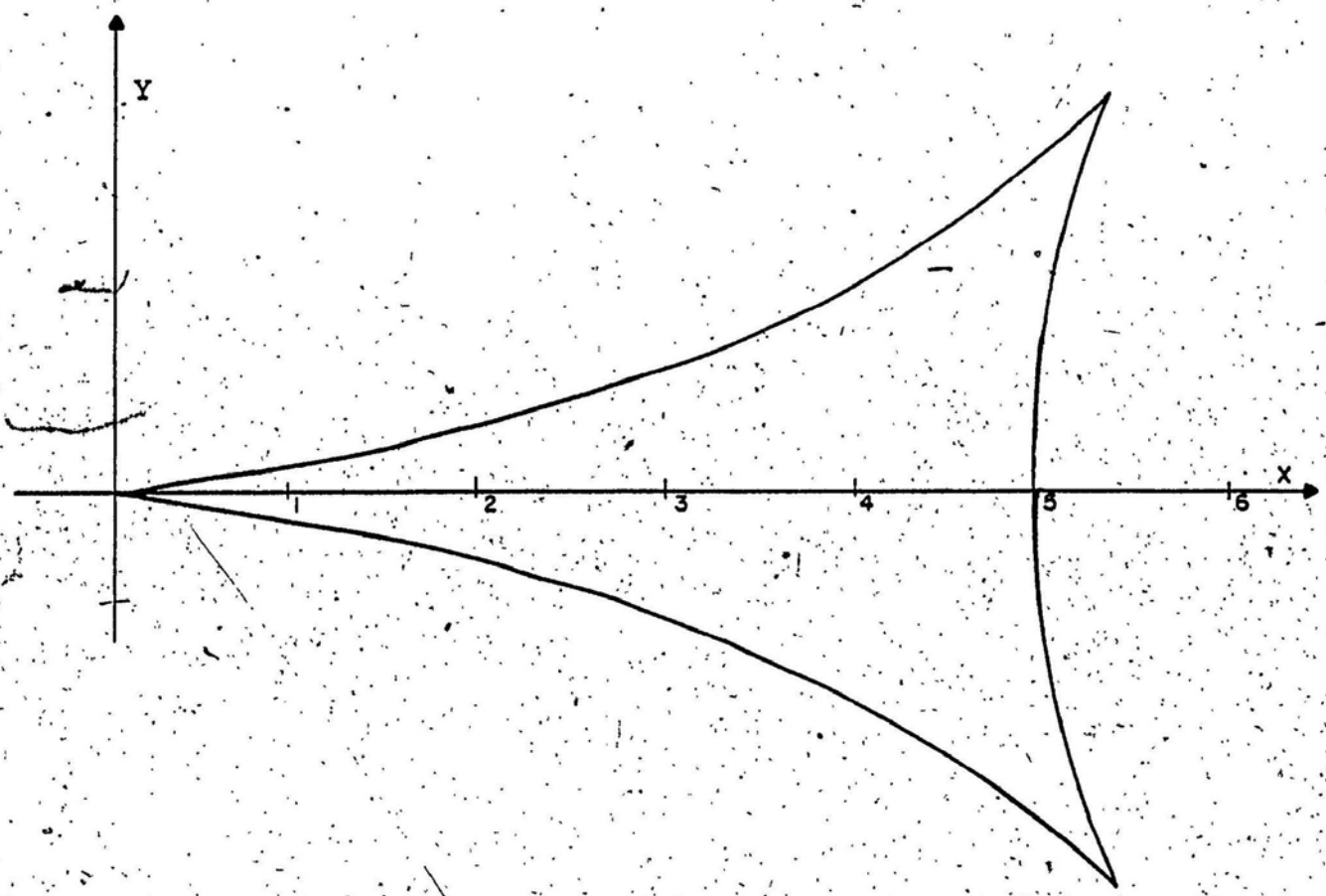

FIGURE 10 KELVIN WEDGE $X_0 = 10$

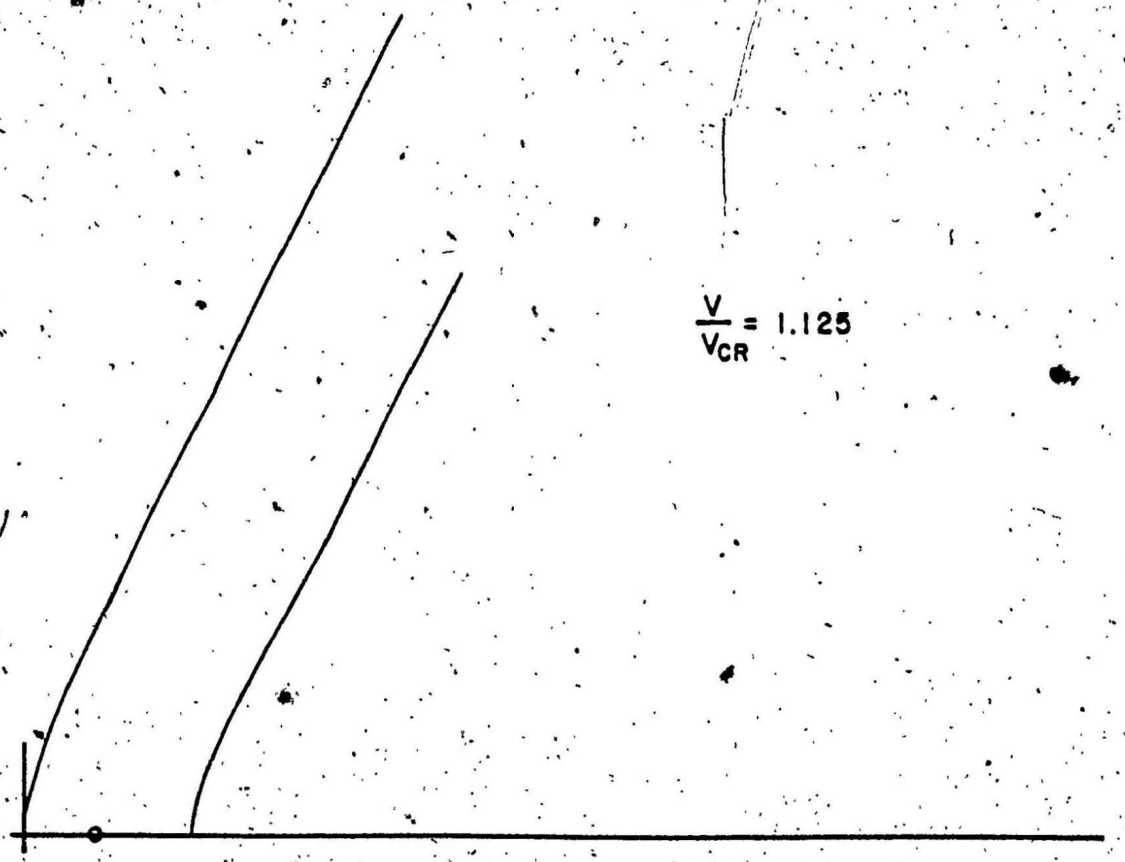

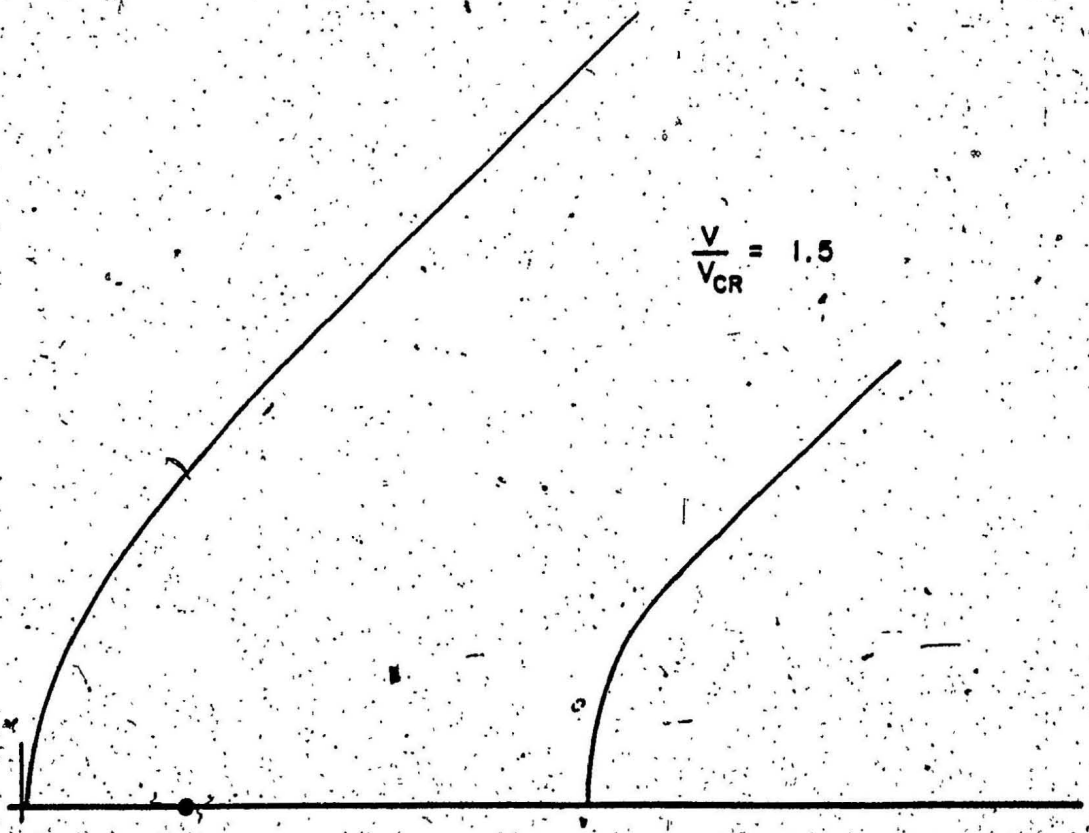

I THIN PLATE WAVE PATTERNS (NO INERTIA)

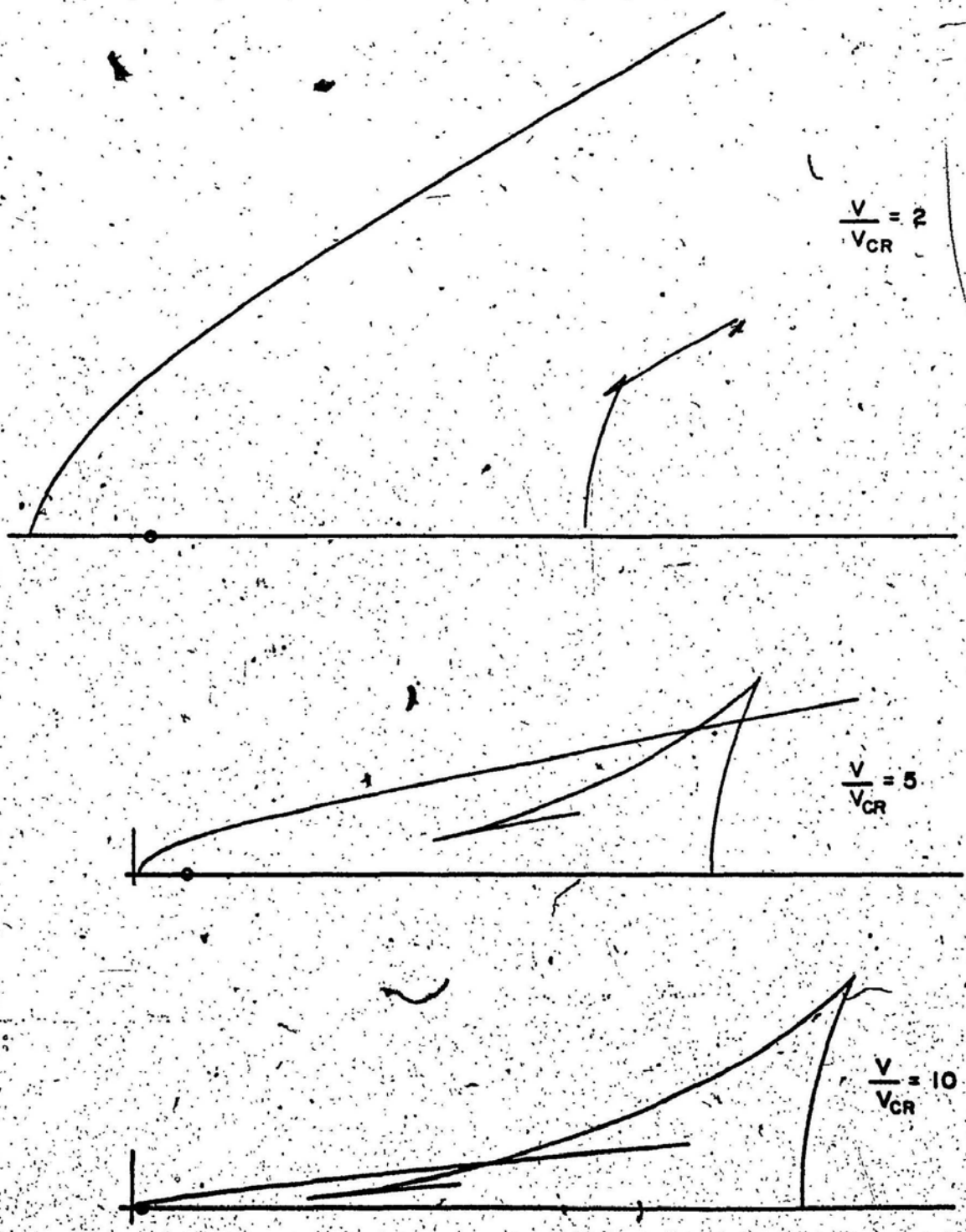

FIGURE 11 CONT'D

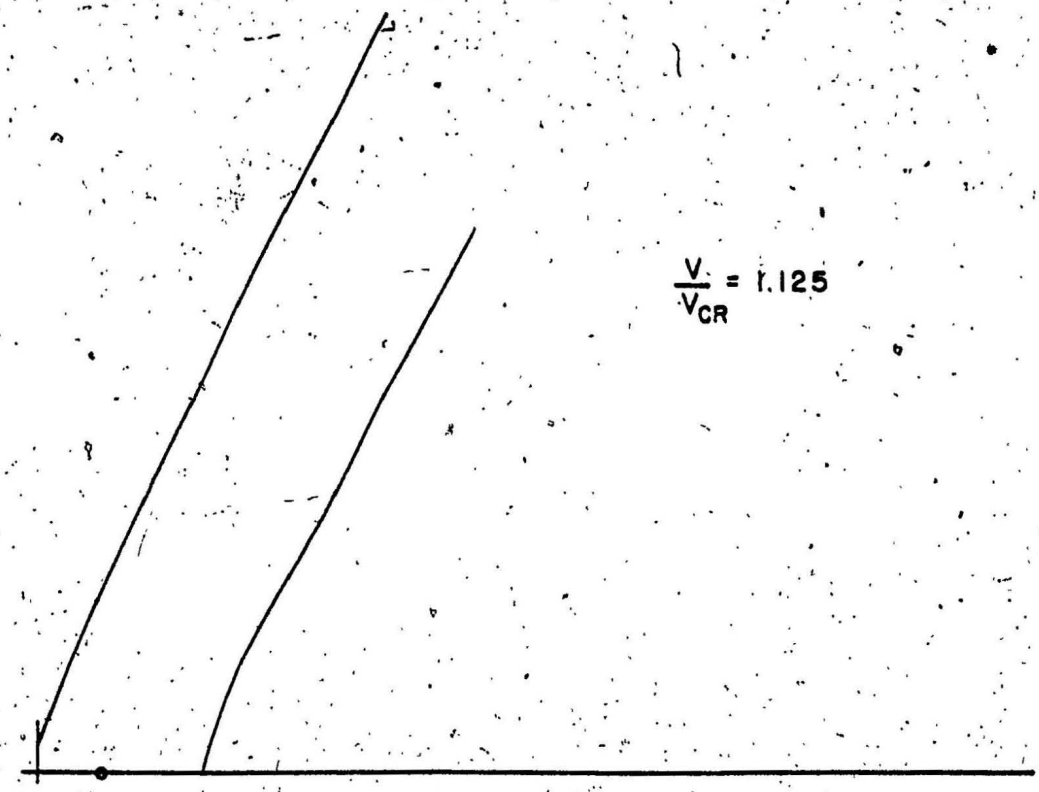

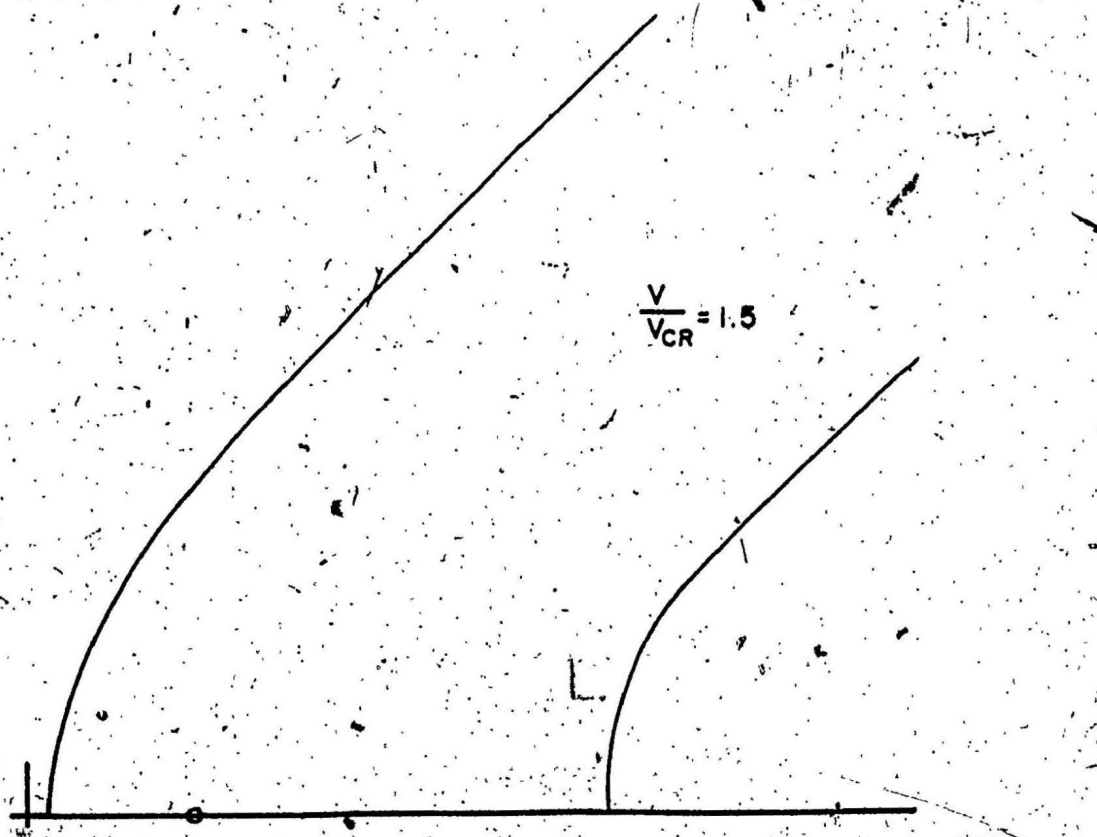

FIGURE 12 WAVE PATTERNS FOR PLATE WITH INERTIA

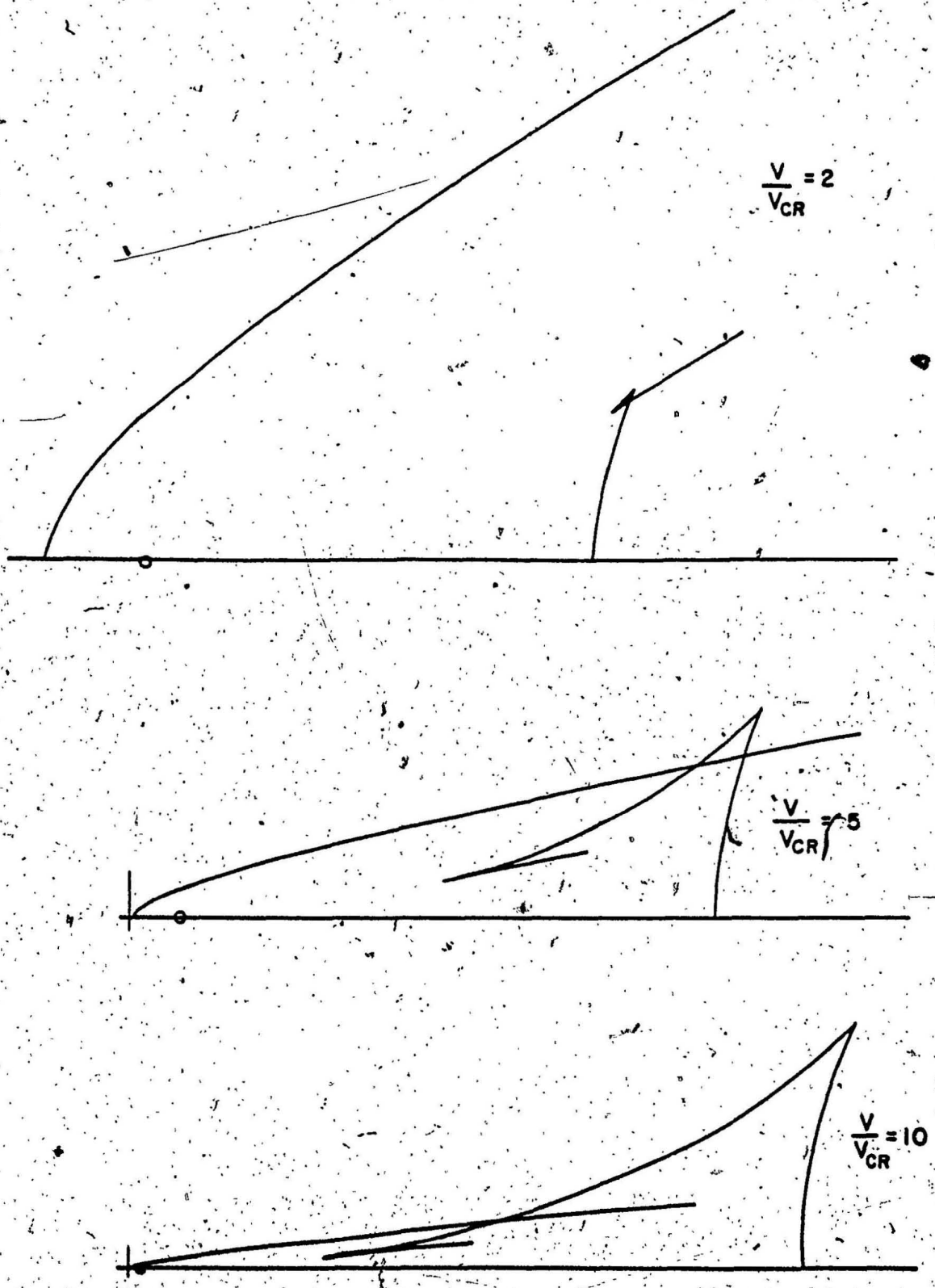

FIGURE 12 - CONT'D

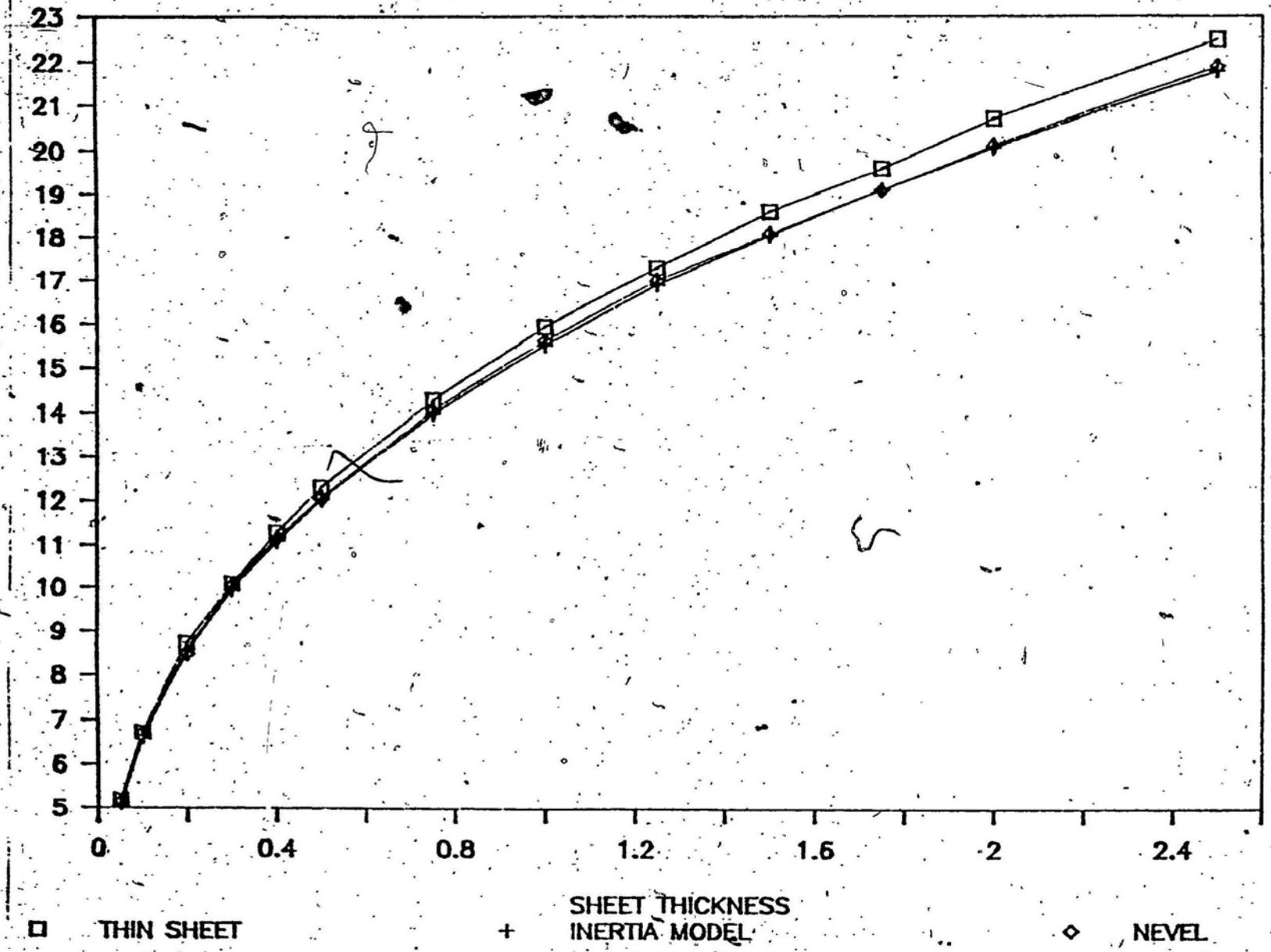

FIGURE 13 CRITICAL SPEED VERSUS THICKNESS

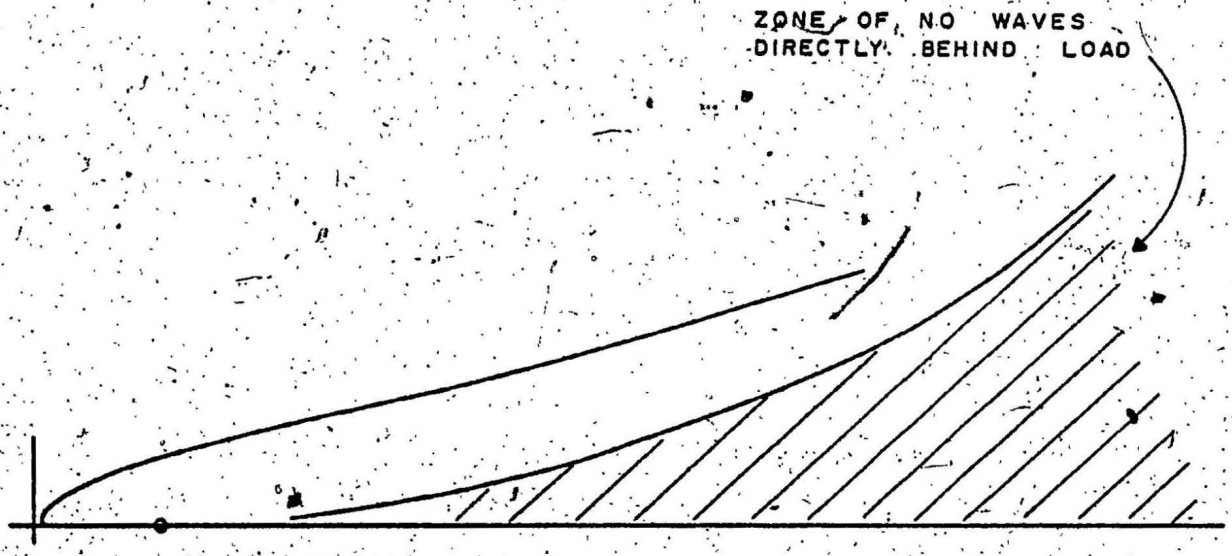

FIGURE 14 PLOT SHOWING SHADOW ZONE

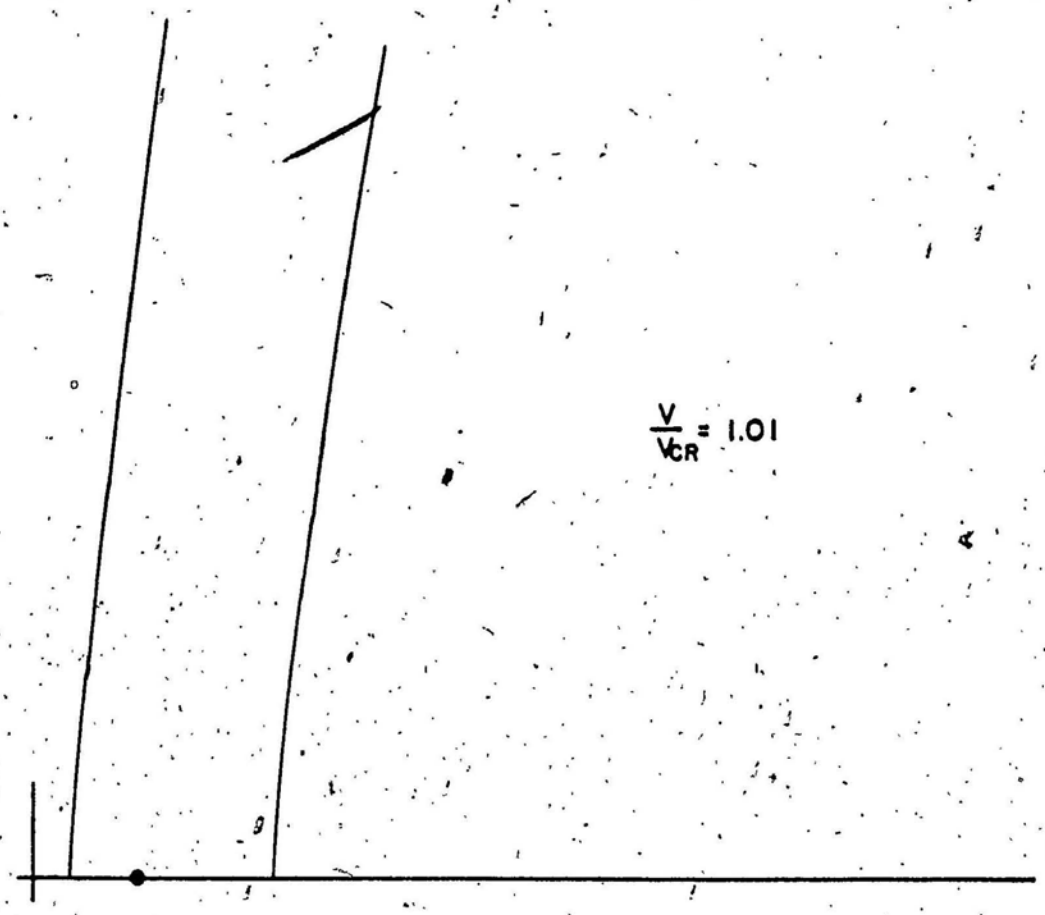

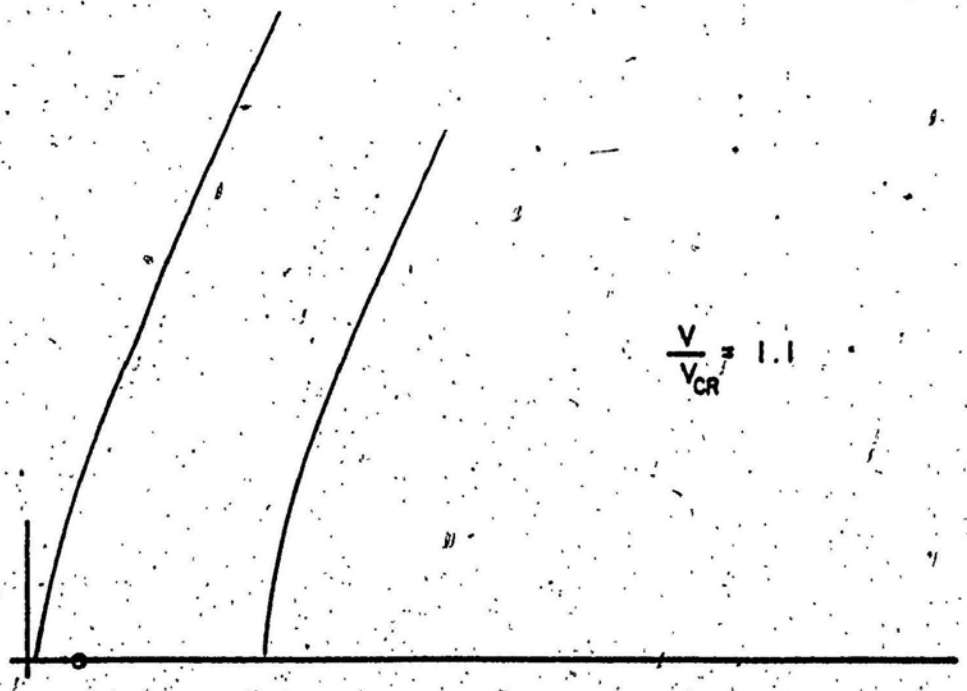

15 SURFACE TENSION WAVE PATTERNS

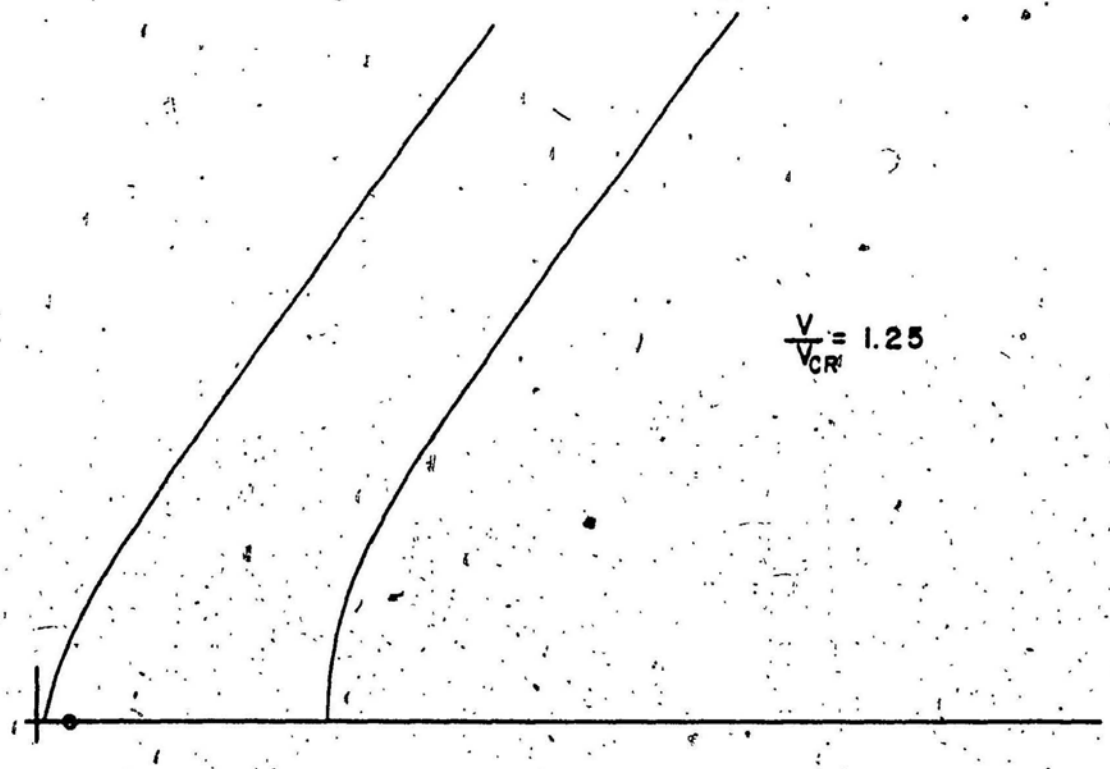

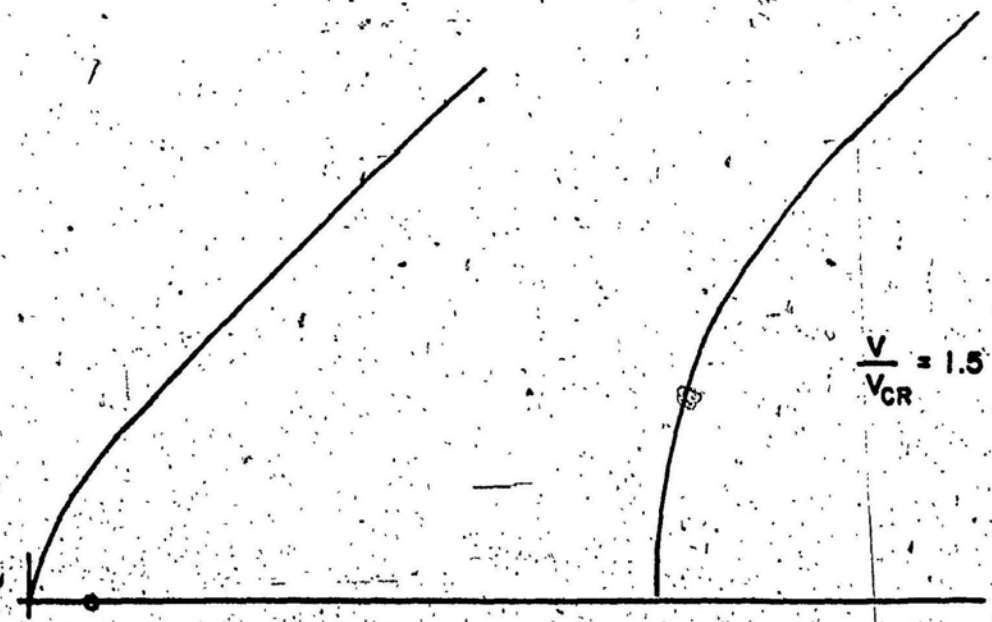

FIGURE 15 CONT'D

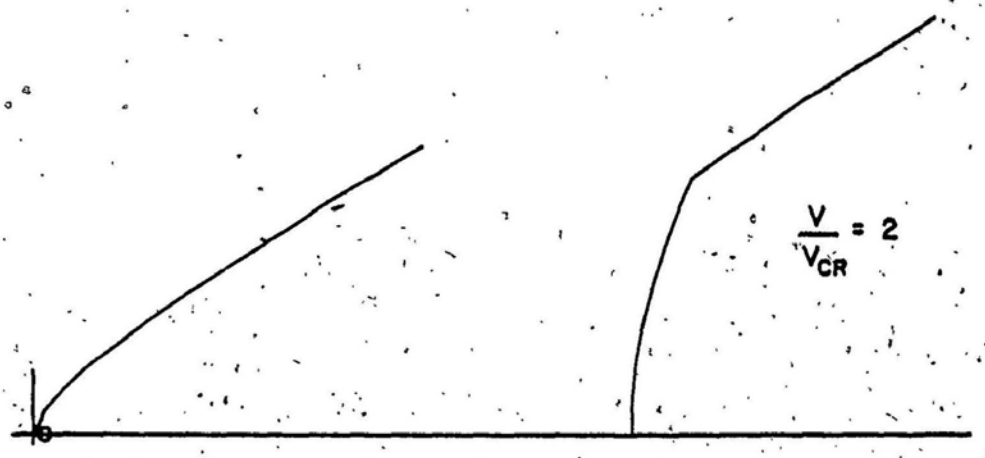

FIGURE 15 CONT'D

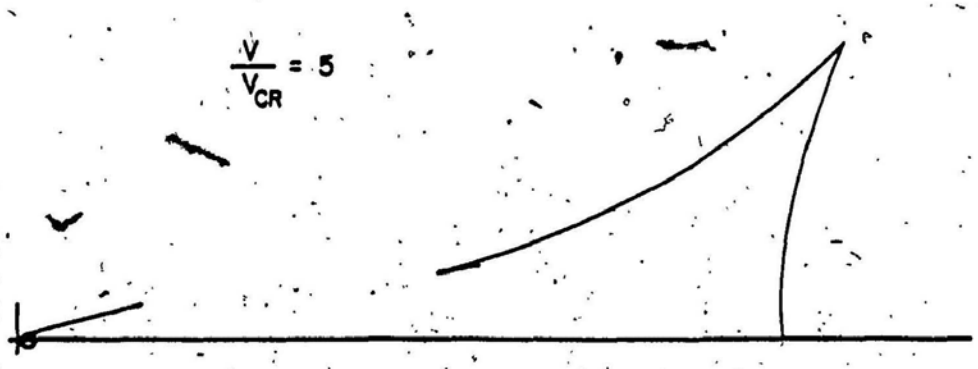

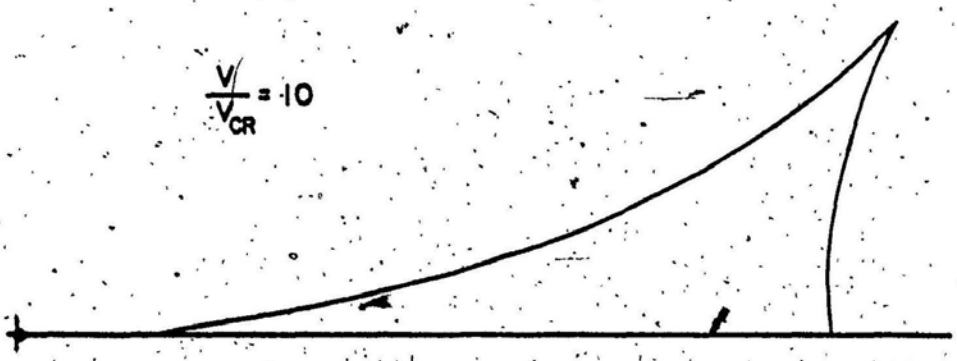

FIGURE 15 CONT'D

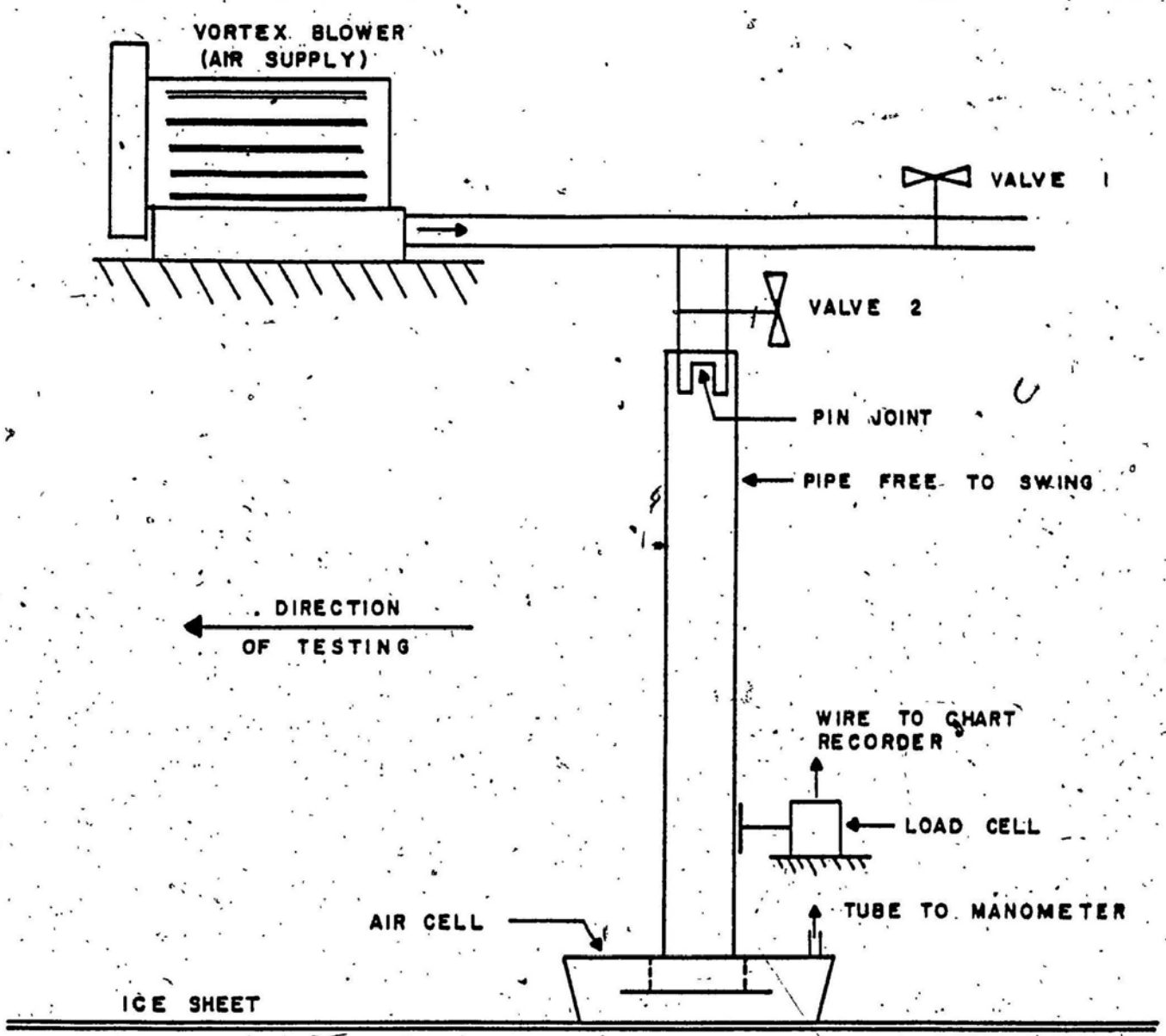

FIGURE 16 AIR CELL MODEL

NOTE: TOTAL WEIGHT OF MODEL AS TESTED WAS 5.0 kg.

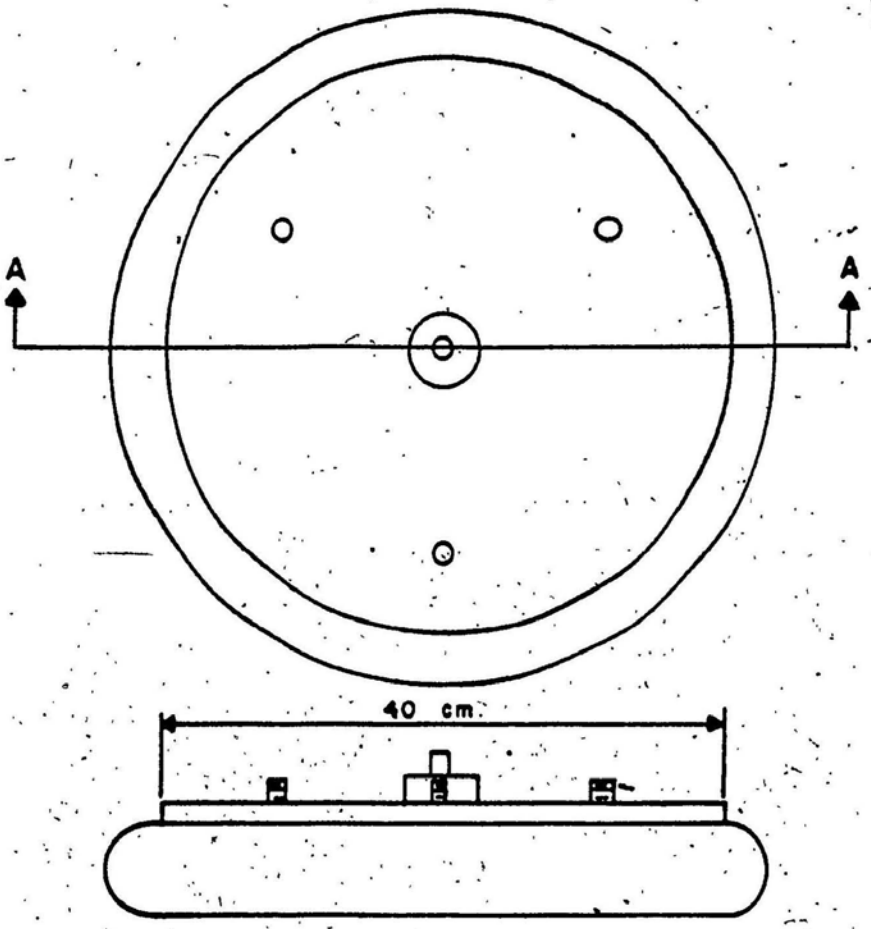

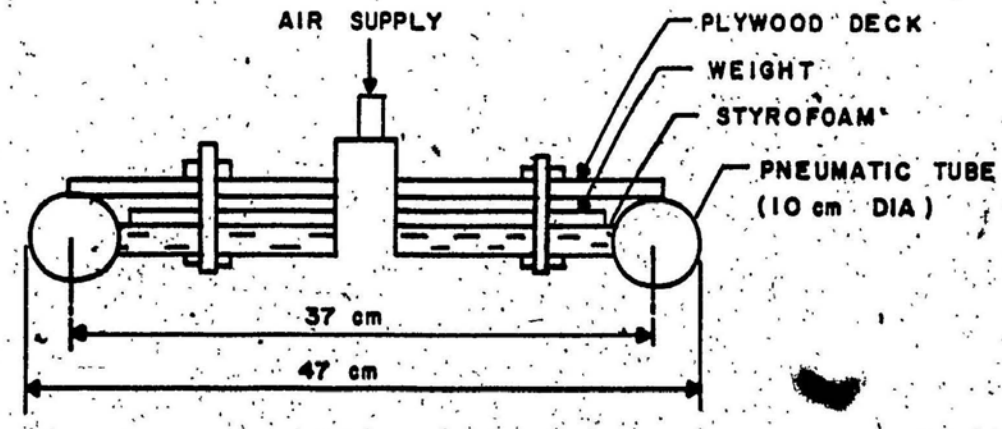

SECTION 'A-A'

FIGURE 17 PNEUMATIC TUBE ACV MODEL

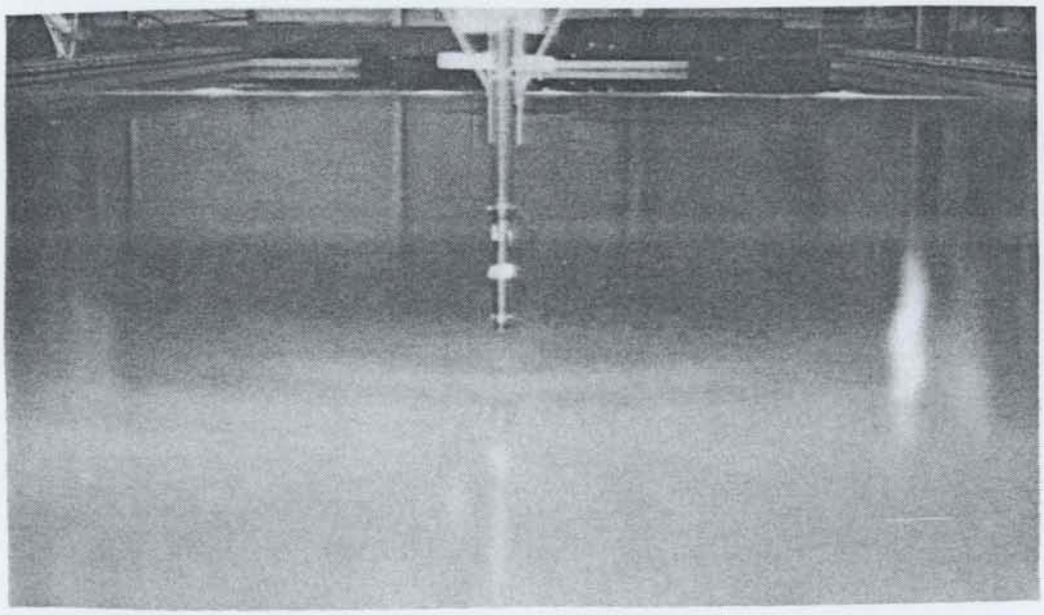

Figure 18 Waves in Ice Sheet at I.M.D.

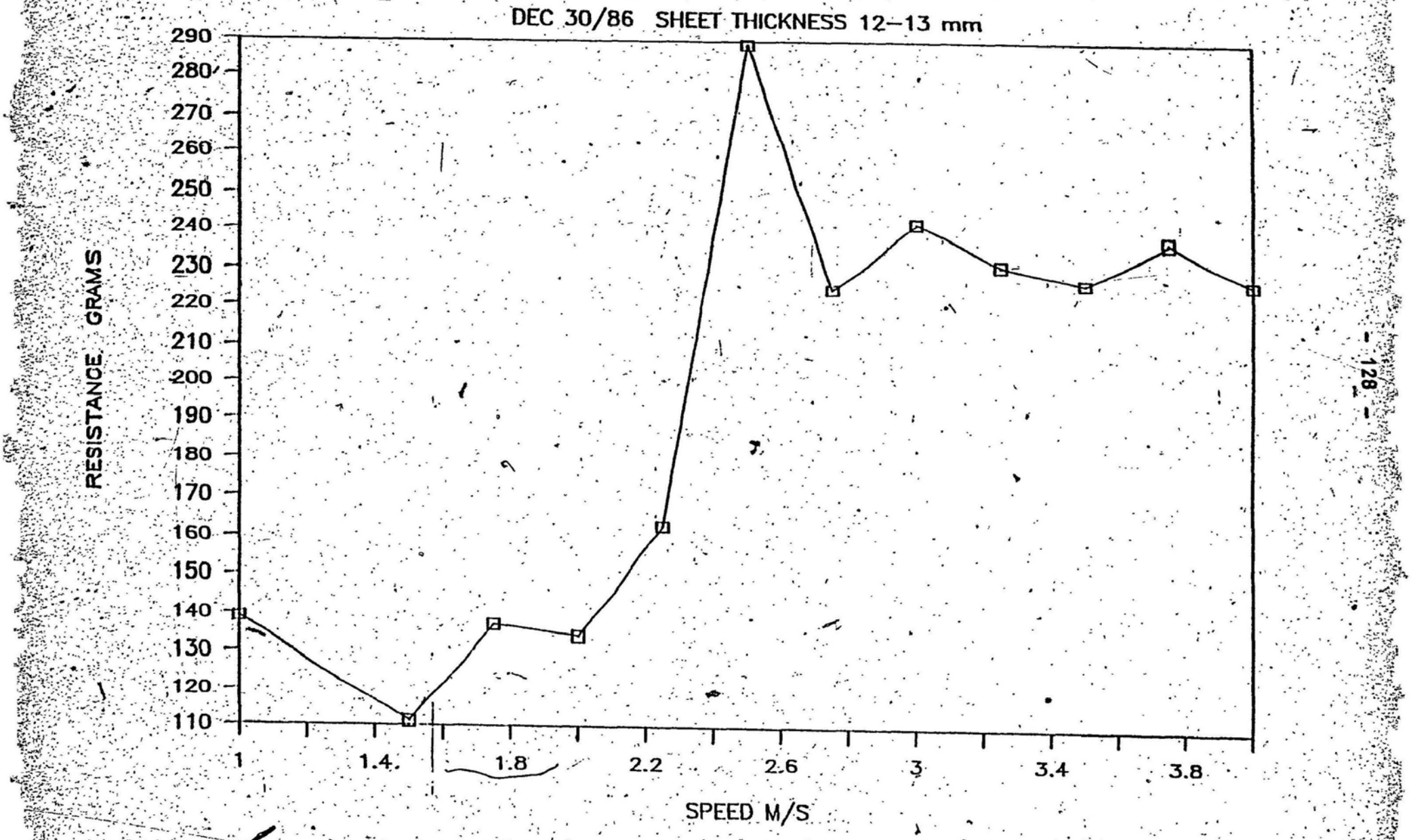

FIGURE 19 HOVERCRAFT RESISTANCE OVER ICE

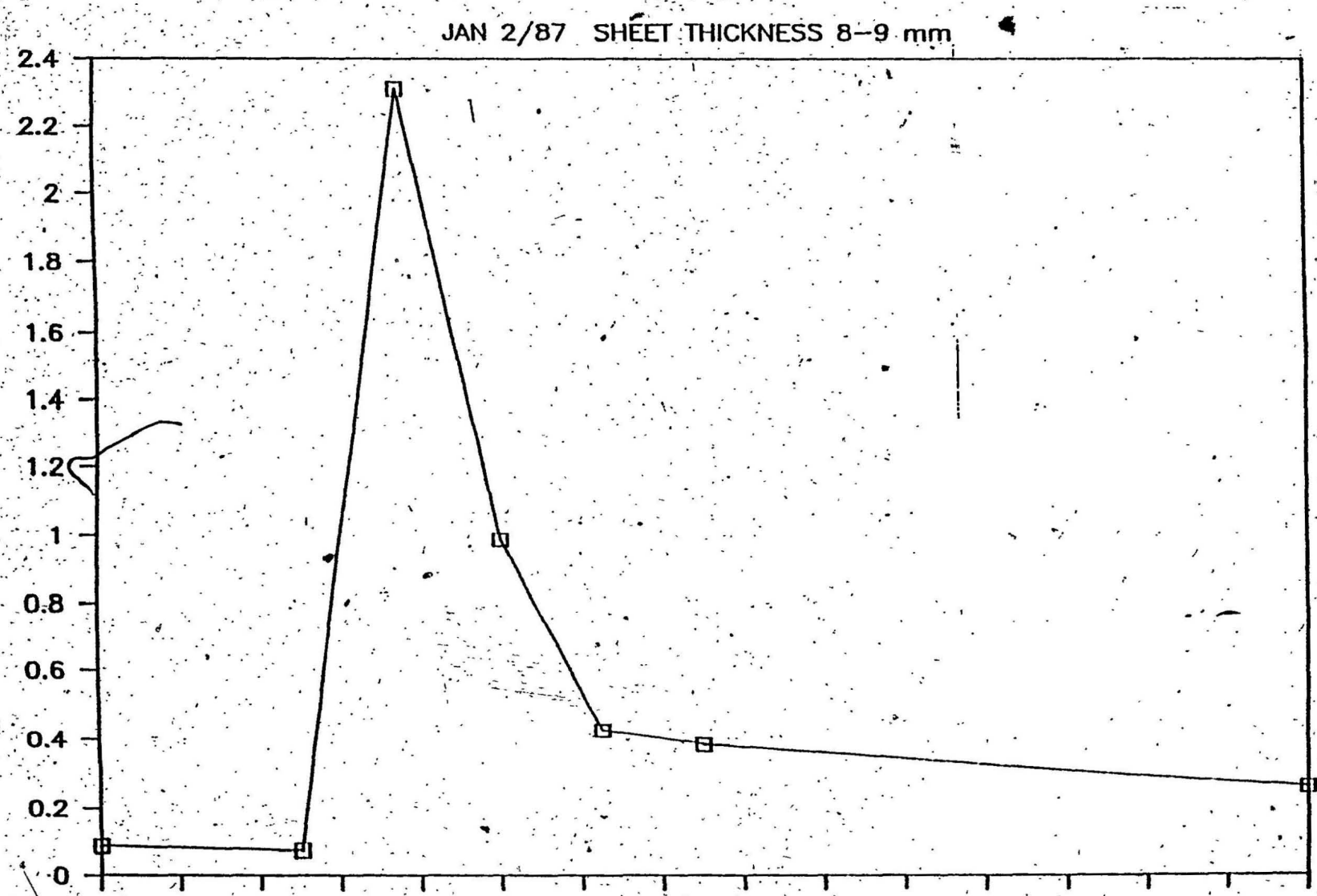

FIGURE 20 HOVERCRAFT RESISTANCE OVER ICE

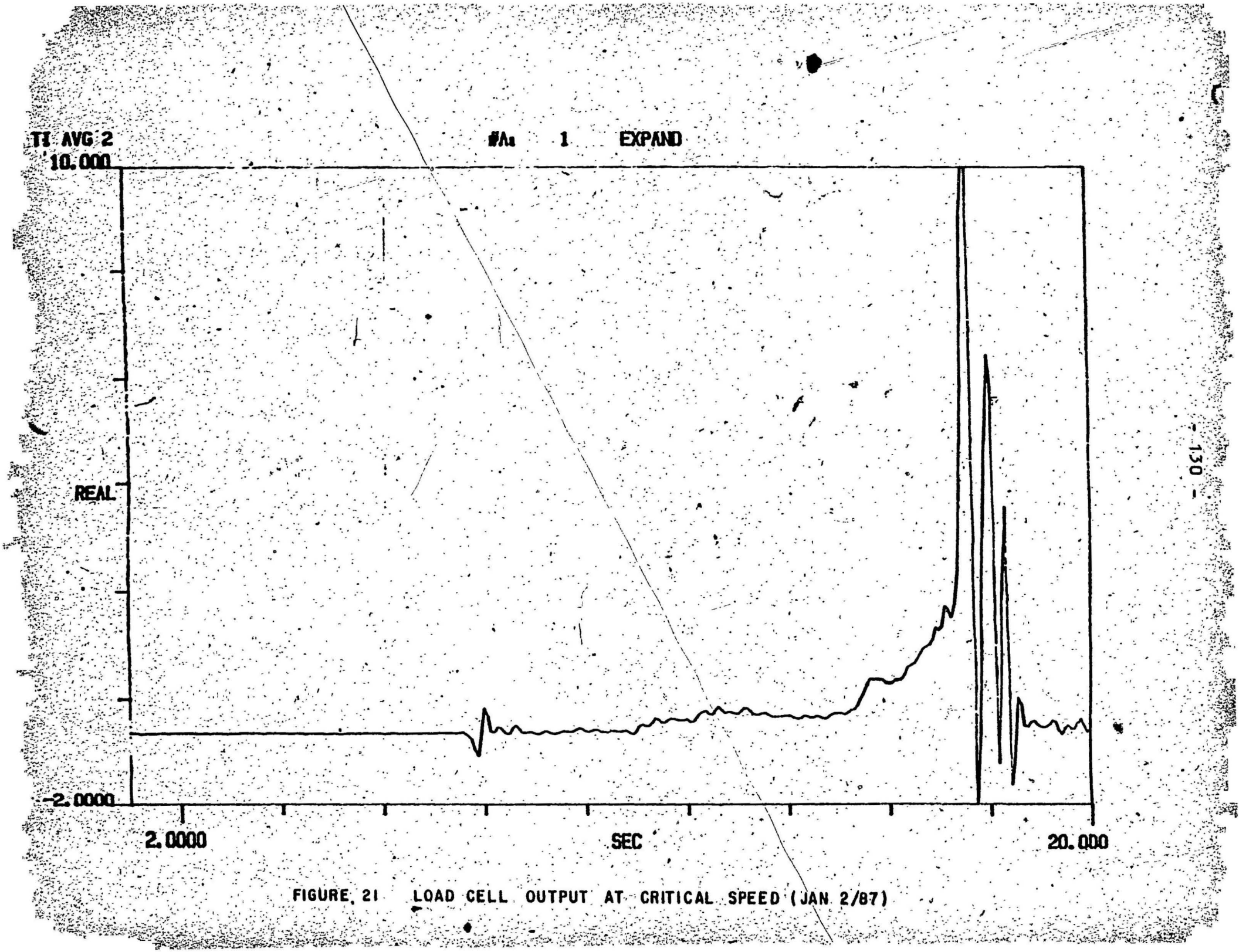

FIGURE 21 LOAD CELL OUTPUT AT CRITICAL SPEED (JAN 2/87)

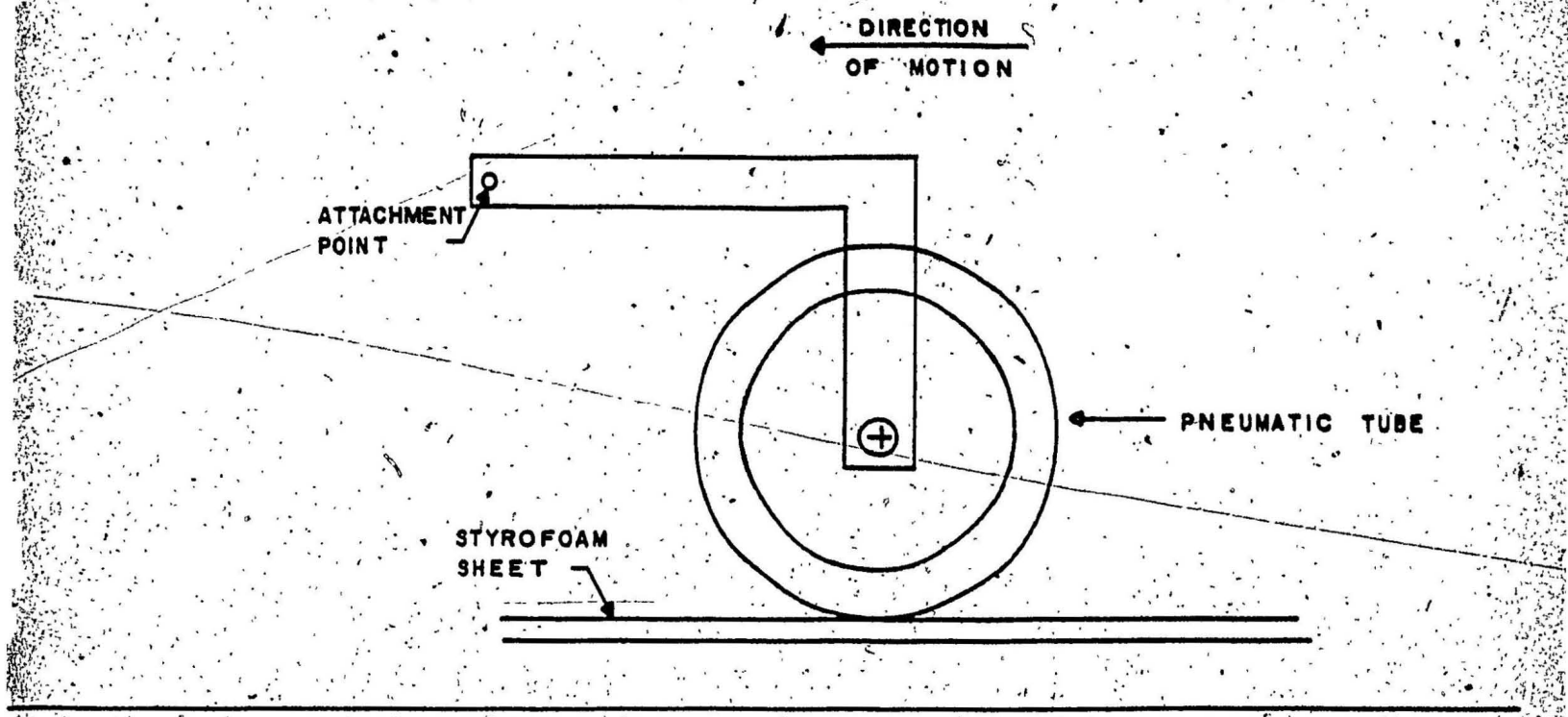

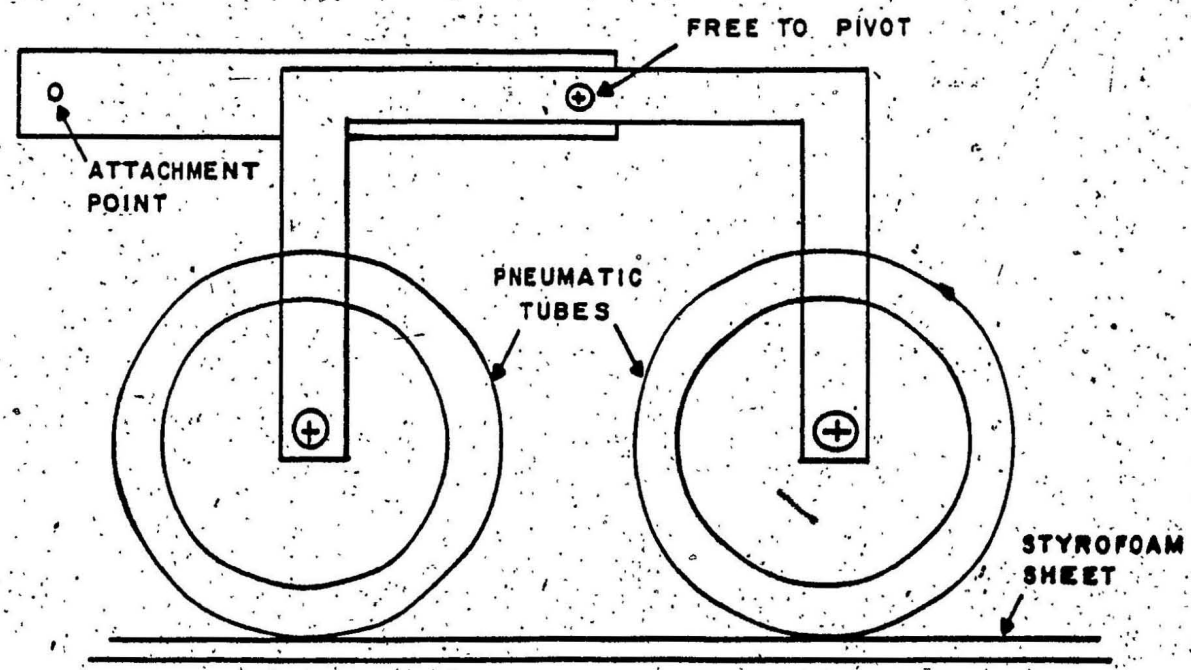

FIGURE 22 SINGLE AND TWO TIRE MODELS USED IN STYROFOAM SHEET TESTS

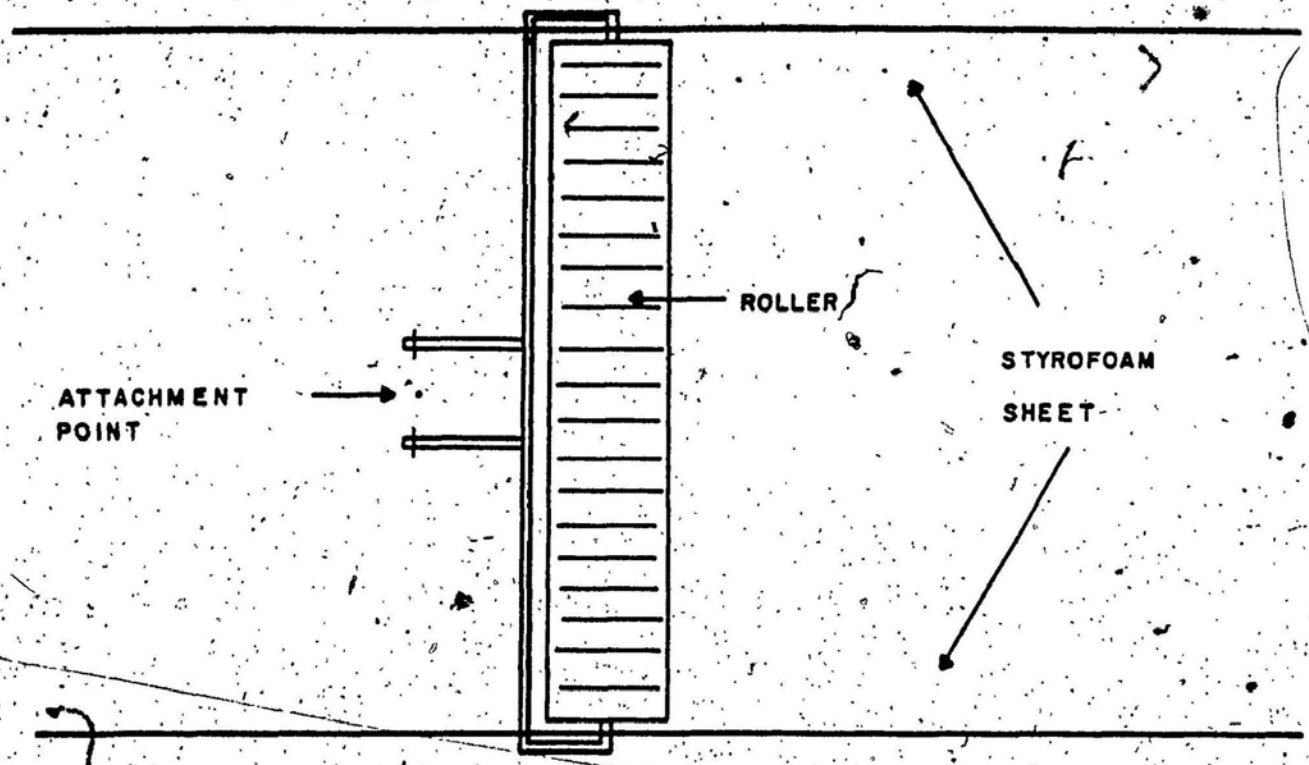

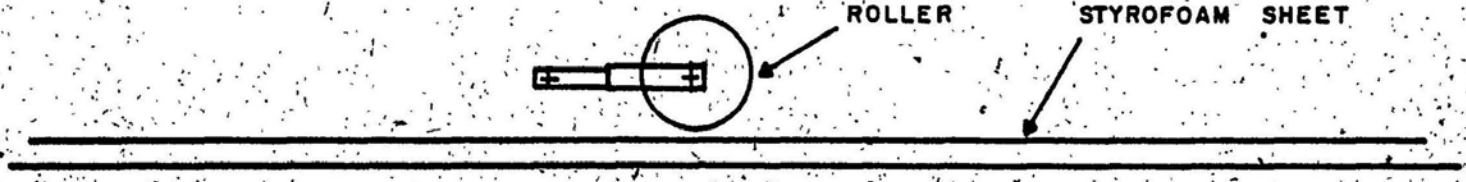

FIGURE 23 ROLLER MODEL USED IN STYROFOAM SHEET TESTS

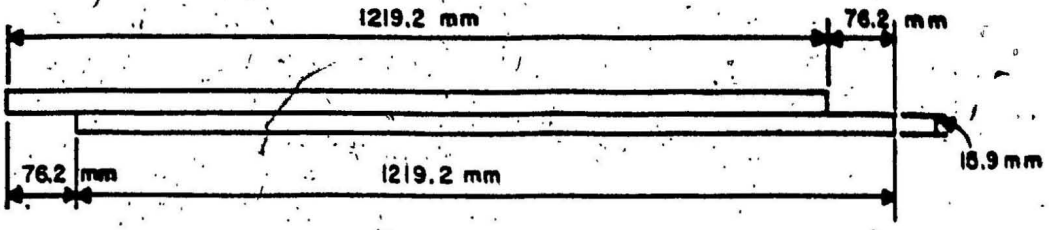

FIGURE 24 LAP JOINT IN STYROFOAM-SHEET

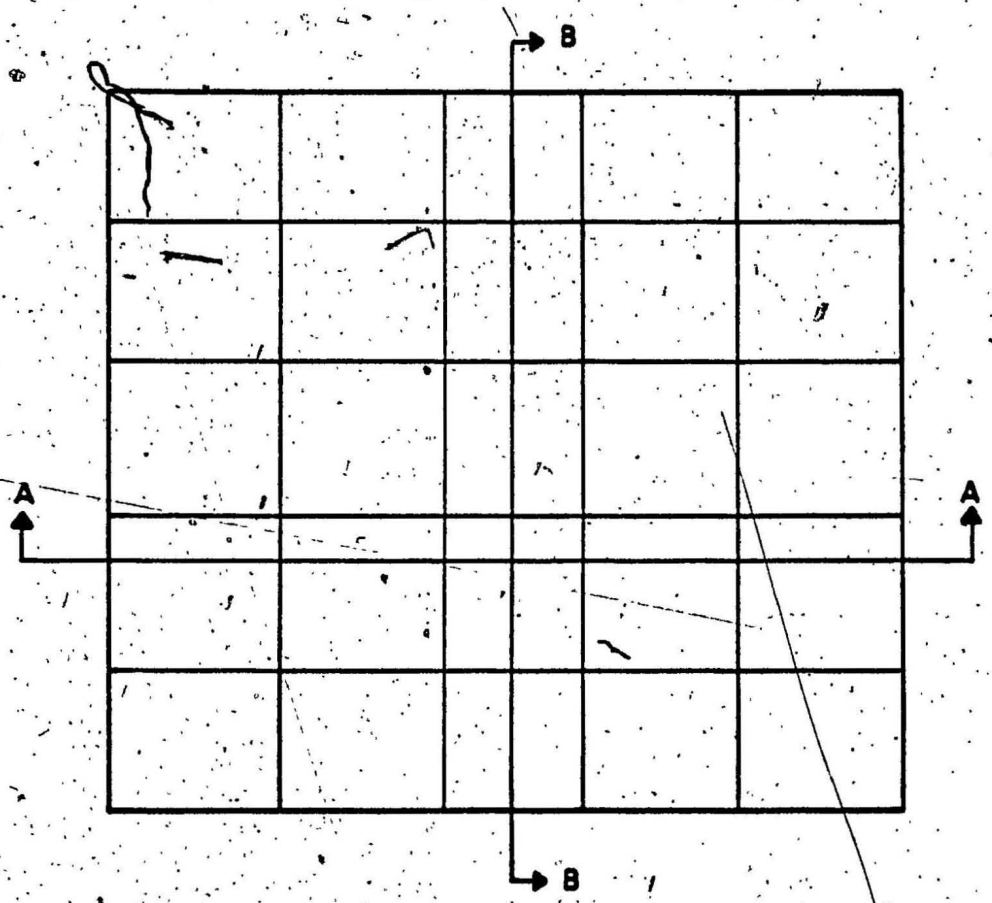

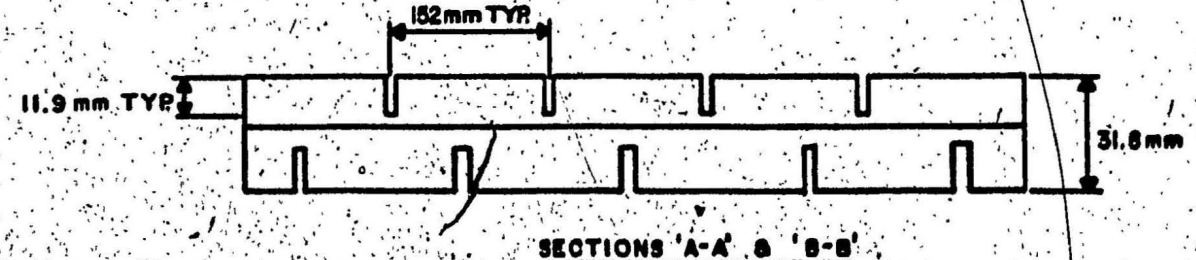

SECTIONS 'A-A' & 'B-B'

FIGURE 25 ARRANGEMENT OF CUTS IN SHEET

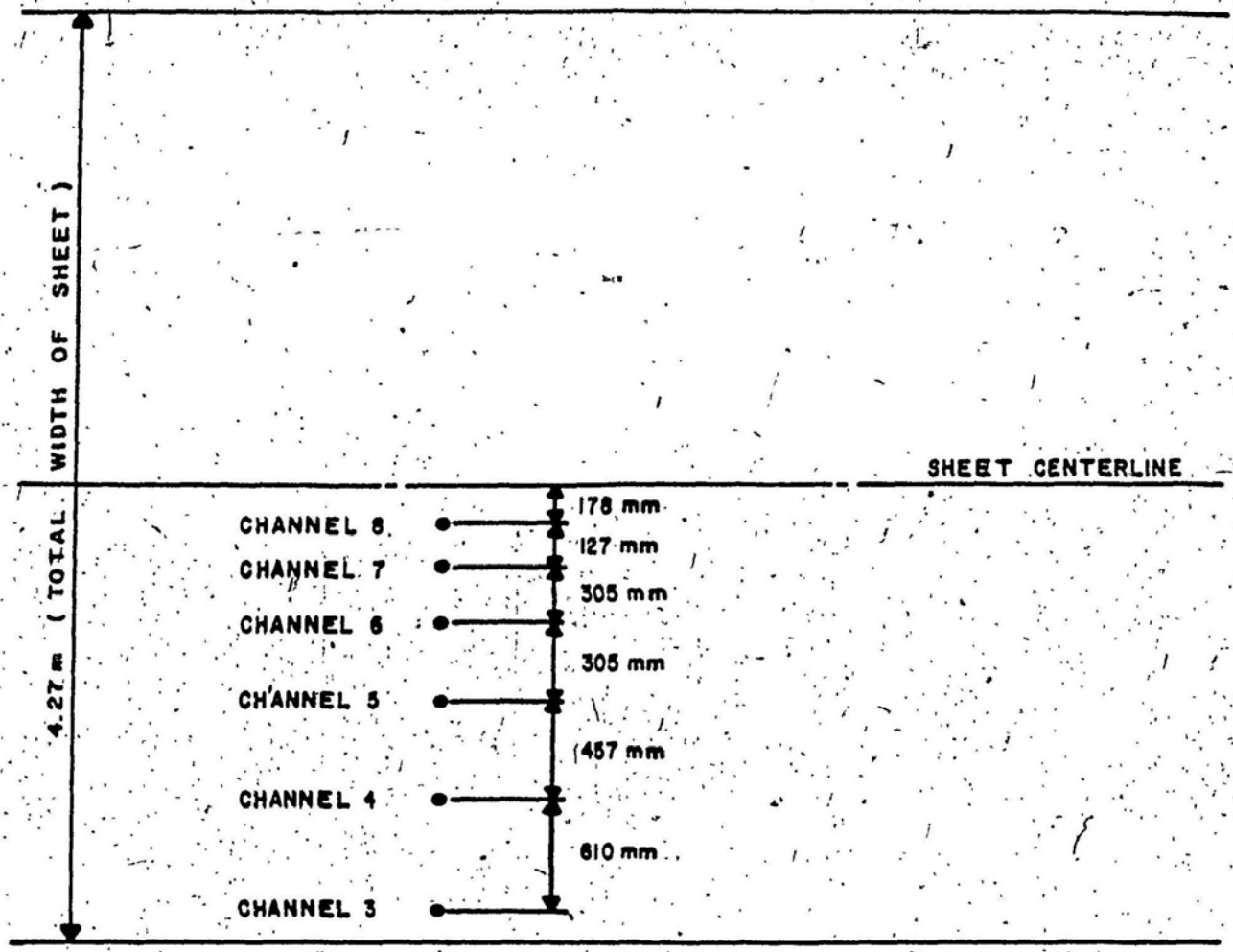

FIGURE 26 LOCATION OF DEFLECTION SENSORS ON SHEET

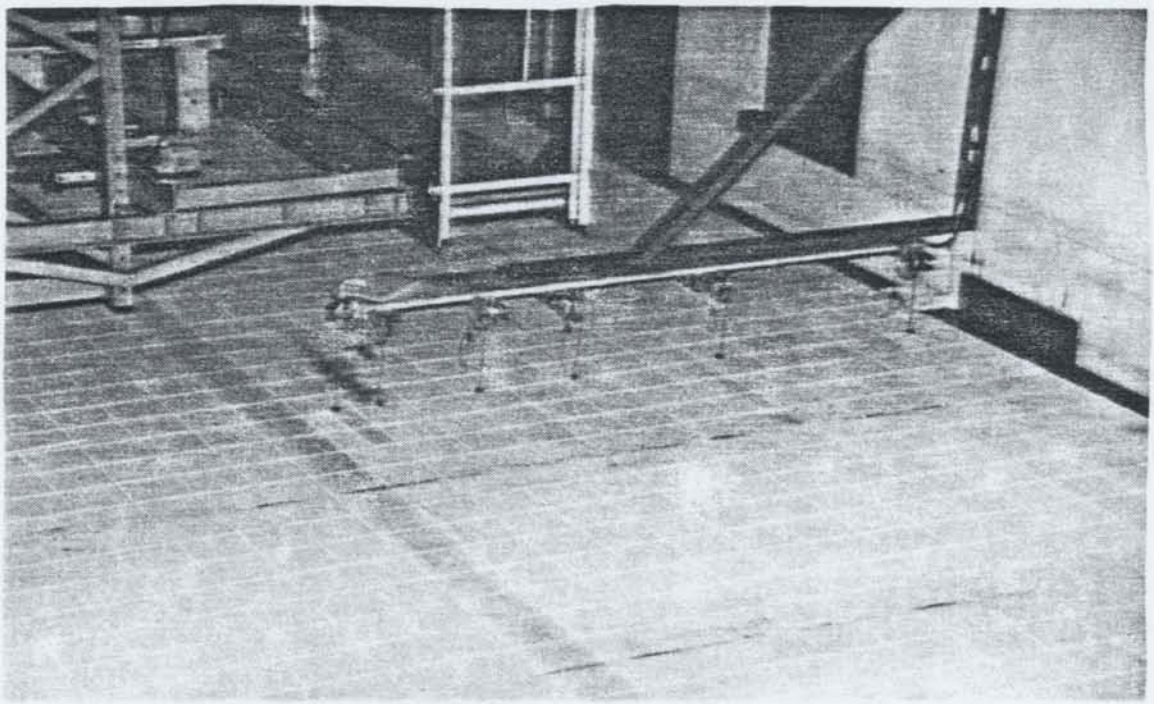

Figure 27 Photo Showing Sensors

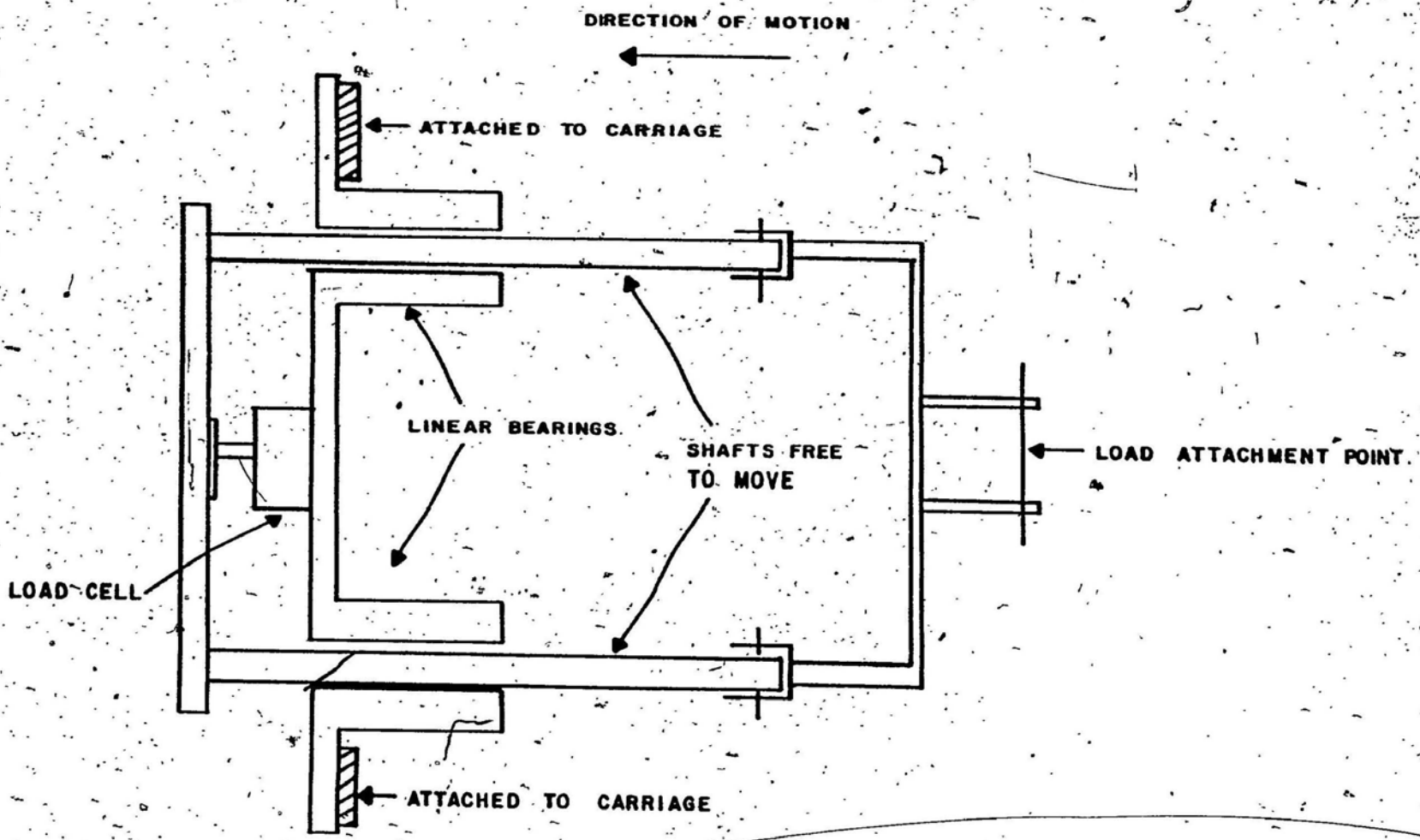

FIGURE 28 . SECTIONAL VIEW OF APPARATUS FOR TOWING MODELS - STYROFOAM SHEET TESTS

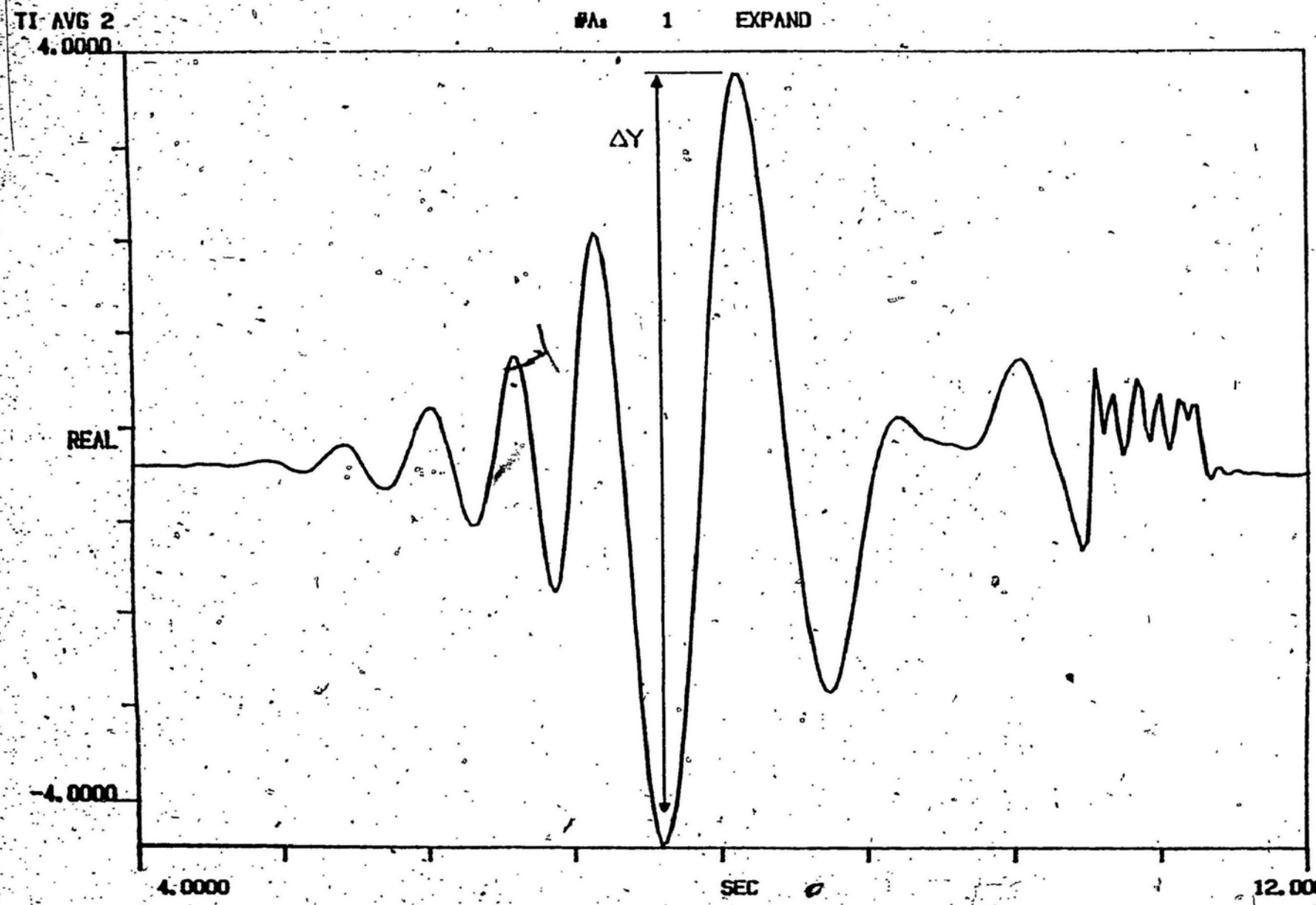

FIGURE 29 DEFLECTION SENSOR OUTPUT

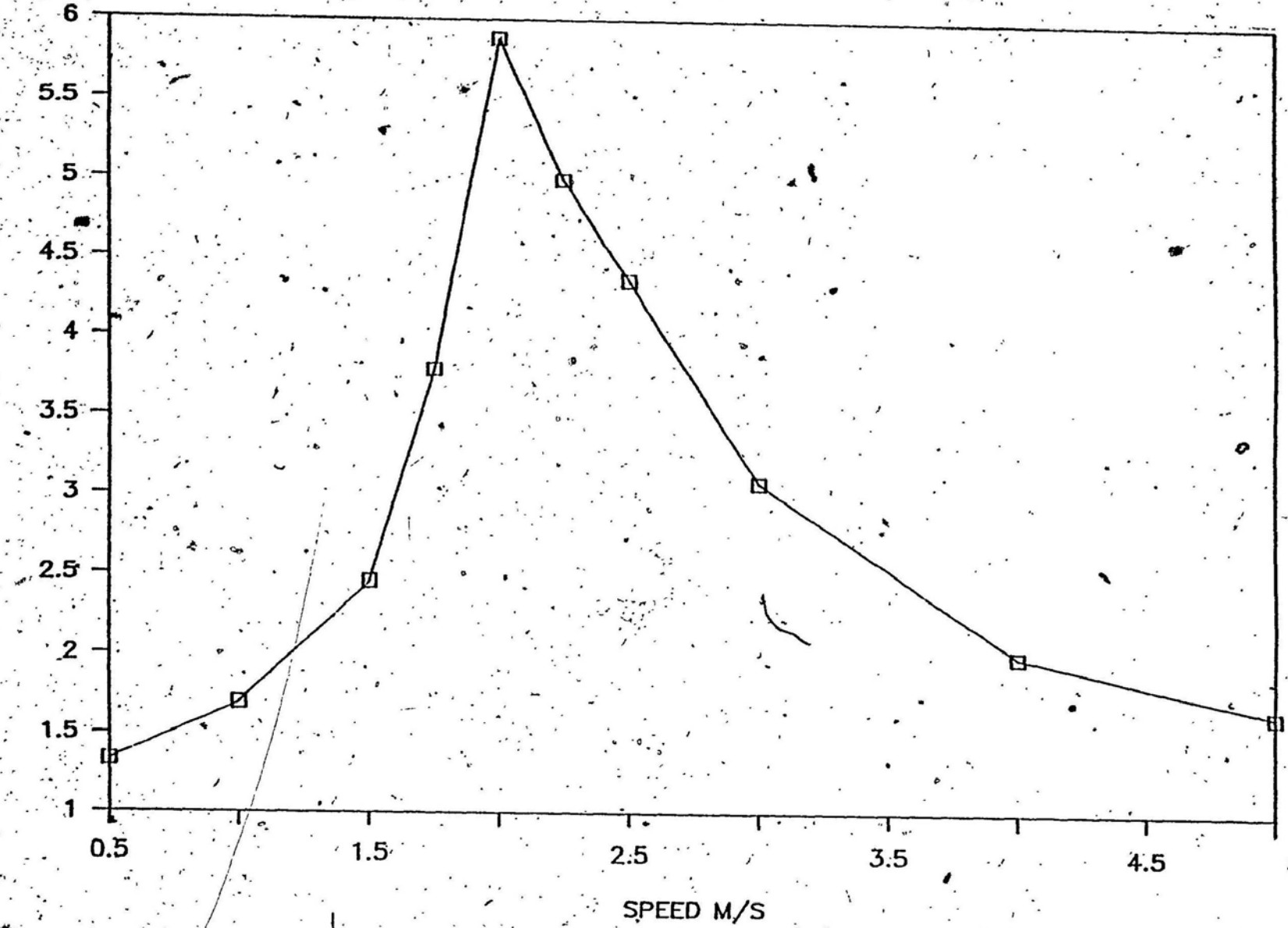

FIGURE 30 SINGLE TIRE DEFLECTIONS
Styrofoam Sheet

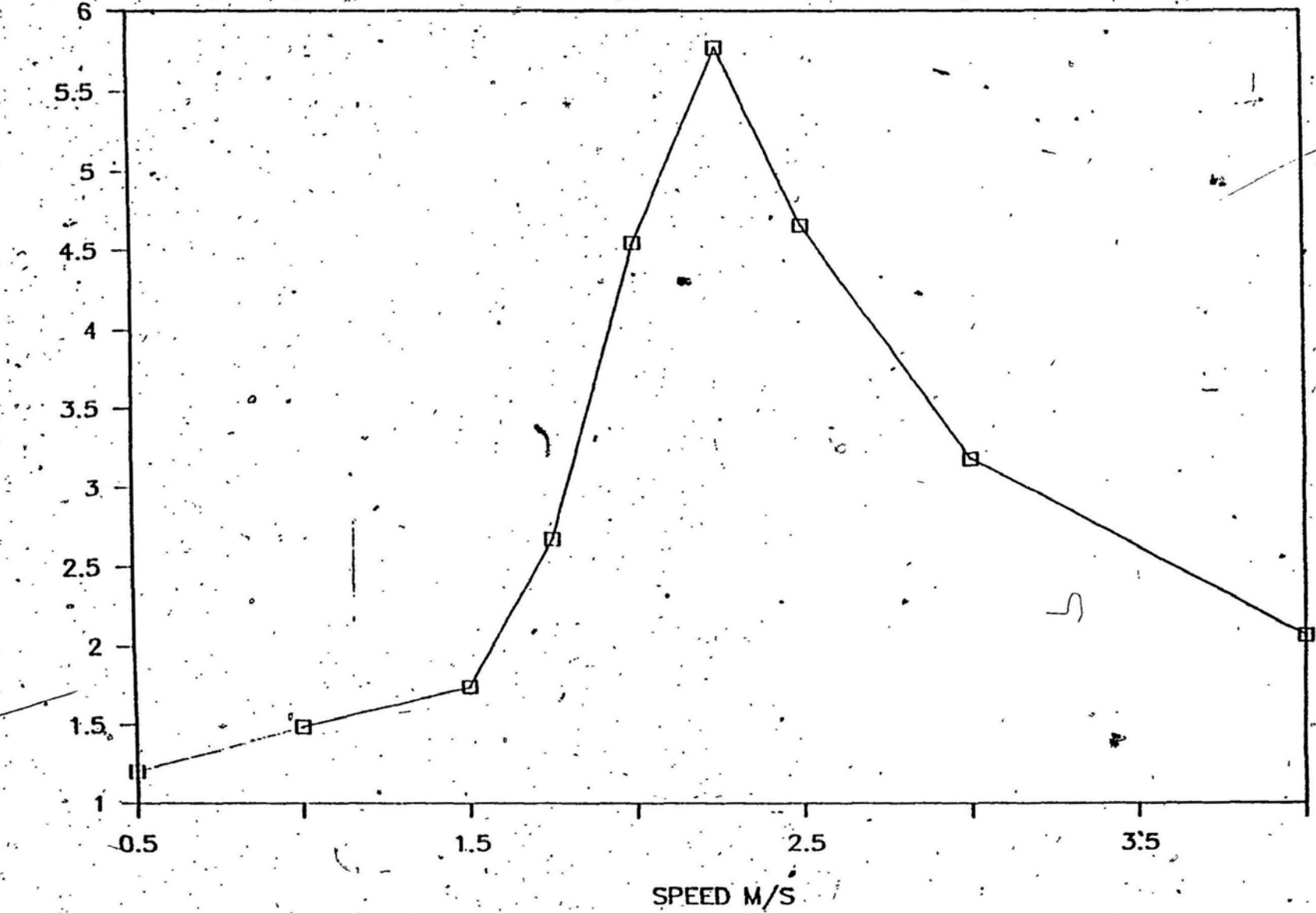

FIGURE 31 TWO TIRE DEFLECTIONS
Styrofoam Sheet

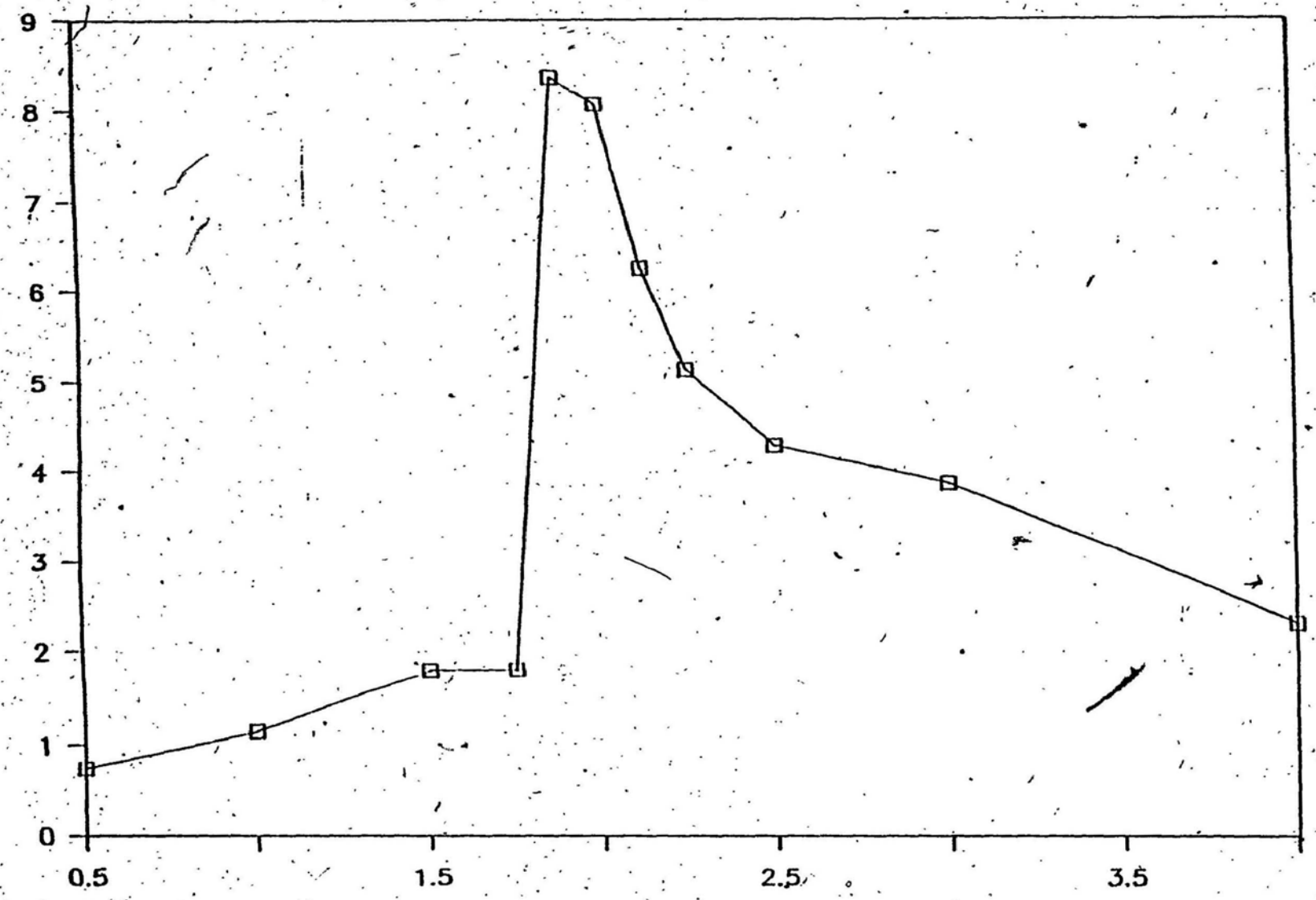

FIGURE 32 ROLLER DEFLECTIONS
Styrofoam Sheet

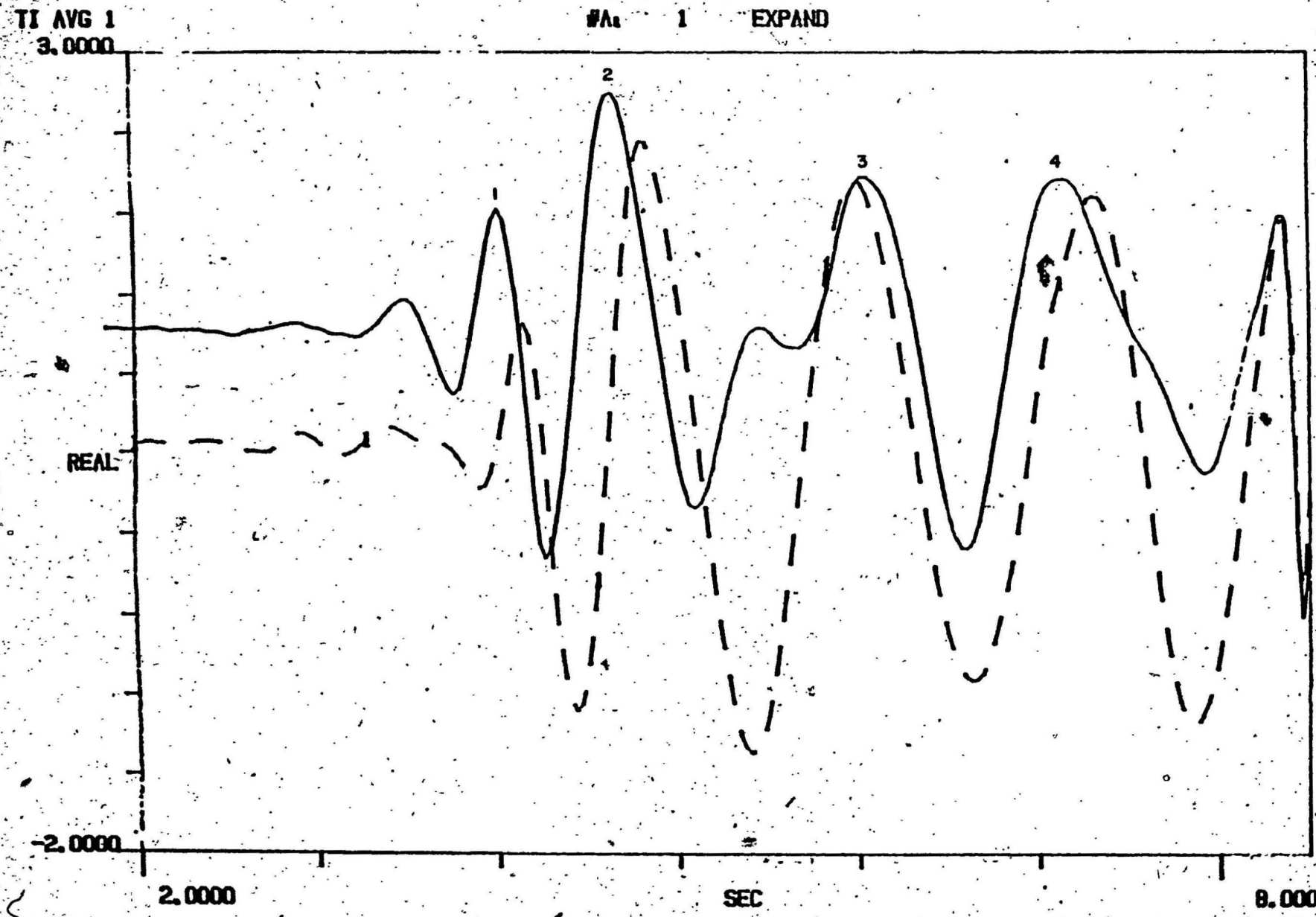

FIGURE 33 DEFLECTION SENSOR OUTPUTS (2 ADJACENT CHANNELS)

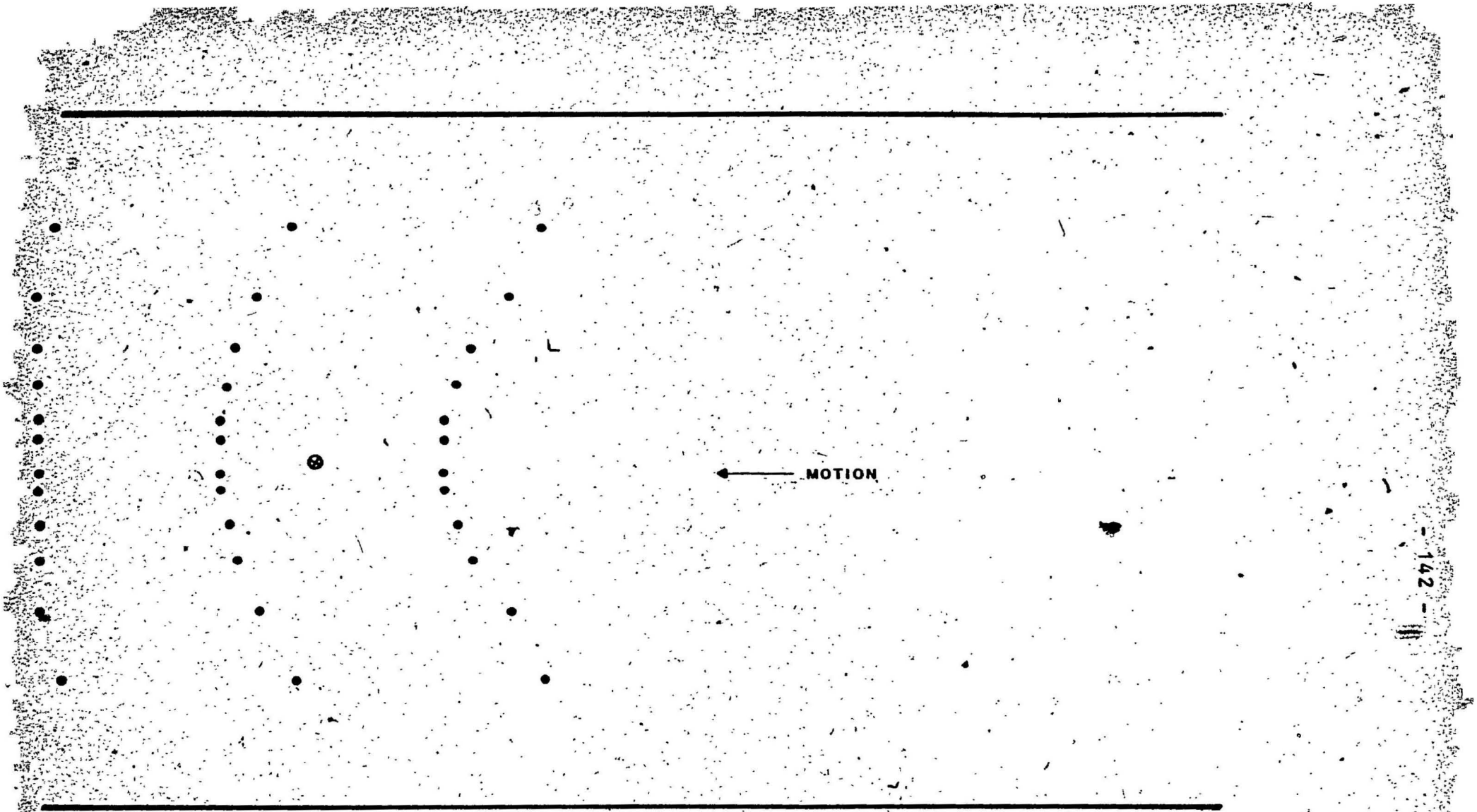

FIGURE 34 WAVE PATTERNS FROM STYROFOAM SHEET

V = 2 m/s V/Vcr = 1

⊗ LOAD LOCATION

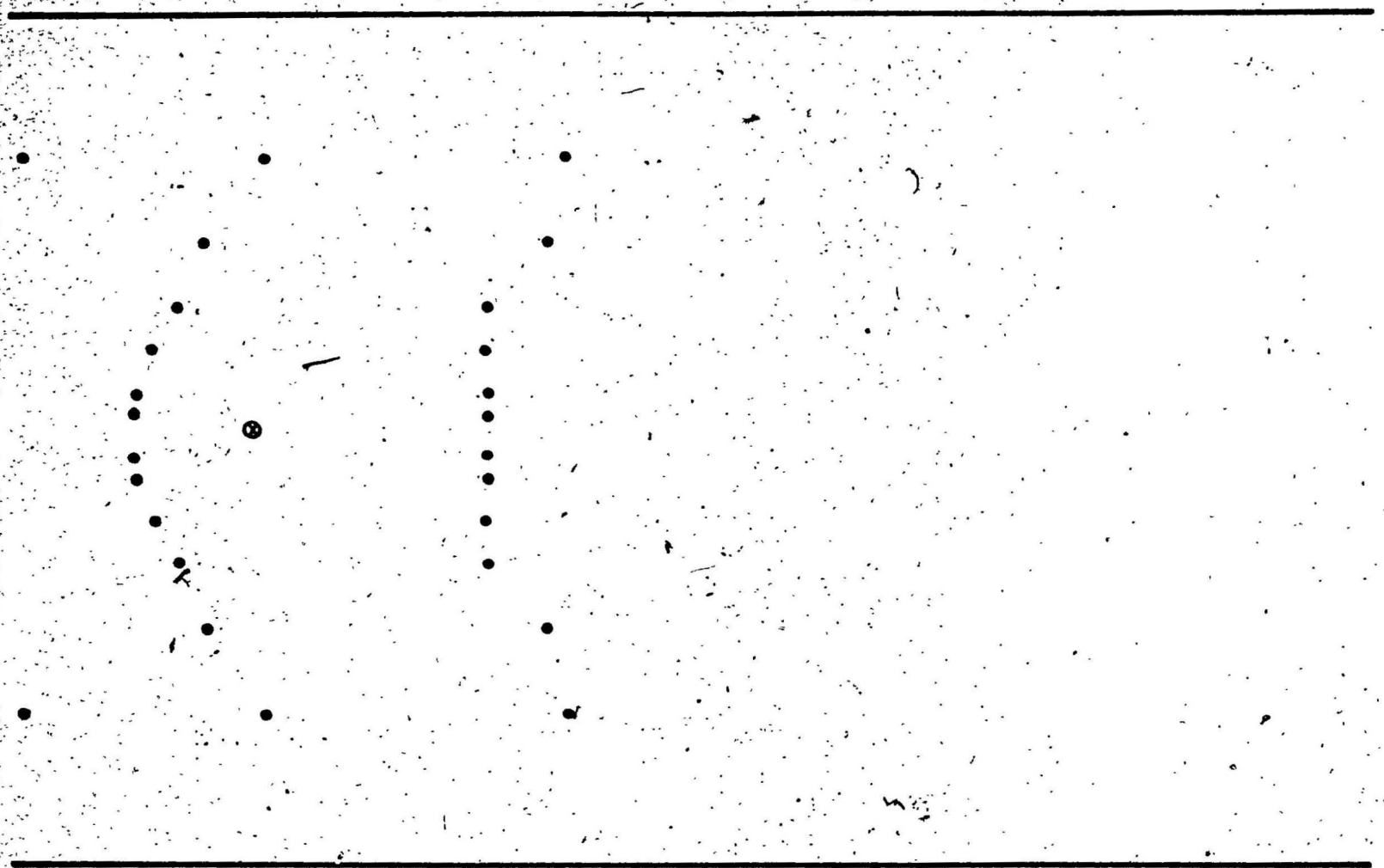

FIGURE 34.1 WAVE PATTERNS FROM STYROFOAM SHEET

V= 2.25 V/Vcr.= 1.125

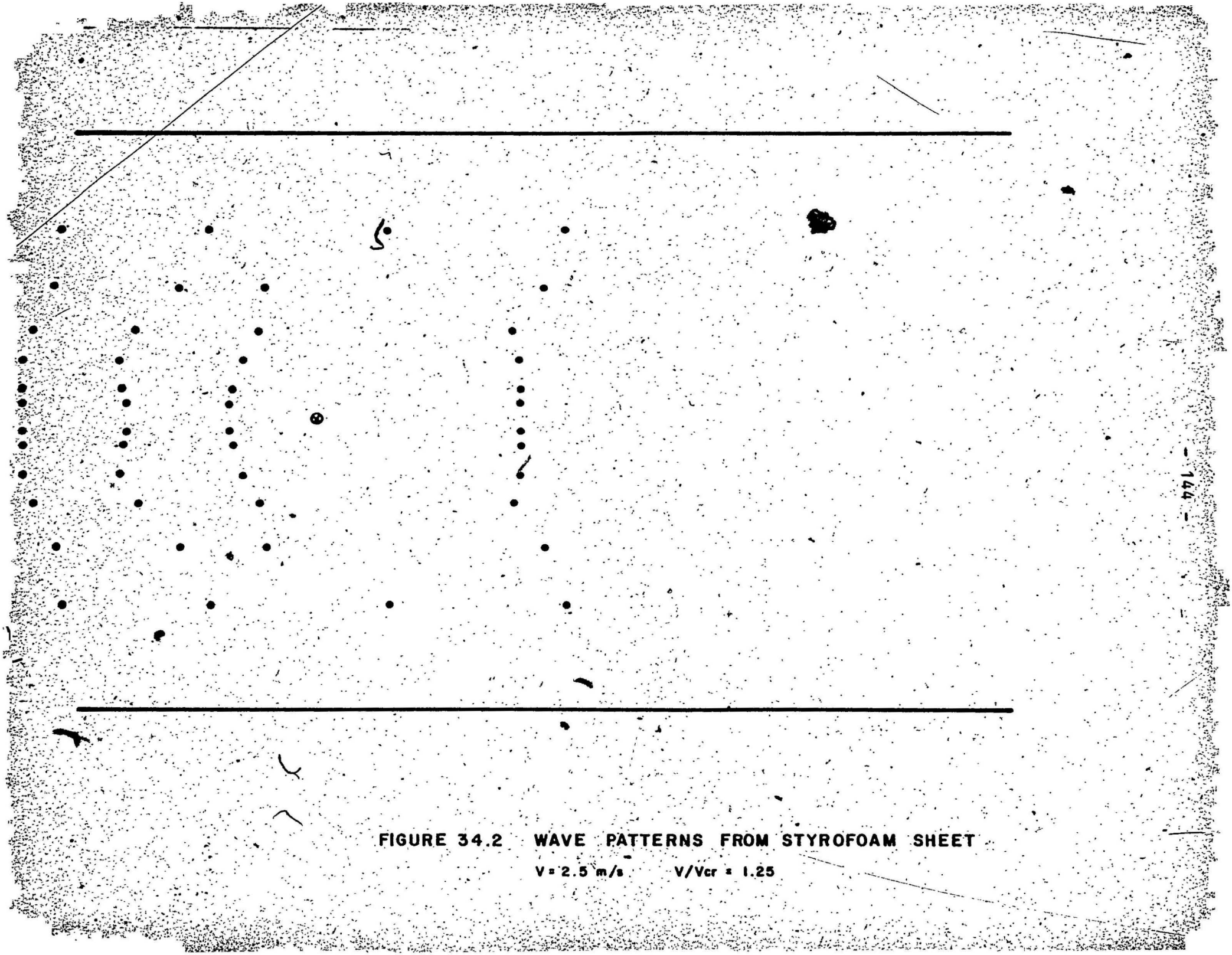

FIGURE 34.2 WAVE PATTERNS FROM STYROFOAM SHEET

V = 2.5 m/s V/Vcr = 1.25

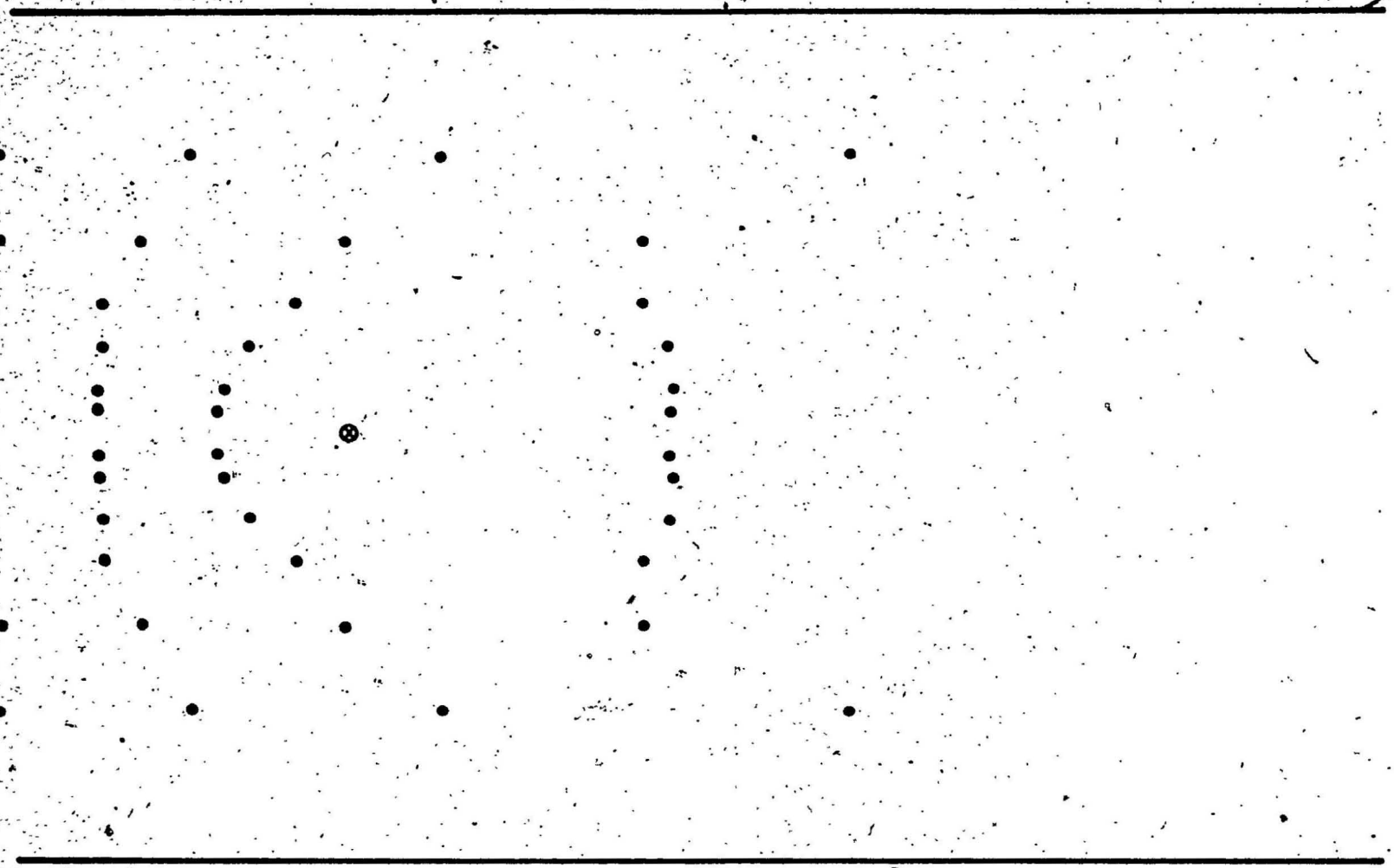

FIGURE 34.3 WAVE PATTERNS FROM STYROFOAM SHEET

V = 3 m/s V/Vcr = 1.5

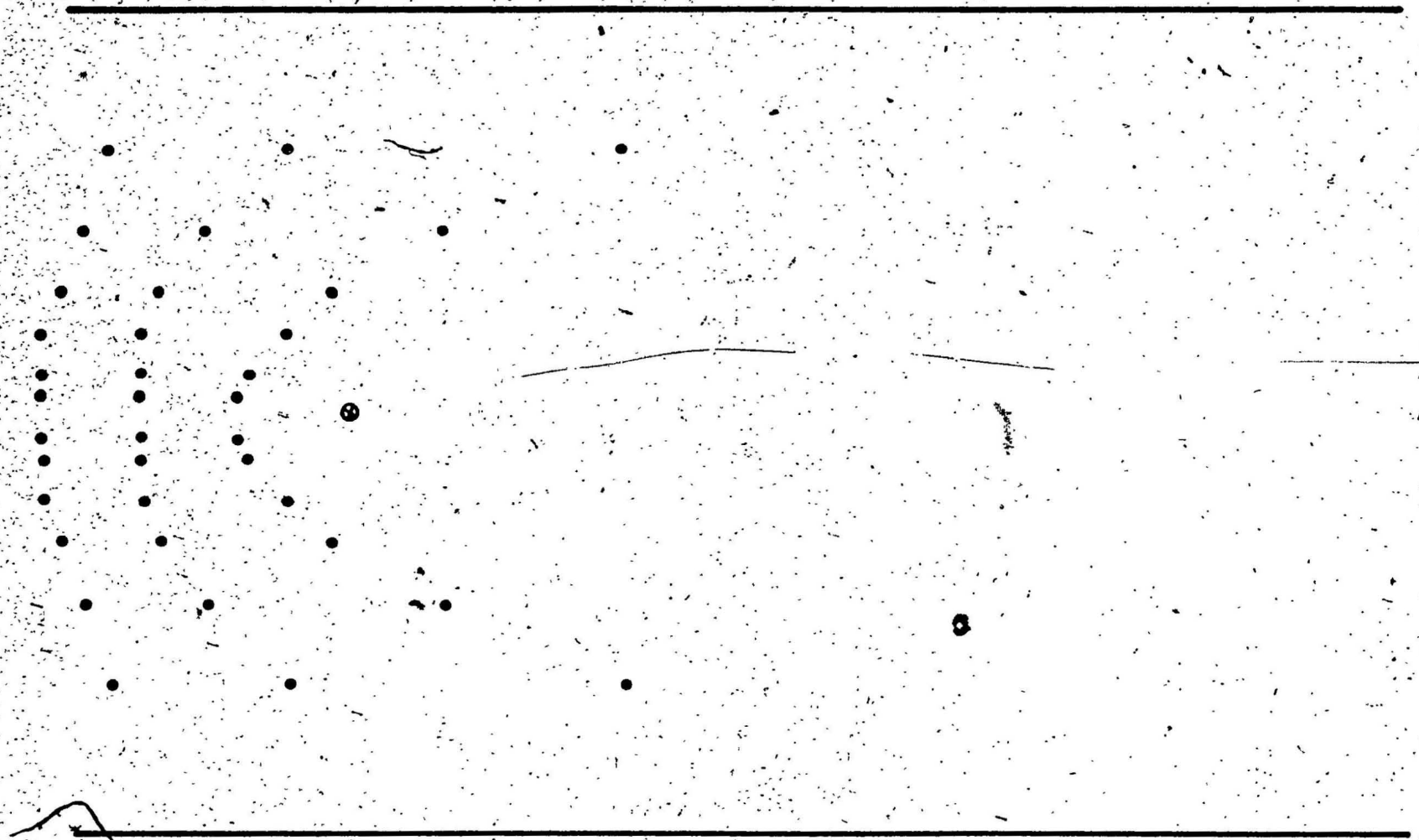

FIGURE 34.4 WAVE PATTERNS FROM STYROFOAM SHEET

V = 4 m/s V/Vcr = 2

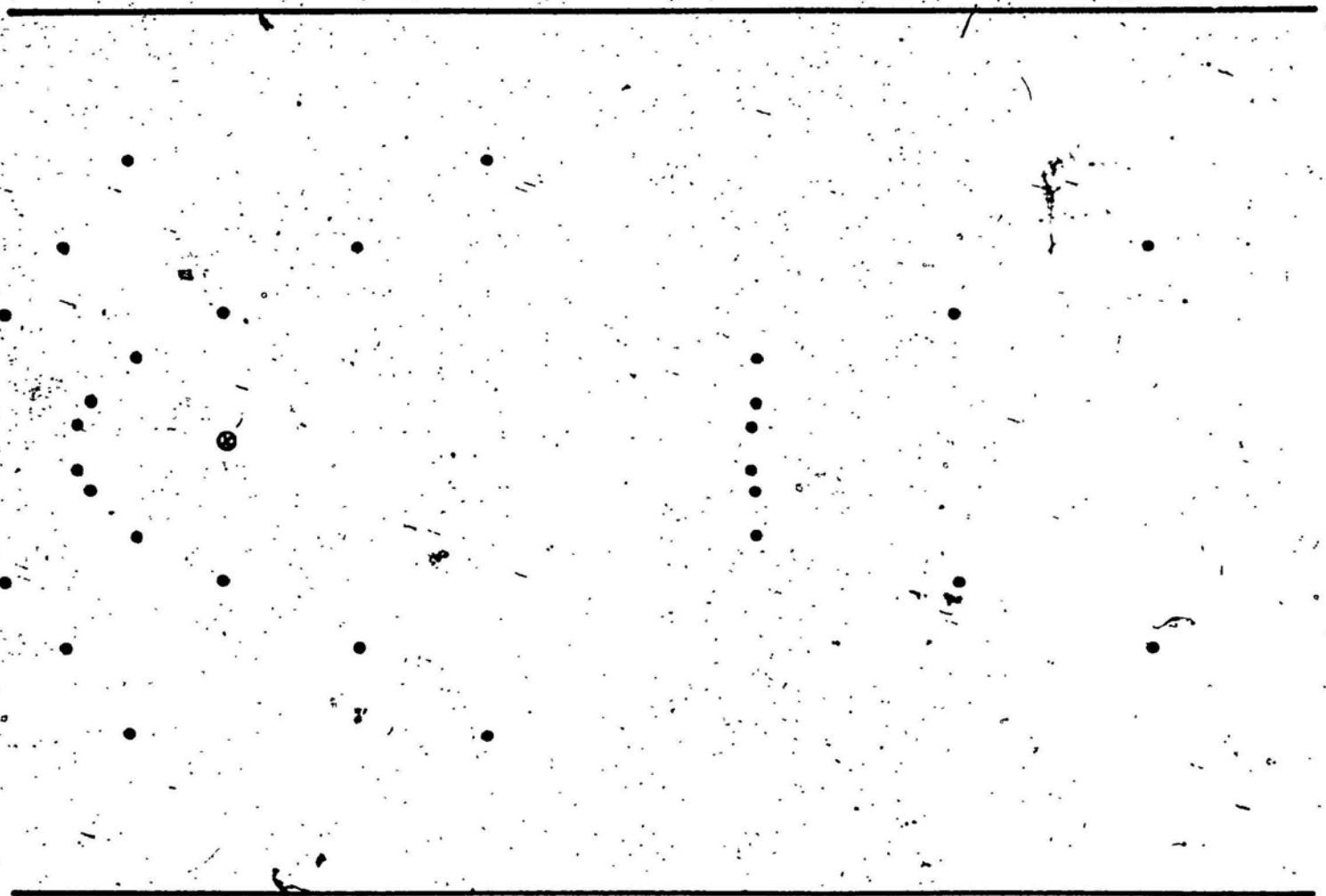

FIGURE 34.5 WAVE PATTERNS FROM STYROFOAM SHEET

V = 5 m/s V/Vcr = 2.5

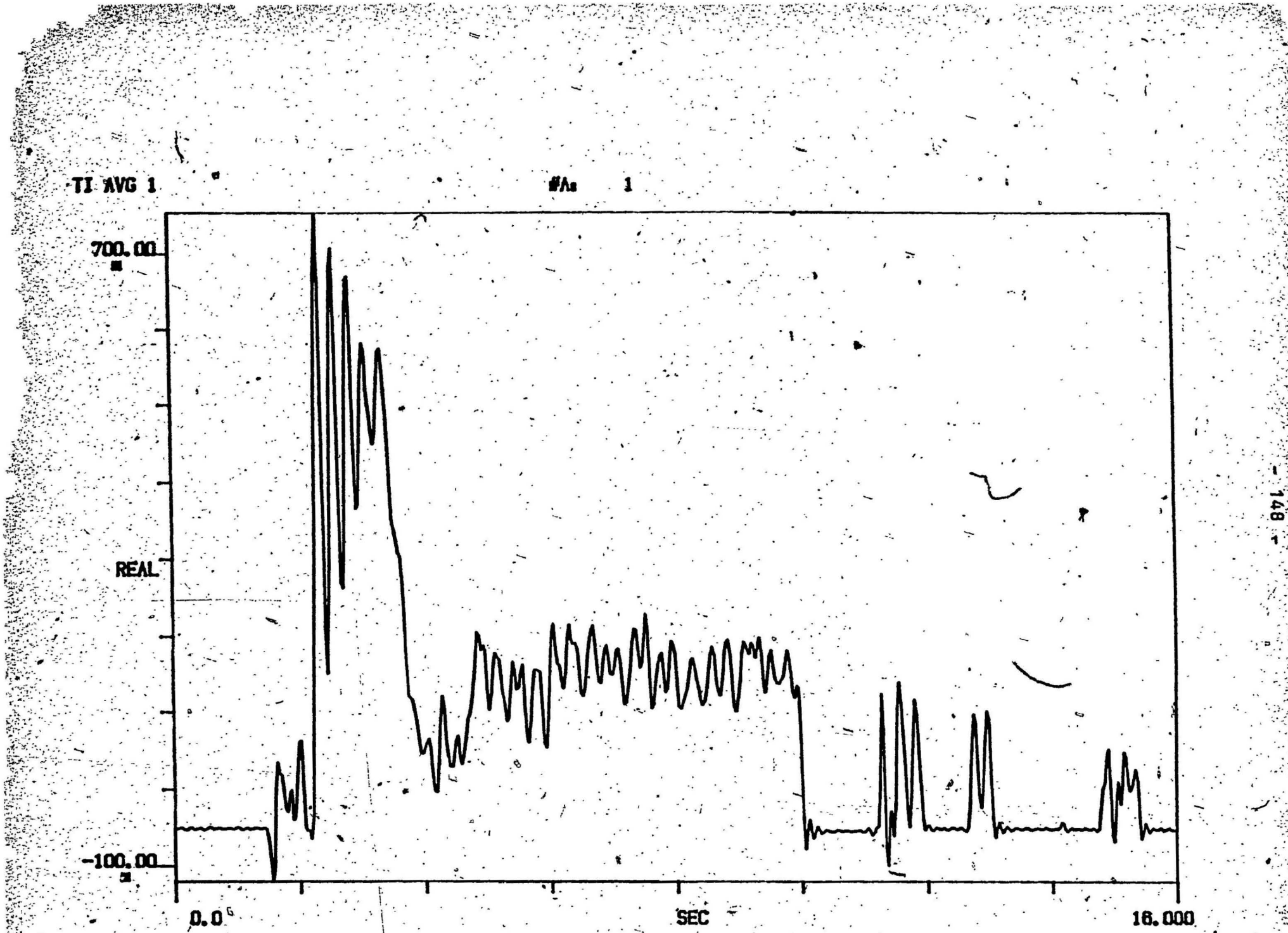

FIGURE 35 LOAD CELL OUTPUT

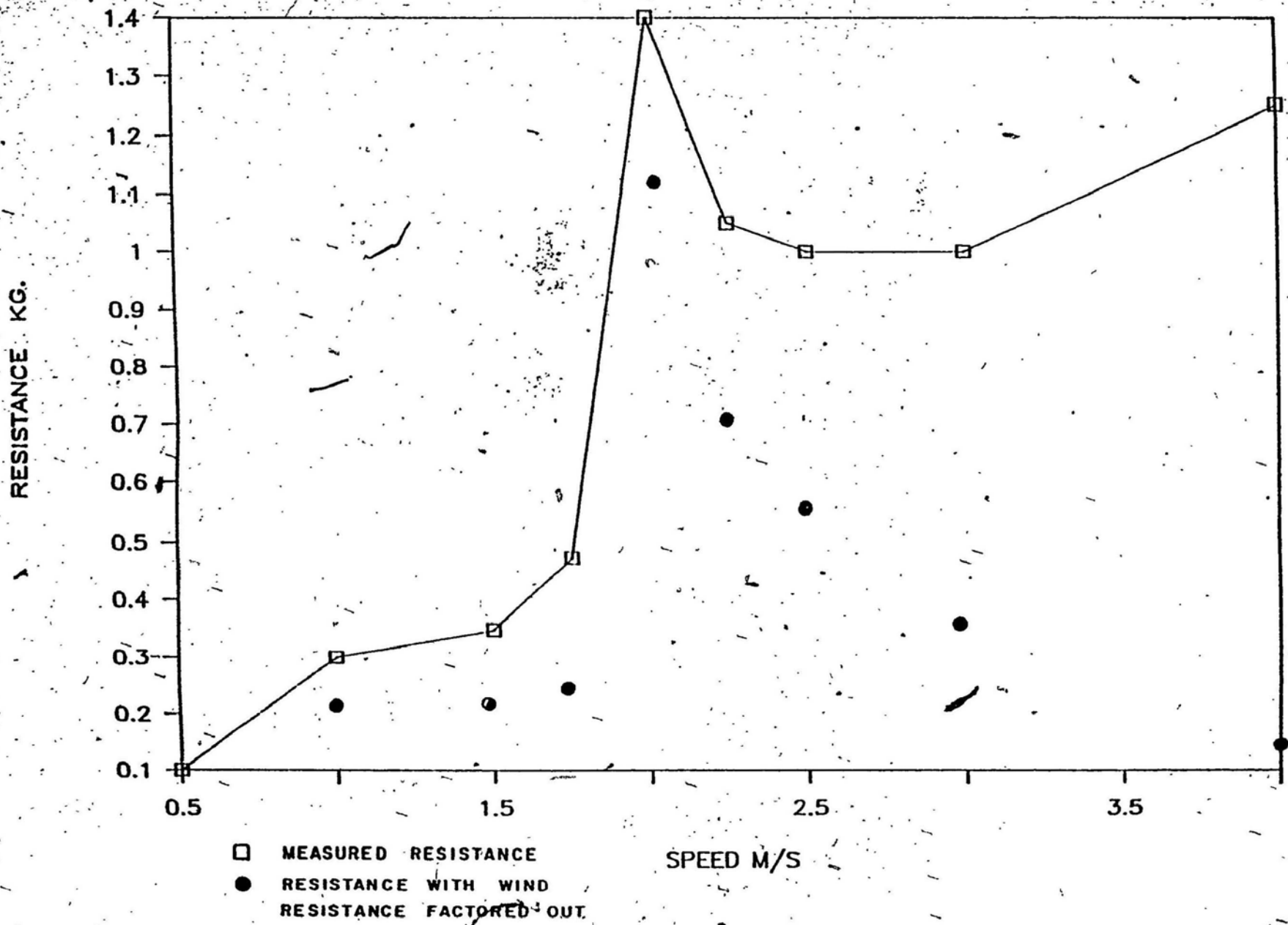

FIGURE 36 ROLLER RESISTANCE
Styrofoam Sheet

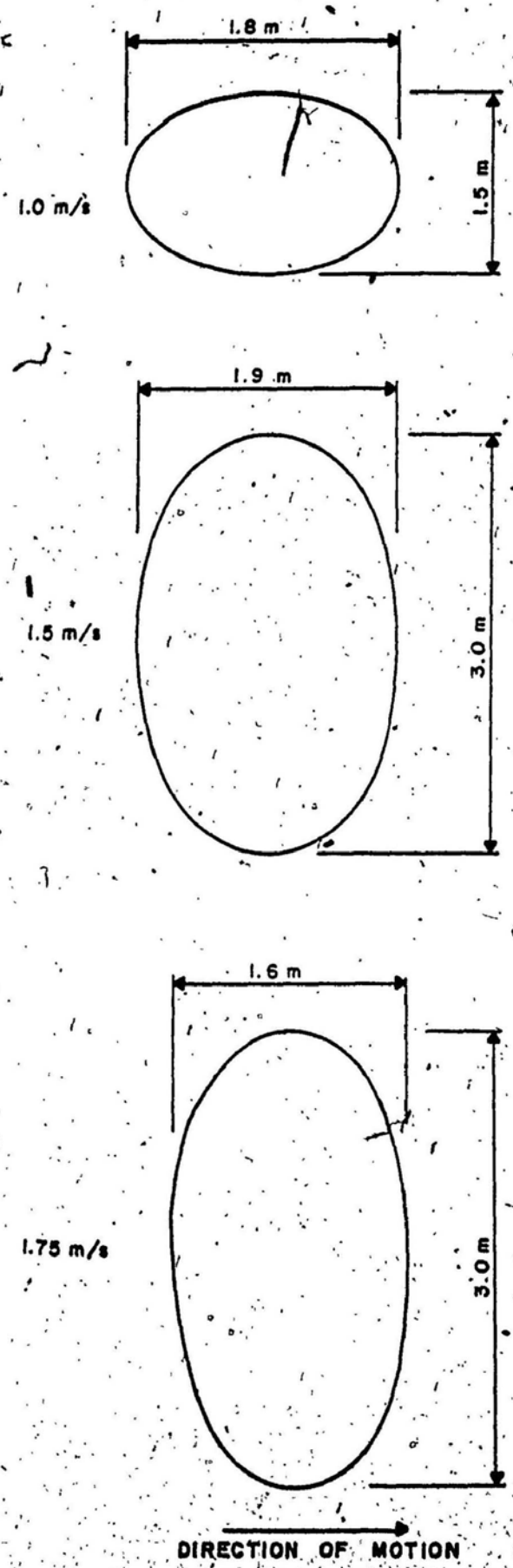

FIGURE 37 DEFLECTION PATTERNS BELOW

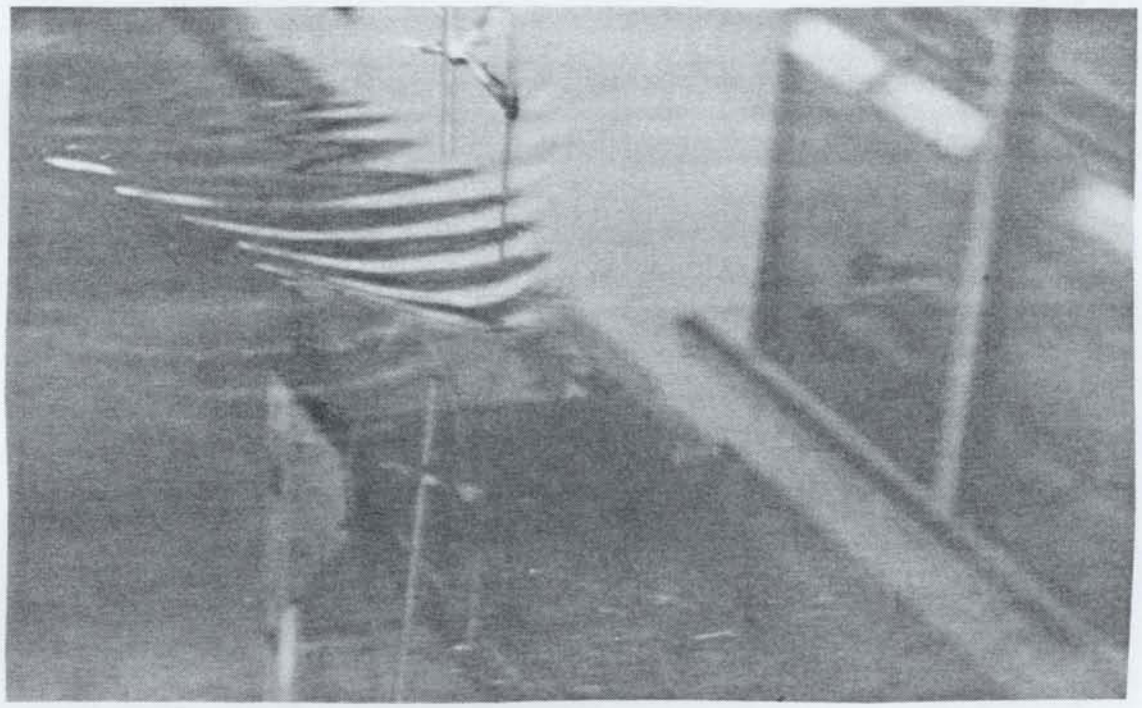

v = .4 m/s

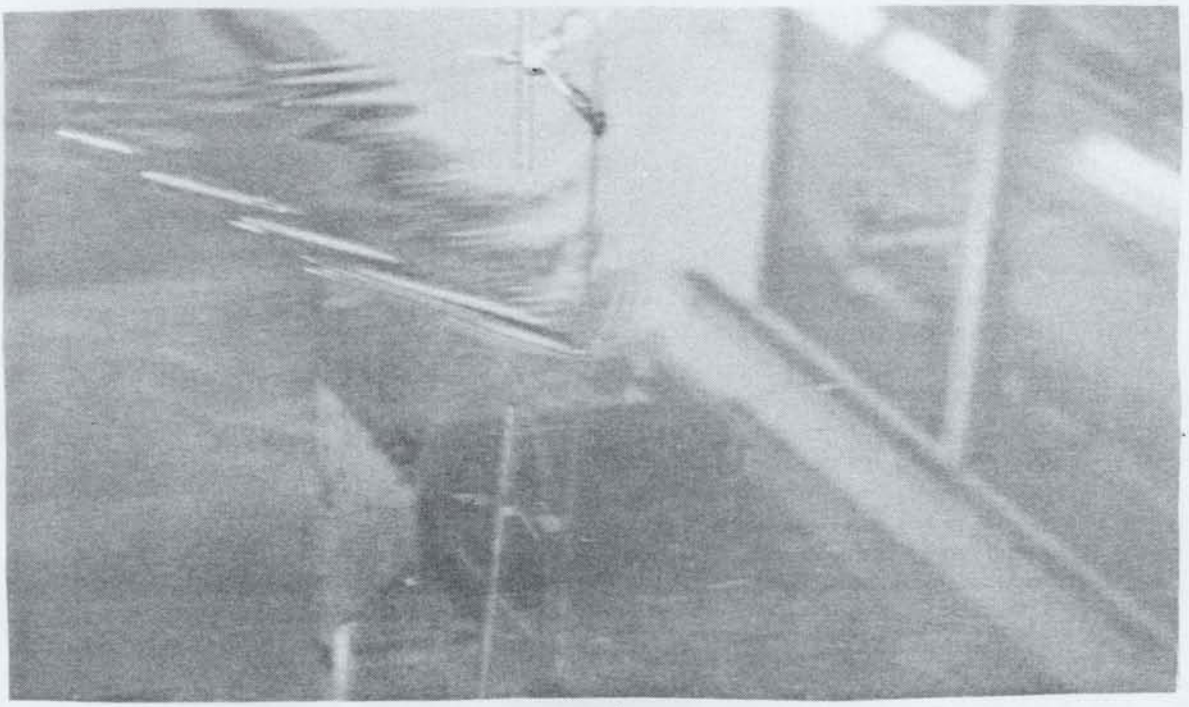

v = .5 m/s

Figure 38 Open Water Wave Patterns

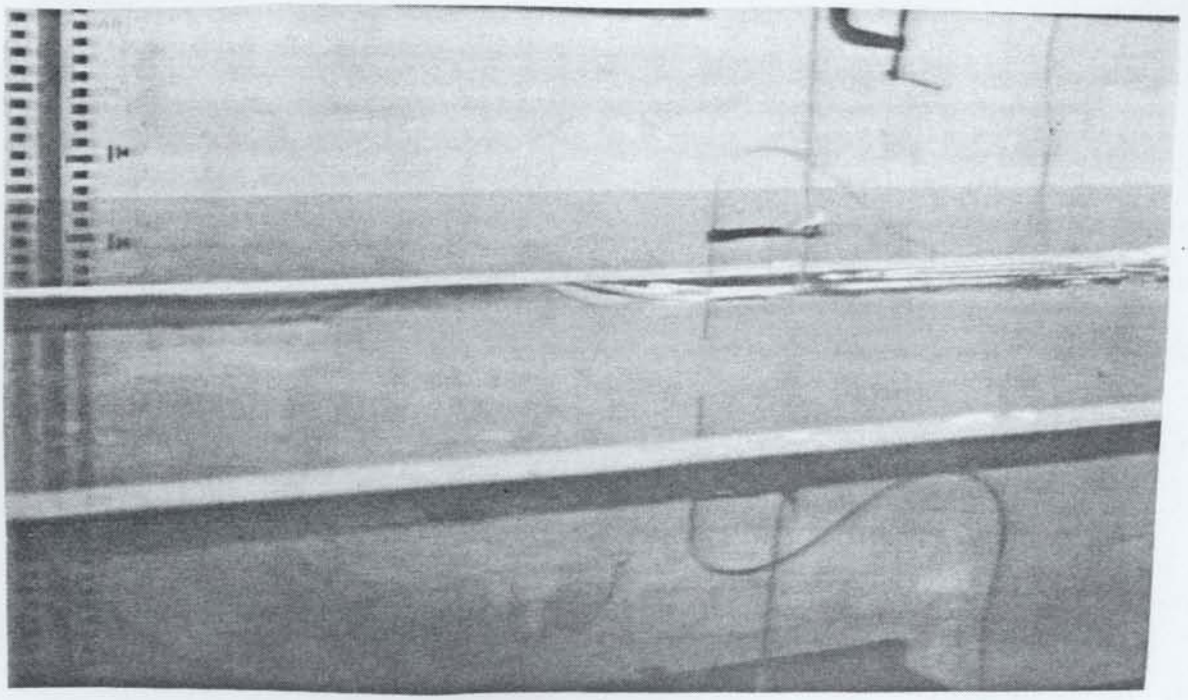

v = .3 m/s

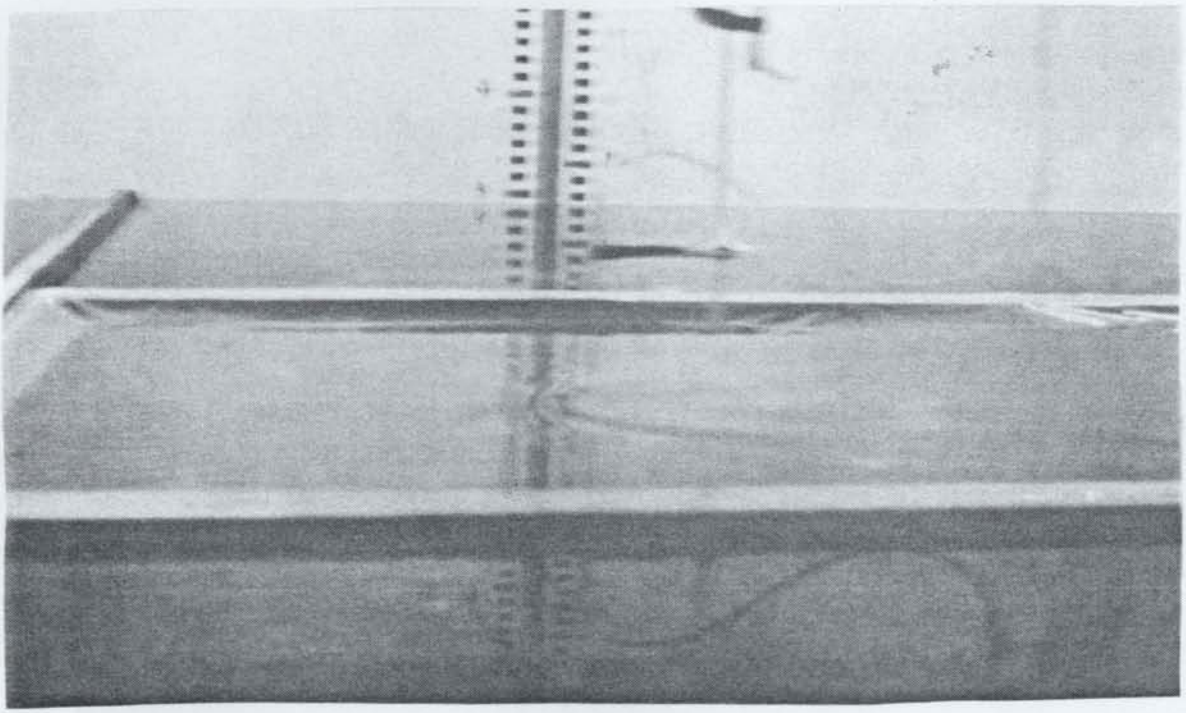

v = 1.0 m/s

Figure 39 Wave Patterns in Polyethylene Sheet